Instantaneous Ultrasonic Assessment of Urinary Bladder Volume

Egon J.W. Merks

ISBN 978-90-8559-542-7

Typesetting in LaTeX 2_ε.
Printed by Optima Grafische Communicatie, Rotterdam, the Netherlands.

Instantaneous Ultrasonic Assessment of Urinary Bladder Volume

Instantane urineblaas volume meting met ultrageluid

Proefschrift

ter verkrijging van de graad van doctor aan de
Erasmus Universiteit Rotterdam
op gezag van de
rector magnificus

Prof.dr. S.W.J. Lamberts

en volgens besluit van het College voor Promoties.

De openbare verdediging zal plaatsvinden op
woensdag 17 juni 2009 om 11.45 uur door

Egon Jacobus Wilhelmus Merks
geboren te 's-Hertogenbosch

Doctoral Committee

Promotors:	Prof.dr.ir. N. de Jong
	Prof.dr.ir. A.F.W. van der Steen
Other members:	Prof.dr.ir. R. van Mastrigt
	Prof.dr.ir. W.A. Serdijn
	Prof.dr.ir. N. Bom

This work has been supported by the Dutch Technology Foundation STW (grant 06652). It was carried out at the department of Biomedical Engineering of the Erasmus Medical Center in Rotterdam, the Netherlands.

Financial support by Verathon Medical Europe B.V. (formerly Diagnostic Ultrasound Europe B.V., IJsselstein, the Netherlands) for the publication of this thesis is gratefully acknowledged.

Financial support for the publication of this thesis by:

- TiePie Engineering (Sneek, the Netherlands)
- Oldelft B.V. (Delft, the Netherlands)

is also gratefully acknowledged.

Contents

1 Introduction **1**
- 1.1 The urinary bladder . . . 2
  - 1.1.1 Bladder shape and position . . . 2
  - 1.1.2 Bladder dysfunction . . . 3
- 1.2 Ultrasound imaging . . . 3
  - 1.2.1 Basic physical properties . . . 3
  - 1.2.2 Echography . . . 5
  - 1.2.3 Display modes . . . 6
- 1.3 Advances in acoustic bladder volume assessment . . . 8
  - 1.3.1 A-mode techniques . . . 8
  - 1.3.2 Two-dimensional B-mode . . . 9
  - 1.3.3 Three-dimensional acquisition . . . 12
- 1.4 Portable ultrasound . . . 12
  - 1.4.1 BladderScan® technology . . . 13
- 1.5 Bladder volume assessment using nonlinear ultrasound . . . 15
  - 1.5.1 Nonlinear ultrasound . . . 15
  - 1.5.2 Volume assessment . . . 17
- 1.6 Thesis outline . . . 18

2 A Pilot Study **21**
- 2.1 Introduction . . . 22
- 2.2 Approach and theory . . . 23
- 2.3 Experiments and methods . . . 28
  - 2.3.1 Single-element transducer . . . 29
  - 2.3.2 Phased-array rotating transducer *in vitro* . . . 29
  - 2.3.3 Volunteer measurements . . . 29
- 2.4 Results and discussion . . . 30
  - 2.4.1 Single-element transducer . . . 30
  - 2.4.2 Phased-array rotating transducer *in vitro* . . . 32
  - 2.4.3 Volunteer measurements . . . 33
- 2.5 Conclusions . . . 34

3 Transducer Design and Realization **37**
3.1 Transducer realization 39
3.1.1 Introduction 39
3.1.2 Materials and methods 41
3.1.3 Results 44
3.1.4 Conclusions and discussion 52
3.2 Transducer modeling 53
3.2.1 Introduction 53
3.2.2 Materials and methods 53
3.2.3 Results 58
3.2.4 Discussion and conclusions 62
3.3 Transducer concepts 63
3.3.1 Introduction 63
3.3.2 Materials and methods 64
3.3.3 Results 68
3.3.4 Conclusions and discussion 69
3.4 Inverted multilayer transducer (IMT) 71
3.4.1 Introduction and literature 71
3.4.2 Materials and method 74
3.4.3 Results 78
3.4.4 Discussion and summary 84

4 Comparison of Computational Methods: A Simulation Study **89**
4.1 Introduction 91
4.2 Methods 93
4.2.1 Computer model 93
4.2.2 Pulse-echo scattering 94
4.2.3 Algorithm definition 95
4.2.4 Simulations 97
4.3 Results 98
4.4 Discussion and conclusions 106

5 Quantitative Bladder Volume Assessment: First *In Vivo* Results **109**
5.1 Introduction 110
5.2 Materials and methods 111
5.2.1 Nonlinear wave propagation simulations 111
5.2.2 *In vivo* volume measurements 111
5.3 Results 115
5.3.1 Nonlinear wave propagation simulations 115
5.3.2 *In vivo* volume measurements 116
5.4 Discussion and conclusion 119

6 Patient Safety **121**
6.1 Introduction . . . 122
6.1.1 Safety regulation . . . 122
6.1.2 Mechanical Index (MI) . . . 124
6.1.3 Thermal Index (TI) . . . 124
6.2 Materials and methods . . . 126
6.2.1 Temperature simulations . . . 126
6.2.2 Temperature measurements . . . 127
6.3 Results . . . 129
6.4 Discussion and conclusions . . . 131

7 Conclusions and Suggestions **133**
7.1 Introduction . . . 133
7.2 General discussion . . . 134
7.3 Future research suggestions . . . 137
7.4 Conclusions . . . 140

Bibliography **143**

Appendix A: Abstract Original Patent Application **151**

Appendix B: Abstract Continuation In Part (CIP) of the Original Patent Application **155**

Dankwoord **159**

Summary **165**

Samenvatting **169**

About the Author **173**

Publications and Presentations **175**

Chapter 1

Introduction

This thesis concentrates on a completely new instantaneous, non-invasive, and simple bladder volume assessment method with the use of nonlinear ultrasound. Before we can introduce this new method, knowledge about the bladder shape and position is essential to understand the issues involving acoustic bladder volume assessment. Explanation about bladder dysfunction and its treatment will clarify the necessity for bladder management, in which noninvasive bladder volume assessment plays an essential role. Additionally, the basic principles of (medical) ultrasound imaging will be introduced together with an overview of the advances in acoustic bladder volume assessment throughout the years. Finally, the outline of this thesis will be given.

1.1 The urinary bladder

The urinary bladder (or Vesica Urinaria) is a hollow muscular organ that stores urine produced by the kidneys. The urine is transported from the kidneys to the bladder via two ureters, which are connected at the back of the bladder. The ureters contain valves proximal to the bladder to prevent the urine from flowing back to the kidneys (urine reflux). The urine is transported outside the body via the urethra. The complete system of kidneys, ureters, bladder and urethra is called the urinary tract.

1.1.1 Bladder shape and position

In adults, the location of the empty bladder is within the pelvis behind the pubic bone (Symphysis Pubis). In males, the empty bladder has a triangular or prism shape, and its largest diameter is oriented perpendicular to the abdominal wall (See Figure 1.1). In females, the bladder is located somewhat lower in the pelvis and the prism-like shape is a bit more flattened. In children, the bladder lies at a higher level than in adults, above the pubic bone. In most cases its shape resembles an ellipsoid, oriented roughly parallel to the abdominal wall. When the bladder fills up, it first distends in depth (towards the spine) and will then expand in height into the abdominal cavity. The lowest part of the bladder, the base, will remain behind the pubic bone.

The maximum amount of urine an adult bladder can hold ranges from 500 ml to 1000 ml and depends on the individual. The urge to void usually starts at a volume of 300 ml. The actual size and position of the bladder depends on the amount of urine it contains and the surrounding organs. Especially, the conditions of the rectum and the uterus have large effect on the bladder shape.

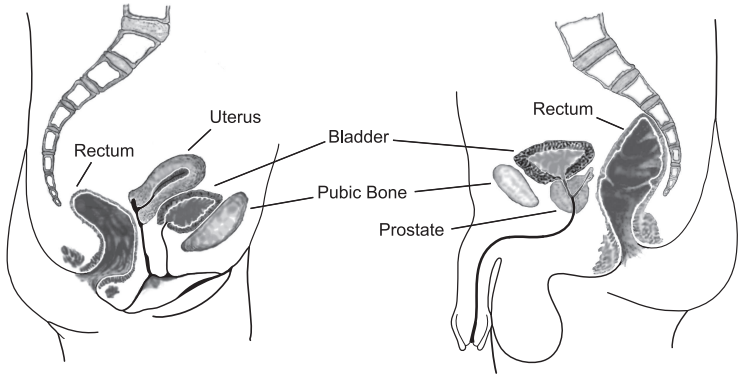

Figure 1.1: Median section of the pelvis of an adult female (left) and an adult male (right).

1.1.2 Bladder dysfunction

Bladder dysfunction is a condition that affects millions of people and is particularly common in the elderly. Several types of bladder dysfunctions are known of which incontinence and urine retention are the most common. Although incontinence is mostly experienced as a social problem, it may result in serious complications, including urinary tract infections (UTI). Urine retention can lead to over distention of the bladder and urine reflux. The unwanted urine reflux may lead to kidney infection and eventually kidney failure.

Age-related changes in the structure and function of the bladder may also lead to dysfunction, including reduced bladder capacity and increased postvoid residual urine volume (PVR). Measurement of PVR is particularly useful in assessing voiding dysfunctions and identifying patients who may have bladder outlet obstruction. PVR is also used to diagnose for an overactive bladder, which is a condition defined as urinary urgency. Clearly, bladder volume assessment, including PVR, is an essential diagnostic tool.

Urinary catheterization remains to be the "golden standard" for bladder volume assessment. It is also used to avoid over distention of the bladder under conditions such as post-operative recovery, where there is temporary loss of bladder sensation and/or loss of the normal voiding mechanism. However, the use of a catheter involves the risk of urinary tract infections and trauma to the urethra and bladder. It was found that 80% of the nosomical (healthcare related) UTIs was caused by urinary catheterization (Sedor and Mulholland, 1999). Noninvasive procedures for bladder volume estimation are known, but are either unreliable or expensive or have some other significant disadvantages. Palpation and percussion are known to be unreliable, while radiography and dye-excretion techniques are known to be inaccurate and clinically impractical. Numerous studies have shown that by the use of portable ultrasound scanners, the number of catheterizations can be reduced significantly, thereby reducing the risks involving this invasive action. It was clinically demonstrated that the use of dedicated portable ultrasound scanners, in place of intermittent urinary catheterization, reduced the incidence of UTI with 50% (Moore and Edwards, 1997; Lee et al., 2007).

Before the advances in acoustic bladder volume assessment can be discussed a brief introduction to ultrasound imaging (echography) is essential and will be given in the next section.

1.2 Ultrasound imaging

1.2.1 Basic physical properties

Sound is defined as the systematic disturbance of the state of equilibrium in matter, where the position of this disturbance in space changes in time. Sound,

or mechanical waves, are characterized by several physical properties such as propagation speed (c), wave frequency (f), wave amplitude (u_0) and wavelength (λ). The propagation speed or sound velocity, expressed in meter-per-second (m/s), primarily depends on the medium through which the wave propagates. For example, the propagation speed in air is about 340 m/s, where in water (at 20°C) it is about 1480 m/s. The wave frequency, expressed in hertz (Hz), describes the amount of vibrations per second. It is the wave frequency that separates audible sound (f between 12 Hz and 20 kHz) from infrasound ($f <$ 12 Hz) and ultrasound ($f >$ 20 kHz). The wavelength, expressed in meter (m), is related to the propagation speed and wave frequency as:

$$\lambda = c/f \tag{1.1}$$

We all know that from shouting into a well or an empty room our voice is reflected and returned to us as one or multiple echoes. In general, reflections occur when a sound wave reaches a boundary between two acoustically different media. The acoustical difference between media is mainly related to their difference in acoustic impedance (Z). The acoustic impedance, expressed in Rayl ($= \mathrm{kg/s \cdot m^2}$), is defined as:

$$Z = \rho \cdot c, \tag{1.2}$$

where ρ is the density ($\mathrm{kg/m^3}$) of the medium. The acoustic pressure (p_0), expressed in pascal (Pa) or $\mathrm{N/m^2}$, is related to the wave amplitude (u_0), or particle displacement, as:

$$p_0 = \rho \cdot c \cdot v_0, \tag{1.3}$$

or with the use of Eq. 1.2 as:

$$p_0 = Z \cdot v_0, \tag{1.4}$$

where v_0 is the particle velocity obtained via du/dt.

When the acoustic impedances of two media are known, the ratio between the amplitudes of the reflected wave and the incident wave at the boundary, also known as the "pressure reflection coefficient," can be calculated by:

$$R = \frac{Z_2 - Z_1}{Z_2 + Z_1}, \tag{1.5}$$

where $\mathrm{Z_1}$ represents the impedance of the medium through which the incident wave was initially propagating and $\mathrm{Z_2}$ represents the impedance of the medium

into which part of the incident wave is transmitted. Equivalently, the pressure transmission coefficient is defined as:

$$T = \frac{2Z_2}{Z_2 + Z_1} \tag{1.6}$$

It must be noted that the given coefficients only apply to cases where the wave propagation is perpendicular to the boundary. When the angle of incidence is not 90 degrees, refraction occurs and the equations should be adjusted according to Snell's law. This will not be discussed here.

1.2.2 Echography

Because of the finite propagation speed of sound, a time delay is experienced between the instant the sound is generated and the moment the echo has returned. In nature, animals like dolphins and bats use this property for positioning of objects and for navigation. The same principle is used with ultrasound imaging. In most medical applications, ultrasonic waves with frequencies between 1 MHz and 20 MHz (1 MHz or "Megahertz" = 1 million Hz) are generated by a transducer and transmitted through the body. In most cases the same transducer is used for transmission as well as reception. This is why transducers are also called "transceivers". The reflections, which occur from inhomogeneities (media with different acoustic impedances) and larger boundaries in the body, are recorded as function of time. By measuring the time delay (Δt) and knowing the speed of sound ($\sim$1540 m/s), the distance (d) to the reflecting boundary, which is half the 2-way travel distance of the sound wave, can be calculated by $d = \Delta t/2 \cdot c$.

The choice for which frequency to use depends on the needed resolution, i.e. the minimal distance between two reflectors for which they still can be seen as separate, and the total distance (or depth) that needs to be scanned. Resolution can be split into two parts: Axial and Lateral resolution. Axial resolution is the resolution in the direction of the sound beam and is approximated as half the effective pulse length. Lateral resolution is the resolution along the direction perpendicular to the sound beam and is determined by the transducer geometry and the frequency used.

For both the axial and lateral resolutions, higher frequencies have shorter wavelengths, allow for shorter pulses and, therefore, give higher resolution. However, sound propagation is also accompanied with frequency dependent attenuation (or loss). In tissue this is approximated at 0.3 dB/MHz/cm, which means that the amplitude of a wave with f=1 MHz is reduced with 3.5% when it propagates over a distance of 1 cm. Because of this frequency dependency, higher frequency waves are attenuated more and thus their penetration depth

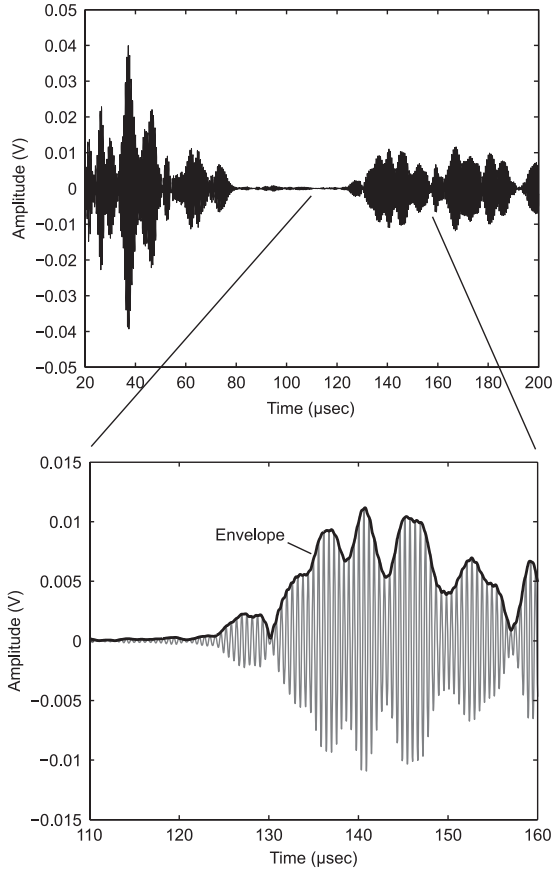

Figure 1.2: RF-signal obtained from a pulse-echo acquisition on a phantom (top) and a zoomed portion (bottom) including the computed envelope.

is limited. Therefore, an application specific trade-off between frequency and the distance that needs to be scanned must be made.

1.2.3 Display modes

The signals that contain the recorded echoes as function of time are often referred to as *Radio Frequency* (RF)-signals. A typical RF-signal as function of time obtained from a pulse-echo acquisition on a phantom is given in Figure 1.2. The part up to 20 μs has been omitted because it contains the very large transmitted signals. Clearly, some parts of the RF-signal have larger amplitudes, indicating that the impedance differences are larger at these locations. Also, the large amplitudes are mainly situated at the left side of the time trace,

which shows the effect of attenuation.

The most basic display mode is called the "Amplitude mode" or "A-mode." In this mode, only the amplitude information of the RF-signal is plotted with respect to time or distance. This so-called "envelope" can be obtained by using a envelope detector, which, in its simplest form, subsequently rectifies and low-pass filters the RF-signal. The lower part of Figure 1.2 shows a zoomed portion of the RF-signals including the calculated envelope. Figure 1.3 shows the complete A-mode of the RF-signal from Figure 1.2.

It may be clear from Figure 1.2 and Figure 1.3 that these 1-dimensional (1D) images are difficult to interpret when no information on the scanned object is available. In the case of these figures, we know that it is a bladder phantom, and therefore we can distinguish between the reflecting tissue regions and the reflectionless urine region.

To be able to determine, for instance, the cross-sectional dimensions of the bladder, a two-dimensional (2D) image would be useful. These 2D images can be obtained by acquiring several A-mode lines from different locations or angles, and displaying the amplitude information as gray scale in 2D space. Because the amplitudes are converted to gray scale, where the larger amplitudes are displayed brighter than the smaller amplitudes, this mode is called the "Brightness-mode" or "B-mode." An example of a B-mode image is given Figure 1.4, which actually shows two cross-sectional B-mode images of a bladder subsequently obtained in the longitudinal and transverse direction.

Because the acquisition of B-mode images can be done very fast, e.g. the A-mode from Figure 1.3 was acquired within 250 μs, tissue motion can be visualized by displaying subsequent B-mode images in time. This allows clinicians

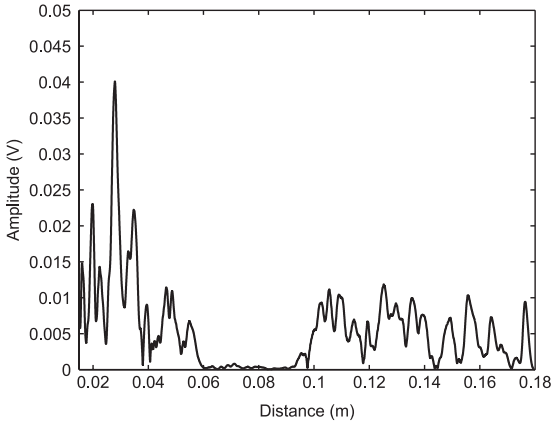

Figure 1.3: A-mode representation of the RF-signal given in Figure 1.2.

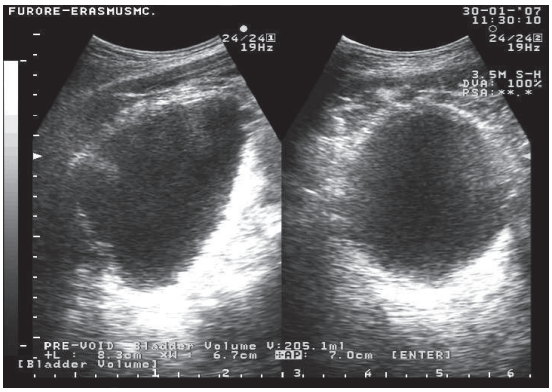

Figure 1.4: B-mode: Cross-sectional images of the bladder in the longitudinal (left) and transverse (right) direction.

to observe, for instance, the functionality of the heart in "real-time." Of course, B-mode images are still cross-sections of a 3-dimensional (3D) space. Currently, imaging systems are available that, with the use of 2D array transducers, are capable of real-time 3D imaging.

1.3 Advances in acoustic bladder volume assessment

In the past 40 years, various non-invasive bladder volume measurement techniques with ultrasound have been described. These methods for bladder volume assessment can be divided into 3 groups:

- A-mode techniques
- Two-dimensional (2D) B-mode
- Three-dimensional (3D) geometry acquisition

1.3.1 A-mode techniques

One of the first publications on using ultrasound for bladder volume measurements was written by West (1967). This paper describes a qualitative method to assess the volume of residual volume using only three A-mode scans in the sagittal plane (See Figure 1.5), with the probe positioned just above the pubic bone. It was shown that the number of A-mode scans that intersect the bladder, as well as the measured distance between the anterior and posterior bladder walls, correlates with the bladder volume. Although, this was only a

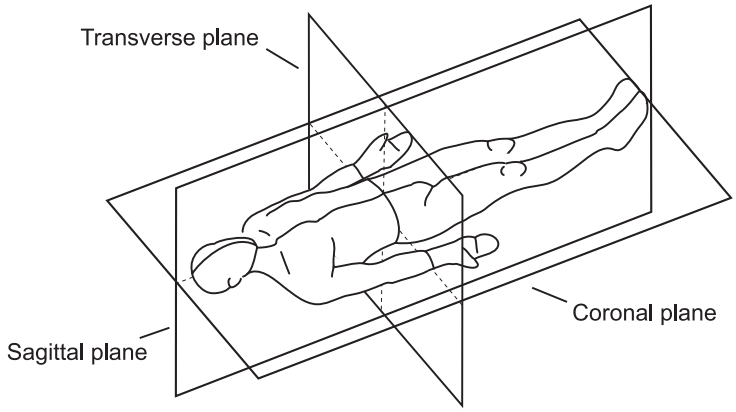

Figure 1.5: Definition of anatomical planes in the human body.

preliminary study without any quantitative results, it was clear that ultrasonic assessment of bladder volume was a promising alternative to catheterization.

At that same time, Holmes (1967) suggested to quantitatively measure the bladder volume using the maximal difference in echo travel time between echoes from the posterior and anterior bladder wall. He concluded that, since the bladder changes in shape when filling, a single distance measurement is not precise enough to predict the entire bladder volume. A-mode scanning with 1 line does indicate the presence of urine but does not allow for accurate volume assessment.

Only recently, the idea of West was modified to allow for real-time quantitative bladder volume measurement (Palanchon et al., 2004). The method uses five ultrasound beams positioned in one plane with predetermined angles. The measurements are performed in only one sagittal plane. Depending on the number of beams intersecting the bladder, the bladder height and depth could be estimated and the volume was calculated using the formula $Height \times Depth \times K$. Here, K represents one of five different and empirically found correction factors, which correspond to the number of intersecting beams. In doing so, the differences in bladder shape, and in particular the bladder width, at different bladder filling were compensated for. Evaluation of this method on 2D B-mode images (N=110) gave a good correlation (r = 0.98) with the true urine volume obtained by catheterization. A relatively low mean error of 11.4% was obtained in a volume range of 23 ml-860 ml.

1.3.2 Two-dimensional B-mode

It was soon found that inter- and intra patient variability of the bladder shape introduced errors in the volume estimations based on geometric models. As

a result, empirically found correction factors were introduced to the existing models.

Hakenberg et al. (1983) reported a simple method that is based on measuring the diameters in a cross sectional image obtained from the midline sagittal bladder plane only. The bladder volume has been related to bladder height and depth as $Height \times Depth \times 6.6$ ml. This formula showed a good correlation coefficient (r=0.942), but with a relatively large mean error of 30.1%.

Most currently available conventional 2D ultrasound systems allow for bladder volume measurement on the basis of static biplane 2D B-mode (Brightness Mode) images. These biplane images consist of two subsequently obtained B-mode scans in the midline saggital plane and the transverse plane of the bladder (See Figure 1.5). The most commonly used methods are:

- Prolate Ellipsoid Method
- Double Area Method
- Double Ellipsoid Method

With the Prolate Ellipsoid Method the bladder shape is assumed to be an ellipsoid. Electronic calipers are used to determine the maximal transverse (W) and longitudinal (L) diameter and the maximal anterior-posterior (AP) diameter (See Figure 1.6a). The volume is calculated as:

$$V = W \times L \times AP \times 0.57, \tag{1.7}$$

where the empirically found correction factor is used to compensate for the variability in bladder shape.

The Double Area Method uses the maximal longitudinal area (A1) and transverse area (A2) of the manually traced contours of the bladder (See Figure 1.6b). The volume is then calculated as:

$$V = \exp\left(C1 + C2 \times \ln\left(A1\right) + C3 \times \ln\left(A2\right)\right), \tag{1.8}$$

where C1, C2 and C3 are again empirically found constants based on 206 patient studies.

The Double Ellipsoid Method (Figure 1.6c) is based on the same principle as the double area method. However, the shape of the bladder is outlined by smooth ellipsoids, which are manually fitted to approximate the two bladder cross-sections. These three methods were reported to be equally accurate with relatively large errors of about 60%. The Prolate Ellipsoid Method was recommended because it was fast and easy. However, because of the large errors care must be taken not to make too rigid conclusions based on these methods.

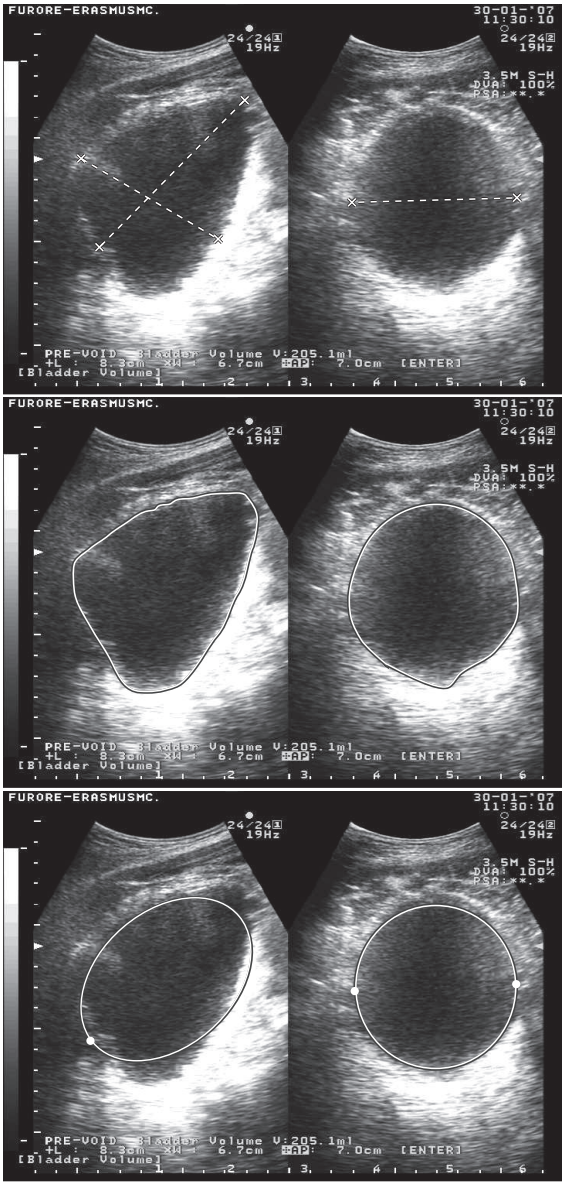

Figure 1.6: Bladder volume measurement using biplane 2D B-mode images. The Prolate Ellipsoid Method (top), Double Area Method (middle) and Double Ellipsoid Method (bottom).

1.3.3 Three-dimensional acquisition

A volume measurement based on 3D echographic sampling of the bladder with a hand guided transducer mounted in a pantograph has been described by Kruczkowski et al. (1988). The sampling covers the entire bladder, follows a given pattern and is not limited to a single or two cross sections of the bladder. For the calculation he needs data from many beam directions. The acquisition procedure is time consuming and thus no instantaneous volume measurement is possible. The hand steered transducer guiding for recording of echo data from the bladder has subsequently gained in acquisition speed by the introduction of constructions whereby the transducer, and thus the beam, is mechanically swept. This nevertheless still requires an acquisition time equivalent to a full acquisition procedure and thus does not yield an instantaneous display of volume. No instantaneous feedback on optimal positioning is thus available. An example of such methods is the BladderScan® technology, which will be described in the next section.

Another 3D ultrasound method is described in a patent by Ganguly et al. (1999). This method is based on bladder wall contour detection with obtained data from echography in a plurality of planes that subdivide the bladder. In each single plane a number of N transducers are positioned on a line to produce N ultrasound beams. In this way, the distance from front to back wall are measured in N positions in the selected plane, from which the surface can be derived. The volume is then calculated from the weighted sum of the surfaces obtained for all planes.

Recently, real-time 3D ultrasound systems are available that use 2D phased array transducers to scan the 3D space. By applying the methods described by Kruczkowski et al. (1988) or Ganguly et al. (1999), these systems should be capable of accurately measuring the bladder volume. However, these instruments are often large, requiring patient transportation to the instrument; they require trained operators and are relatively costly.

1.4 Portable ultrasound

Portable ultrasound devices have gained interest as they allow for bedside diagnosis and thus avoiding the need for patient transport. Dedicated portable ultrasound devices for bladder volume assessment additionally have the advantage of being fast and easy, and hence do not need a trained operator. The use of a portable ultrasound scanner for bladder volume assessment was first published by Henriksson and Maršál (1982) and Ravichandran and Fellows (1983). They used the MiniVisor (Figure 1.7), a small portable battery operated real-time ultrasound device, to determine the PVR. Although it was mentioned

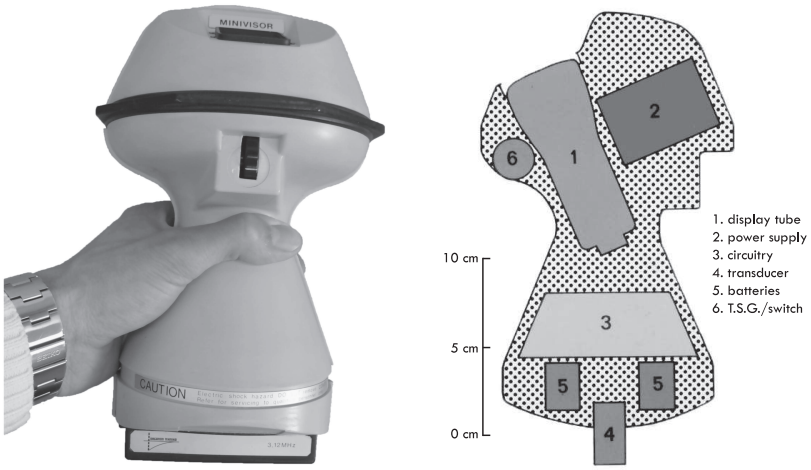

Figure 1.7: MiniVisor (Organon Teknika). *Courtesy N. Bom*

that this device was not suitable for exact measurement, it allowed the user to detect significant residual volumes and thus reduced the number of catheterizations. Additionally, it was demonstrated that portable ultrasound devices made quick and safe bedside examinations possible.

1.4.1 BladderScan® technology

In 1988, the company Diagnostic Ultrasound Corp., currently named Verathon, patented and introduced the BladderScan® Technology. They commercialized the first dedicated portable Bladder Volume Instruments (BVI) for ultrasonic assessment of bladder volume. It consisted of an instrument box with a screen for digital display and a separate motorized scanhead that was capable of mechanically sweeping a transducer through a 97 degree arc in steps of 1.9 degrees. The first BVIs (BVI 2000) used the so-called 2-step technology, which is comparable to the Double Area Method previously described. Firstly, the user needed to scan the sagittal plane, on which the device software automatically detects the bladder and calculates the cross-sectional area. Then, the user had to rotate the scanhead with 90 degrees to perform a second scan, perpendicular to the first scan. After the second scan was completed the volume was automatically calculated and displayed for the user. In 1993, the 2-step method of the BVI 2000 was modified to the 1-step technology (BVI 2500, see Figure 1.8, left). With this new technology the bladder volume was

measured by interrogating a 3D region containing the bladder and performing image detection. The 3D scan was achieved by performing 12 planar scans rotated 15 degrees apart. The bladder volume is then computed using the detected 3D geometry. The results obtained with the BVI 2500 were superior to those from the BVI 2000 and were found equally accurate as catheterization. Since then, subsequent BVI devices brought improved accuracy, larger scan areas (120 degree arc instead of 97) and expanded in functionality. Also, smaller versions became available with integrated scanhead (BVI 6000-series) that allow clinicians to view B-mode images from exams via the Internet. The latest addition to the BVI family is called the BVI 9400 (See Figure 1.8, bottom right). This device uses new technology, directly derived from the study described in this thesis, to ensure faster and more accurate bladder volume assessment.

Figure 1.8: BladderScan® Technology: Automated portable bladder volume instruments. Top Left: BVI 2500 (1993). Bottom Left: BVI 6100 (2005). Right: BVI 9400 (2007). *Courtesy Verathon Medical*

1.5 Bladder volume assessment using nonlinear ultrasound

The previously discussed ultrasound methods require a large amount of ultrasound beams or a mechanical movable transducer to acquire the necessary amount of data of the whole bladder or cross-sections of the bladder. The method described in this thesis only requires a single diverging ultrasound beam and uses the effect of nonlinear wave propagation to determine the urine volume.

1.5.1 Nonlinear ultrasound

It has been demonstrated in literature that the propagation of ultrasound waves is in principle a nonlinear process (Humphrey, 2000). The nonlinear effects have been predicted and demonstrated at frequencies and intensities used in the diagnostic range either in water or in tissue. The nonlinear effects manifest themselves by gradually deforming the acoustic wave shape as it propagates through a medium. As a result, harmonic frequencies at integer multiples of the original frequency are developed. These so-called "higher harmonics" were not present in the wave transmitted by the transducer and cannot be explained by linear wave theory.

Figure 1.9 shows the effect of nonlinear wave propagation on a typical ultrasound pulse transmitted by an transducer. The top left part of the figure shows the initial transmitted waveform at distance $x = 0$ cm from the transducer. Its normalized frequency spectrum (bottom left) contains only the fundamental frequency (in this case 2 MHz). The top right part of Figure 1.9 shows the same ultrasound pulse after it has propagated through water over a distance of $x = 12$ cm. Clearly, the wave shape has changed from a sinewave to an asymmetric sawtooth-like waveform with sharp positive peaks. The normalized frequency spectrum now shows a significant amount of higher harmonics.

The progressive change in wave shape is explained by the variation in phase speed (ν_t) at different points on the wave. Because the phase speed increases with the increase in density, it is higher in the wave compressions than in the wave rarefactions. The relationship between phase speed and particle velocity (u_t) in fluids was derived from the nonlinear wave equation (Hamilton and Blackstock, 1998) and can be approximated as:

$$\nu_t = c_0 + \left(1 + \frac{B}{2A}\right) \times u_t, \tag{1.9}$$

where c_0 is the wave speed at equilibrium and B/A is the nonlinearity pa-

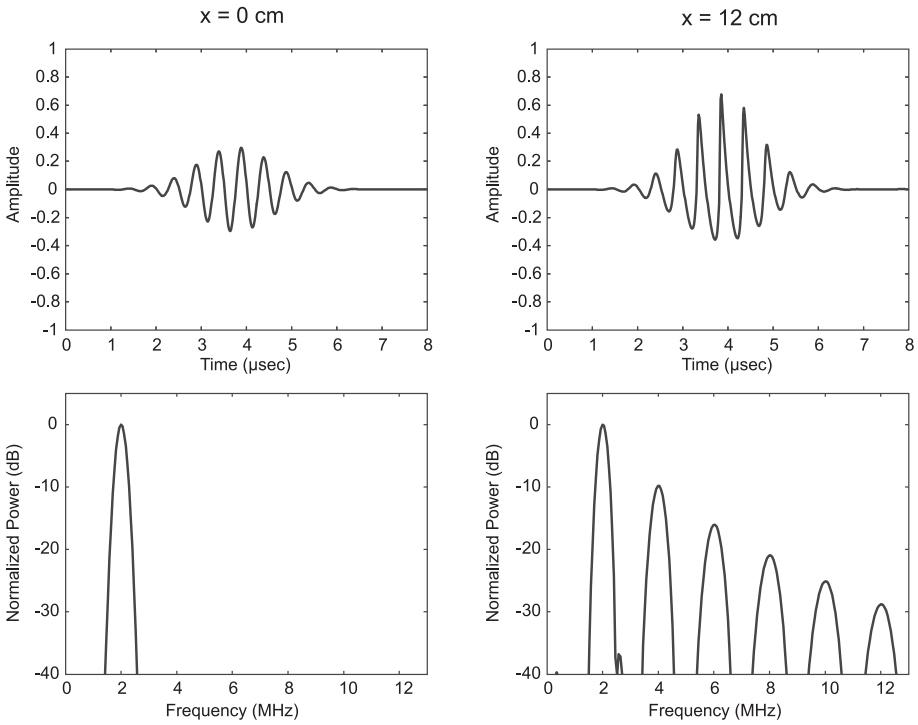

Figure 1.9: Pressure waveforms of an ultrasound pulse at the transducer surface (top left) and after propagation over a distance of 12 cm (top right) in water. Their corresponding normalized frequency spectra are plotted below.

rameter. The nonlinearity parameter relates variations in pressure in a medium to variations in density and is thus a property of the medium. Table 1.1 gives the acoustical properties of some biologic media.

Despite the fact that Table 1.1 shows comparable nonlinearity parameters for all media except fat, it is known that nonlinear effects most strongly occur when ultrasound waves propagate through liquids. In tissue (fat and muscle), acoustic attenuation (α) influences the nonlinear wave propagation, making the nonlinear effects less dominant. The relationship between nonlinearity and attenuation within a medium is reflected in the so-called "Gol'dberg number," which is defined as (Hamilton and Blackstock, 1998):

$$G = \frac{2\pi f p_0 \beta}{\rho_0 c_0^3 \alpha}, \tag{1.10}$$

where β is the coefficient of nonlinearity defined as:

Table 1.1: Acoustical properties of different tissues at 37°C (Duck, 1990; Verma et al., 2005).

Tissue	Sound velocity (m/s)	Density (g/cm^3)	B/A	Acoust.loss (α) ($dB/(mm \cdot MHz^b)$)	b
Fat	1436	0.928	9.6	0.30	0.9
Muscle	1550	1.060	5.8	0.05	1.1
Blood	1584	1.060	6.0	0.01	1.2
Urine	1551	1.025	6.1	0.00047	1.67
Water	1524	0.993	5.4	0.00014	2.0

$$\beta = 1 + \frac{B}{2A}. \tag{1.11}$$

When G is less than 1, the attenuation dominates the nonlinear effect. For values of the Gol'dberg number higher than 1, the nonlinear effect dominates the attenuation. For example, the Gol'dberg number of urine (104) is almost 380 times that of soft tissue (0.27) at an acoustic pressure of 1 MPa and a transmit frequency of 3 MHz. This indicates a much stronger nonlinear behavior for urine than for tissue. From (1.10) it is clear that G depends proportionally on the transmit frequency (f) and the excitation pressure (p_0). Chapter 2 will elaborate further on the implications of the Gol'dberg number and nonlinear wave propagation.

1.5.2 Volume assessment

With the new method described in this thesis, a pulsed ultrasonic signal is transmitted at a certain fundamental frequency. The received echoes that originate from a certain depth beyond the average position (at approximately 12 cm for adults) of the posterior bladder wall are analyzed for the presence of higher harmonics of the fundamental transmit frequency. The received echo signal will contain information about almost the entire bladder as the wide ultrasound beam encompasses the largest part of the bladder. Due to nonlinearity, higher harmonic components will build up during propagation through urine, which can be detected in the returning echo. With empty bladders, the higher harmonics are less apparent (Figure 1.10).

In contrast to the previously described methods for bladder volume assessment, this method does not use a geometrical model to approximate the bladder shape, nor does it need to scan the 3D space with the subsequent application of border detection algorithms. Using only a single element transducer that generates a diverging beam, the information about the amount of liquid present in the insonified 3D space is instantaneously translated, through the physics

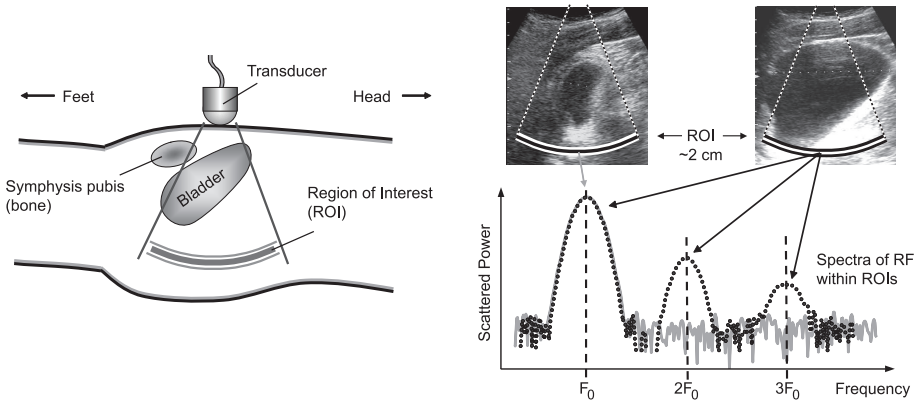

Figure 1.10: Set-up for bladder volume measurements on the basis of nonlinear wave propagation. With the patient in supine position (left) and a single element transducer producing a diverging acoustic beam, the bladder volume is obtained from spectral analysis (right) on a fixed region of interest behind the bladder.

of nonlinear wave propagation, to the amount of harmonics present within the received echoes. Additionally, this beam instantly captures the whole bladder, which avoids aiming problems.

With respect to catheterization, the previously discussed methods using ultrasound have the advantage of being noninvasive, comfortable to the patient, low cost and relatively easy. The additional advantage of the method described in this thesis is that it is instantaneous (or real time) and, because of its simplicity and low cost, is especially suitable for miniaturization and thus monitoring purposes and private use.

1.6 Thesis outline

As was already mentioned, this thesis concentrates on a completely new instantaneous, noninvasive, and simple bladder volume assessment method with the use of ultrasound. The main goal is to obtain the relationship between the detected harmonic components and the urine volume present in the bladder, and to develop a functional prototype that can be evaluated in the clinic. It is expected that this technique can be fitted into a handheld device that does not require experienced operators, facilitates fast bladder volume assessment, and has low cost. Hence, the device will be suitable for personal use and daily clinical practice will benefit from the development of this fast and user independent technique.

Chapter 2 introduces the new method and explains the principle of measurement. Feasibility was proven using *in vitro* measurements on bladder phantoms.

Also, volunteer measurements showed that bladder volume assessment on the basis of nonlinear wave propagation is feasible *in vivo*.

The system used with this first attempt consisted of a conventional ultrasound system, adjusted for experimental purposes, and an experimental fast rotating phased array probe developed for 3D harmonic cardiac imaging. This system was clearly too advanced and costly for the intended application. Also, the system was limited to receiving up to the 2^{nd} harmonic, where, up to that point, the influence of the 3^{rd} and higher harmonics on the volume detection were also of interest. Chapter 3, therefore, describes the design and implementation of a dedicated measurement system. Because of the extreme requirements on sensitivity, bandwidth and beamforming, the main emphasis lies on the design, modeling and implementation of the special ultrasound transducer. Together with the design of a practical and dedicated measurement system, the computational method for deducing the volume from the received echo signals needed to be developed. From initial clinical measurements it became clear that patient variability played an important role on the volume estimation.

Chapter 4 describes a simulation study that compares different computational methods with respect to their ability to estimate the bladder volume from the acquired data and their sensitivity to patient variability.

The dedicated measurement system and the computational method derived from Chapter 4 were put into practice on volunteer measurements. The first *in vivo* results are given in Chapter 5.

The use of ultrasound, at diagnostic pressure levels, is considered to be harmless as no adverse effects have been reported. However, safety limits on the exposure of ultrasound, taking into account pressure and frequency, have been regulated. Chapter 6 discusses the aspects of patient safety using simulations and measurements. It ensures that the safety limits were not exceeded and that bladder volume assessment on the basis of nonlinear wave propagation is safe. Finally, Chapter 7 concludes this thesis with future perspectives and advices on the further development of the method.

The appendices at the end of this thesis give the abstracts of the original patent application and the continuation in part (CIP) related to the method of bladder volume assessment using nonlinear ultrasound.

Chapter 2

A Pilot Study

Based on:
 Bouakaz A., Merks E., Lancée C.T., and Bom N. Noninvasive bladder volume measurements based on nonlinear wave distortion. *Ultrasound in Medicine & Biology*, 30(4):469–476, 2004.

Abstract - The purpose of this study is to suggest a new approach to measure noninvasively the fluid content of a human cavity; in particular, the bladder volume. Determination of bladder volume is important clinically for patients suffering from bladder dysfunction. Several ultrasonic methods were proposed in the past for such a purpose. Most of these methods are based on multiple cross-sectional images and detection of echoes from the bladder wall. We propose here, in a first step, a simple approach that is able to provide an indication of whether or not the bladder volume has exceeded a certain threshold volume. Second, the possibility of accurate volume assessment will be discussed. The approach takes advantage of the difference in harmonic generation of liquids (urine) and tissues. We know that nonlinear effects occur most strongly when ultrasound (US) propagates through liquids with relatively low acoustic attenuation, such as water or urine. However, within soft tissues, the tendency for wave distortion to occur is limited as a result of different acoustic characteristics, most notably the attenuation. Our method is based on measuring the presence of harmonics in an echo from a region-of-interest (ROI) at fixed depth beyond the bladder. The harmonic content in the echo will increase with increase of fluid in the echo path. Phantom measurements were carried out with a single-element transducer and a phased-array transducer. Phantoms containing different volumes were used. Furthermore, measurements on volunteers were performed. The results confirmed that the harmonic content of an echo measured at a deep ROI increases for a full bladder and decays strongly after the volunteer has voided. These preliminary results demonstrate the feasibility of the approach.

2.1 Introduction

It is well known that bladder dysfunction is associated with a number of clinical conditions requiring treatment. In many of these cases, it is important to accurately determine the volume of the bladder (Harrison et al., 1976; Newman and Palmer, 1999; Topper et al., 1993). Under other conditions, such as postoperative recovery, where there is temporary loss of bladder sensation and/or loss of the normal voiding mechanism, too much distension of the bladder has to be avoided. Under those conditions, voiding by catheter introduction is carried out. For assessing bladder volume, catheterization remains the "gold standard". However, serious disadvantages are associated with catheterization, ranging from the uncomfortable situation for the patient to real possibilities of infection (Binard et al., 1996; Çevik et al., 1996; Hakenberg et al., 1983). To ascertain that the bladder needs to be emptied and, thus, avoid unnecessary catheterization, the need for a noninvasive and quick measurement of bladder volume is required. The clinical importance is particularly apparent in anesthesiology, for example. In some situations, accurate determination of volume is needed; in others, however, an indication of the bladder filling is sufficient.

Noninvasive procedures for bladder volume estimation are known, but are either unreliable, expensive or have some other significant disadvantages (Çevik et al., 1996; Hakenberg et al., 1983; Harrison et al., 1976; Ireton et al., 1990). Palpation and auscultatory percussion are unreliable, and radiography and dye-excretion techniques may provide inaccurate volume estimations. Diagnostic ultrasound (US) is today well known for real-time cross-sectional imaging of human organs. Using US waves, volume is sometimes calculated using organ contours obtained in two orthogonal planes with a geometric assumption of organ shape. For 3-D or volumetric echography, the sound beam has to be swept through the entire 3-D space containing the organ of interest. This will further increase the complexity, data-acquisition time and the costs of the instrument. Various methods of bladder volume assessments have been described that utilize the advantages of US waves (Ganguly and Guiliani; Ganguly et al., 1999; Hakenberg et al., 1983). In calculating ultrasonic bladder volume, most of these methods use assumptions about the bladder shape. 2-D echo devices, for instance, use bladder models in the shapes of ellipsoids and/or prisms. Their working principle is based on the bladder information obtained by scanning multiple planes. This information is fitted to the model and, finally, the volume is calculated. Because of the large number of scans needed to provide the model with enough data, the devices become very complex and, therefore, very expensive.

Recent studies (Kruczkowski et al., 1988; Lewis, 1995) have demonstrated, using portable US scanners, that the number of catheterizations can be reduced significantly, thereby reducing the risks of this invasive procedure. An example of a portable US scanner is the Bladderscan® manufactured by Diag-

nostic Ultrasound (Bothell, WA). This device measures the bladder volume by interrogating a 3-D region containing the bladder and then performing image detection on the US signals returned from the insonified region (Coombes and Millard, 1994). It is noninvasive and is claimed to be as accurate as catheterization (Çevik et al., 1996; Sulzbach-Hoke and Schanne, 1999). Although the 3-D scanning requirement makes this instrument complex, such an instrument provides a portable, rapid and accurate method for bladder volume determination.

Nevertheless, the proposed methods based on US waves have shown that the use of bladder models introduces significant errors, because the bladder can take different and complex shapes at different filling stages (Hakenberg et al., 1983; Palanchon et al., 2004; Topper et al., 1993). To avoid errors related to the different bladder filling stages and to reduce device complexity and cost, Palanchon et al. (2004) describes a new approach that uses a limited number of US beams and does not make any assumptions about the bladder shape. From this research, it was shown that it is possible to estimate the bladder volume with just a limited number of US beams with predefined orientations in only one sagittal plane.

The approach described in this study will not make any assumptions about the bladder shape and will further reduce device complexity and cost. It takes advantage of the difference in harmonic properties of liquids (urine) and tissues. We know from literature that US waves undergo different degrees of harmonic distortion depending on the propagation medium, with a strong harmonic generation for propagation through liquids such as water, amniotic fluid or urine. To take advantage of these harmonic differences, echo signals returning from a large distance beyond the posterior wall of an average filled bladder are then analyzed for harmonic contents and compared with an empty bladder. The harmonic content is then correlated to the bladder volume.

2.2 Approach and theory

The approach is based on the differences in nonlinear wave distortion capabilities between urine and surrounding tissue. It is known from available literature that harmonic generation due to nonlinear wave propagation changes with the medium properties, where US waves undergo strong wave distortion in liquids (such as water, amniotic fluid or urine) compared with soft tissue (Duck, 1990). To take advantage of such differences for our purpose, a wide acoustic beam that encloses the entire volume of a full bladder is required. Such a wide beam can be obtained using a single-element transducer with a defocusing lens, for example. The method, as illustrated in Figure 2.1, consists of measuring the harmonic content in the posterior bladder wall and correlating the harmonic content to the fluid present in the propagation path that was responsible for

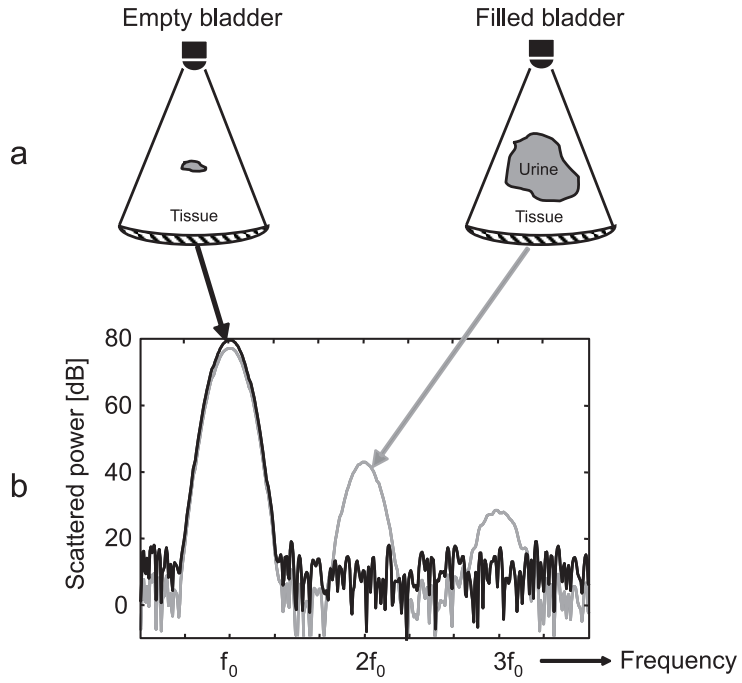

Figure 2.1: A schematic illustration of the principle of the approach

the harmonic generation.

Nonlinear wave distortion has been demonstrated theoretically and experimentally for many years. These nonlinear effects have been predicted and demonstrated at frequencies and intensities used in the diagnostic range either in water or in the human body (Averkiou, 2000). The distortion is due to slight nonlinearities in sound propagation and manifests itself in the frequency domain with the appearance of additional harmonic signals at integer multiples of the original frequency. Acoustic propagation in fluids gives rise to extreme nonlinear effects at diagnostic frequencies (Haran and Cook, 1983). Within soft tissues, nonlinear processes also take place, but are attenuated and modified as a result of different acoustic characteristics, mainly high acoustic absorption. To illustrate the differences in harmonic generation capabilities between urine and tissue, some simple theory is introduced in the following section.

To quantify the harmonic wave distortion, one can calculate the shock formation distance, also known as discontinuity distance σ (Hamilton and Blackstock, 1998). This concept comes from the fact that the waveform progressively steepens as it propagates due to the nonlinearity of the medium; thus, creating shocks or discontinuities in the waveform (Hamilton and Blackstock, 1998).

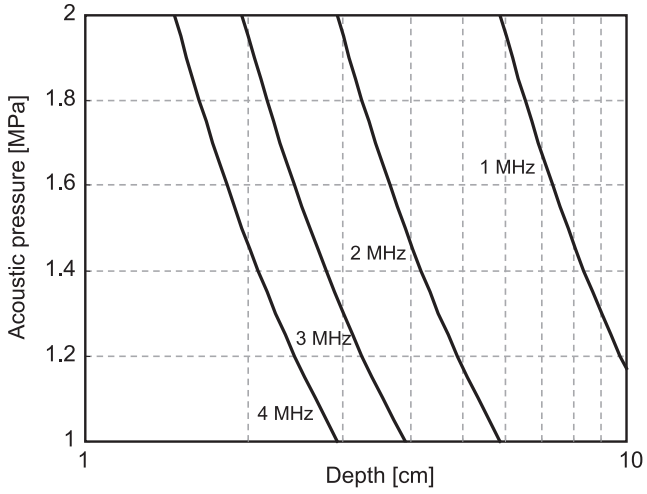

Figure 2.2: Shock formation distance calculated at different acoustic pressures and frequencies for US propagation in urine

Shocks are indicators of the presence of energy at higher harmonic frequencies. This parameter depends on different factors and is given for a plane wave by the expression (Hamilton and Blackstock, 1998):

$$\sigma = \rho c^3 / \beta \omega p \tag{2.1}$$

where ρ and c are the density and propagation speed of the medium, β is the coefficient of nonlinearity, ω is the angular frequency and p is the acoustic pressure. For low values of σ (< 1), the wave has not been distorted enough, whereas $\sigma = 1$ is an important benchmark for the shock formation distance. At this distance, the pressure discontinuity has just formed, the originally sinusoidal wave has distorted enough and the harmonics have grown to nonnegligible proportions. Figure 2.2 displays how the shock formation distance changes with acoustic pressure and frequency. In this calculation, urine was considered as the propagation medium. The density and nonlinearity coefficient were $\rho = 1025$ kg/m^3, $\beta = 4.36$, as given in (Duck, 1990). For the speed of sound, it was calculated by simply approximating urine as a saline mixture of water and salt. This approximation is simple because urine is not composed of a single liquid with standard properties, even though water dominates the constituents. It contains, however, a range of constituents that also can change over time. Based on this simple approach, the speed of sound was calculated using the formula given by Coppens (Duck, 1990) and was found to be 1538.7 m/s at 30°C. From the figure, we see that, for typical diagnostic pressures and frequencies, significant harmonic generation will occur at rather short distances,

especially for higher frequencies and pressures. For example, transmitting a wave at 3-MHz frequency, the shock formation distance is less than 4 cm for an acoustic pressure of 1 MPa and is less than 3 cm if the acoustic pressure is higher than 1.3 MPa. These curves agree with previous statements (Haran and Cook, 1983; Szabo et al., 1999) and demonstrate that significant nonlinearities can occur in urine at diagnostic frequencies and pressures.

In addition to being nonlinear, all the media have acoustical losses due to absorption. The acoustical loss is described by the power law: $\alpha = \alpha_0 f^b$, where α_0 is constant and b ranges from 1 to 2, depending on the medium. For water, the rate of absorption is quadratically related to the frequency ($b = 2$). However, the rate of energy loss due to absorption is considered small and, most of the time, the dissipationless theory is applicable over short ranges for US propagation in water. Biologic media have high rates of energy loss and the frequency dependence has an exponential value of 1 to 1.5. This attenuation is called here ordinary attenuation, to make a distinction with the attenuation due the harmonic energy transfer between the harmonic frequencies, which further attenuates the fundamental frequency component. Again, here, the simple way to consider urine is to assume the same attenuation function as water with the same square law frequency-dependence of attenuation. By considering both attenuation due to absorption loss and nonlinearity, the exchange of energy between the two processes is complicated, because attenuation diminishes the amplitude of the generated harmonic components with propagation distance and nonlinearity builds up these harmonics. Accordingly, harmonic distortion generally tends to enrich the higher harmonic components at the expense of the lower ones (energy transfer), and absorption damps out the higher components more rapidly than the lower ones. One of the parameters that expresses the balance between attenuation and harmonic generation for an US wave is the Gol'dberg number G (Hamilton and Blackstock, 1998), which represents a measure of which likely attenuation or harmonic distortion will prevail. When $G = 1$, nonlinear effects become comparable to attenuation effects. If the Gol'dberg number is higher than 1, nonlinear processes dominate the wave propagation behavior. For values of the Gol'dberg number below 1, attenuation is more significant in governing the amplitude of the harmonic components than the energy transfer due nonlinear distortion. Figure 2.3 shows a diagram that gives the calculated Gol'dberg number of different media: urine, blood, liver, muscle and fat tissue. The Gol'dberg number was calculated at an acoustic pressure of 1 MPa and a transmit frequency of 3 MHz. Both values lie within the diagnostic range. The calculations demonstrate that, for these transmission parameters, only fat has a Gol'dberg number below 1 (0.27). All other media show values greater than 1, of which urine has the highest (104). This is caused primarily by the attenuation, which is very low for urine

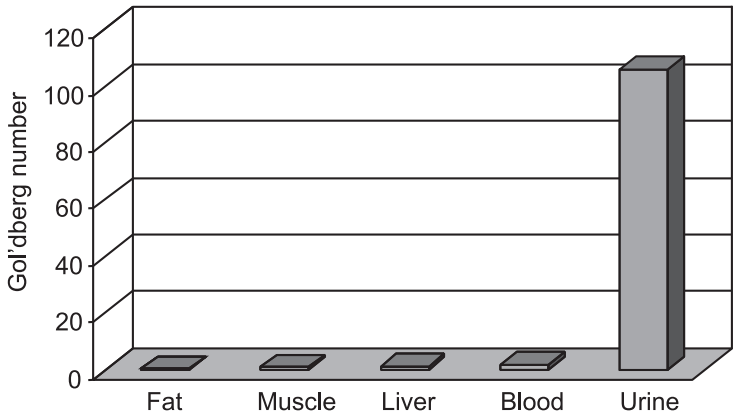

Figure 2.3: Gol'dberg number calculated for different media at a transmit frequency of 3 MHz and acoustic pressure of 1MPa

and very high for fat, although the nonlinearity coefficient of fat is higher than that of urine. These simple calculations demonstrate the difference between different media in causing waveform distortion. Urine has a higher ability to provoke strong nonlinear distortion compared with other body tissues.

To illustrate the differences in harmonic generation ability in a more evident way, simulations of nonlinear wave propagation was carried out in two different propagation media, liver and urine. The simulation considered a single-element transducer focused at 100 mm with an aperture of 30 mm and operating at 3 MHz. The transmit acoustic pressure at the surface was 150 kPa. The simulation model is based on the KZK nonlinear wave equation (Kuznetsov, 1971; Zabolotskaya and Khokhlov, 1969), which is solved in time domain using finite differences (Bouakaz et al., 1999, 2003a). The equation was modified to account for attenuation with a nonquadratic relation with frequency (Bouakaz and de Jong, 2003b). For both media, the attenuation coefficient had the following expression: $\alpha = \alpha_0 f^b$, where $\alpha_0 = 0.42$ dB/cm and $b = 1.1$ for the liver and $\alpha_0 = 0.002$ dB/cm and $b = 2$ for urine, which is the same as for water. Figure 2.4a shows time waveforms after propagation through urine (solid) and in liver tissue (dotted) as calculated at the focus of the transducer, and in Figure 2.4b are given the corresponding frequency spectra rescaled to their respective maximal values. We should recall that these signals correspond to a single ultrasonic line and not to a volume. Because urine induces stronger waveform distortion than the liver, as was predicted by the Gol'dberg number, the time waveform propagated in urine shows clear nonlinear wave distortion as characterized by the asymmetry of the wave, where the positive peak pressure

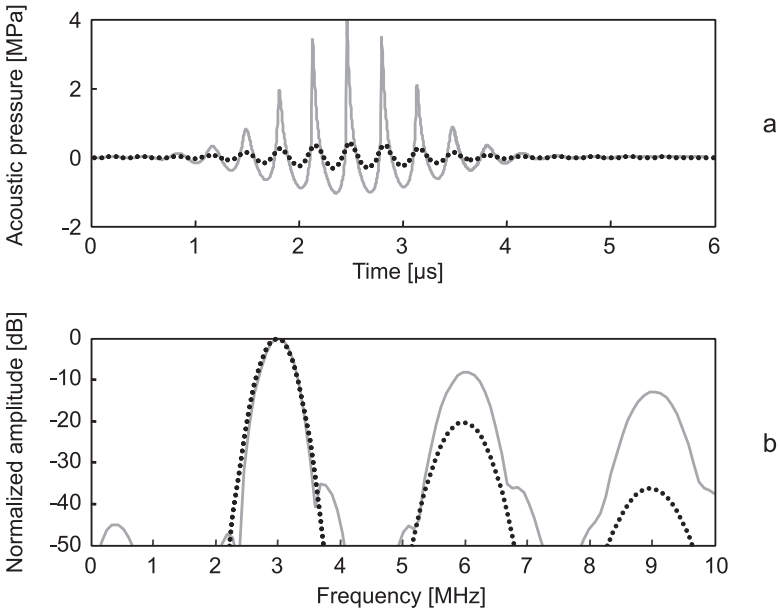

Figure 2.4: (a) Time waveforms as calculated for a single-element transducer (focal depth = 100 mm, excitation pressure 150 kPa, aperture 30 mm) at the focal distance of the transducer after propagation in urine (solid) and tissue (dotted); (b) frequency spectra of the time waveforms

is approximately 3 to 4 times higher than the peak negative pressure. This is confirmed by the frequency spectra, where we see the second harmonic after propagation through urine only 8 dB below the fundamental level, whereas it goes down to 20 dB for propagation in liver tissue. In conclusion, the principal difference between these media is their attenuation coefficients. Urine has a low coefficient and, hence, the distance at which attenuation will dominate the propagation process is too long from an anatomical point of view. On the contrary, tissue presents a higher attenuation coefficient and, therefore, the ordinary attenuation dominates the behavior of the waveform much earlier, prohibiting significant harmonic distortion from occurring.

2.3 Experiments and methods

Two sets of measurements were carried out with the purpose of demonstrating the feasibility of the approach. The first measurement was carried out using a single element focused transducer and the second experiment was performed using a rotating phased-array transducer. Different bladder phantoms (CIRS,

Norfolk, VA) were used in the measurements. The phantoms consisted of a cavity of a liquid surrounded by a tissue-mimicking material. Three phantoms were used with three different volumes: 0 ml, 130 ml and 500 ml.

2.3.1 Single-element transducer

The single-element transducer had an aperture of 14 mm with a center frequency of 5 MHz and was focused at 75 mm. The transmit frequency was set to 2.8 MHz to be able to receive with the same transducer at the second harmonic frequency. The transmitted burst contained 5 cycles and had a peak negative pressure at the focal point of 2.14 MPa, as was measured in water. For such a pressure, the corresponding mechanical index is 1.27, which can be considered within the midrange of mechanical indices used in medical diagnosis. In this experiment, the transducer was positioned on the top side of the bladder phantom and sequential scannings were taken manually over the full width of the phantom at a constant spatial step of 1 cm, making a total of 13 scans over the total width. An ROI at the posterior wall of the fluid cavity was selected from each of the 13 radiofrequency (RF) echoes, and the harmonic content was analyzed. The analyzed depths of the ROI extended over 2 cm.

2.3.2 Phased-array rotating transducer *in vitro*

A fast rotating US transducer dedicated to 3-D echocardiography was used in this experiment (Djoa et al., 2000). The array contained 64 elements with a pitch of 0.21 mm and was tapered into an octagonal shape, approximating a circle with a radius of 7 mm. The center frequency was 3.1 MHz and the fixed focus of the acoustic lens in the elevation direction was 60 mm. The frequency band width was wide enough to permit second harmonic imaging (Voormolen et al., 2002). The transducer was connected to a General Electric-Vingmed Vivid 5 system (Horten, Norway). To create the wide acoustic beam configuration required for volume measurements, the probe was rotated over the target to make 30 scans. The harmonic analysis as performed with EchoMat® (GE-Vingmed) consisted of selecting a ROI over the full width of each 2-D scan and extending from 10 to 12 cm depth. The harmonic content was averaged from all the scans. Different transmit frequencies and numbers of periods were evaluated and the optimal harmonic performance was reached by transmitting a pulse at 2.7 MHz containing 2.5 periods. The measured acoustic pressure in water was 1.25 MPa at the focal distance.

2.3.3 Volunteer measurements

To have more convincing evidence, a harmonic measurement was carried out on a volunteer. The measurement was carried out with the rotating phased-array

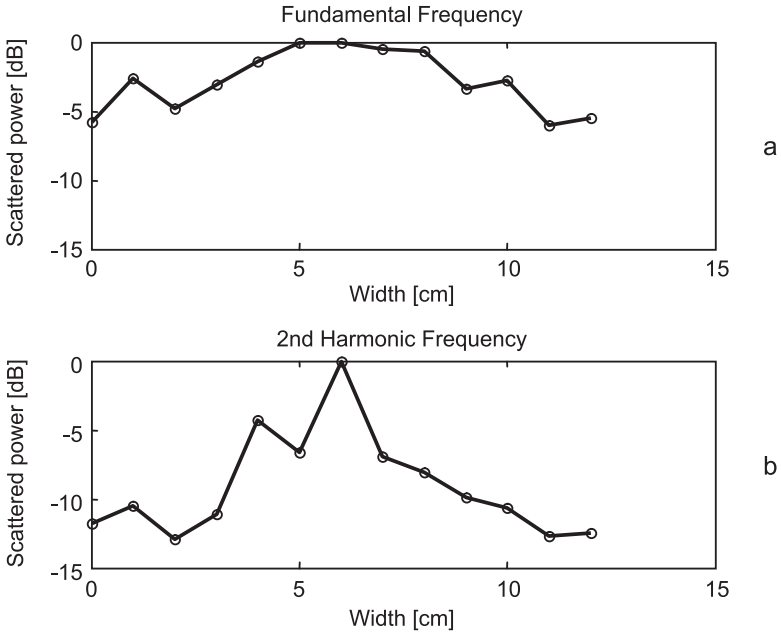

Figure 2.5: (a) Fundamental frequency component as measured across the phantom width at a depth ROI from 8 to 12 cm, (b) second harmonic frequency component as measured across the phantom width in the same region

transducer following the same procedure as described in the previous section. In these measurements, optimal performances were obtained at a transmit frequency of 1.8 MHz with 2.5 periods. The acoustic pressure as measured in water was 0.85 MPa. The selected ROI started at 14 cm depth. It was 2 cm deep and its width was selected over the full 2-D image width.

2.4 Results and discussion

2.4.1 Single-element transducer

These measurements were carried out using the bladder phantom with 130 ml cavity. Spectral analysis was carried out from segments selected from all the RF signals (total 13) and the results are given in Figure 2.5. Figure 2.5a shows the corresponding fundamental frequency components over the width of the bladder phantom. The curve shows maximal power at the fundamental frequency around the center position, which corresponds to propagation through the full cavity path; therefore, ordinary attenuation is less significant. At the

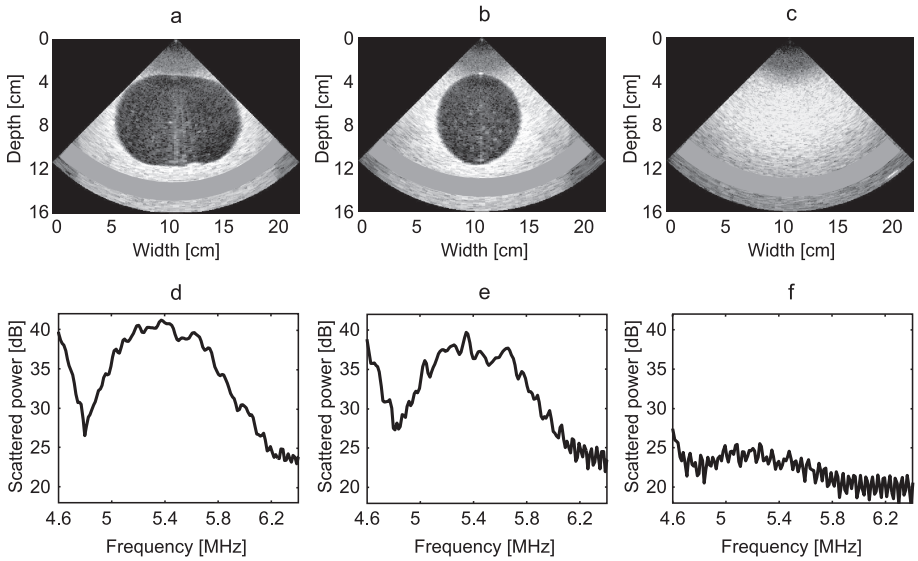

Figure 2.6: B-mode images and frequency spectra as obtained with the rotating phased-array transducer using bladder phantoms. (a) 0°and (b) 90°orientation of the probe with 500-ml cavity phantom; (c) 0°orientation of the probe with no-volume phantom; (d) frequency spectrum of the scattered power around the second harmonic obtained from image in (a), (e) the image in (b), and (f) image in (c).

sides of the phantom where propagation occurs only in tissue, the signal power drops because the attenuation of US waves in the tissue is higher than in the fluid cavity. A wide shape is demonstrated here that corresponds relatively to the width (or diameter) of the fluid cavity. Figure 2.5b shows the same curve at the second harmonic frequency. First, it is noted that the second harmonic power is mainly concentrated or created only in the center where US waves cross the largest path of fluid. When we step aside from the center, the second harmonic generation declines because the liquid path diminishes. At both sides of the phantom, because propagation occurs only in tissue, the creation of the second harmonic power is very limited, due to the high attenuation of tissue. These curves corroborate the theoretical predictions described earlier. The generation of harmonic components (second harmonic) can be correlated to the amount of liquid that is traversed by the US wave, where longer paths give rise to more harmonic generation.

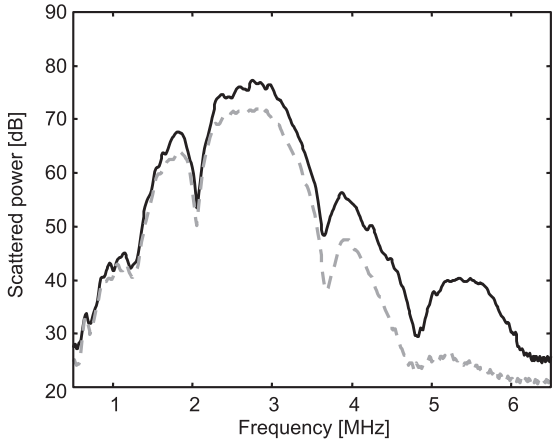

Figure 2.7: Frequency spectra of the scattered power averaged over 30 scans for both 500 ml-volume (solid) and no-volume (dashed) phantoms.

2.4.2 Phased-array rotating transducer *in vitro*

To encompass the full volume of the cavity, measurements with the rotating 3-D probe were carried out. These measurements were performed with the bladder phantom containing a fluid cavity of 500 ml volume and a second phantom containing only tissue (no volume) for comparison. A total of 30 scans were made with each phantom by rotating the probe. In Figure 2.6, the first two images, Figure 2.6a and b, correspond to B-mode images of the phantom cavity taken in two perpendicular planes by rotating the probe (0°and 90°) and the last image, Figure 2.6c, was taken with the tissue phantom only (no volume). From each image, an ROI, as shown by the dashed area, was selected and the corresponding Fourier transforms around the second harmonic frequency were plotted (Figure 2.6d, e and f). The results demonstrate a substantial harmonic scattering difference between the nonvolume frame (Figure 2.6f) and the largest volume-path frame (Figure 2.6d). This observation correlates with the theoretical presumptions where propagation through tissue generates hardly any harmonic components and the presence of liquid (water or urine) through the propagation path provokes significant waveform distortion and, thus, harmonic generation. The difference in this case at the second harmonic frequency is approximately 15 dB. Figure 2.6b, where a slightly smaller volume-path was present due to the different position of the probe, shows also significant second harmonic component (Figure 2.6e), but with less amplitude than in Figure 2.6d. Figure 2.7 shows the frequency spectra averaged over 30 scans for both 500 ml-volume (solid) and no-volume (dashed) phantoms. The averaging was performed to approach the wide beam situation. The ROIs are the same as in

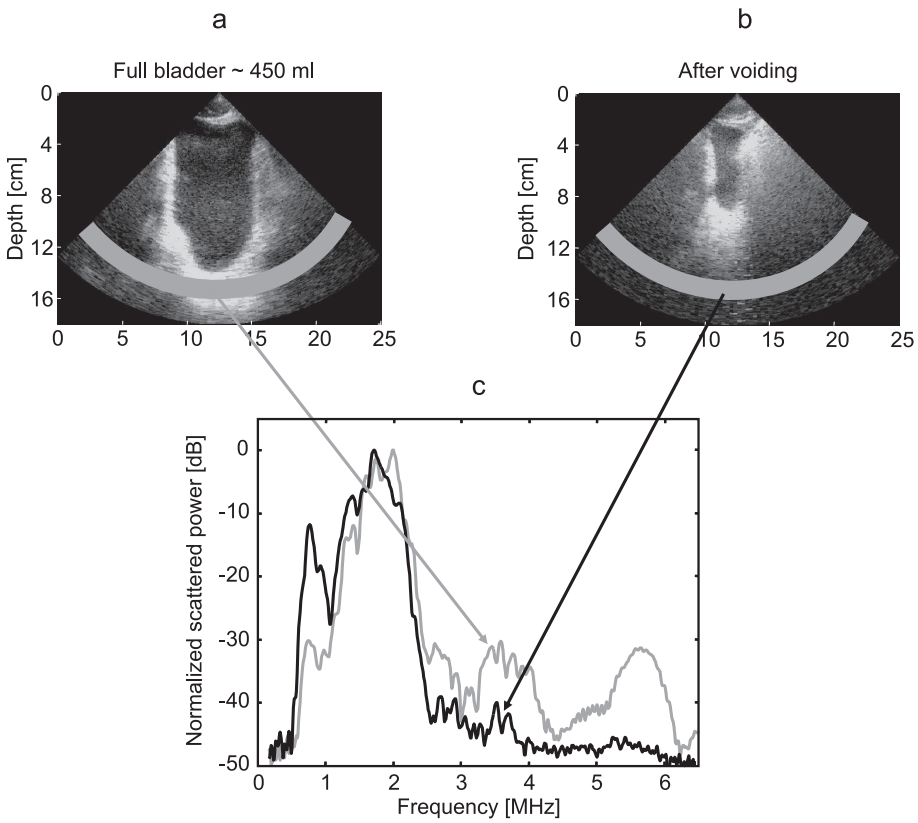

Figure 2.8: Volunteer measurements showing B-mode images of a (a) full bladder, (b) bladder after voiding and (c) corresponding frequency spectra.

Figure 2.6. The curves demonstrate two main differences. The fundamental component of the wave propagation through tissue only has undergone more attenuation than the fundamental component that has propagated through the liquid cavity. The second difference lies in the second harmonic frequency band, where we observe more harmonic generation when the US path contains liquid. The difference in second harmonic energy is more than 14 dB.

2.4.3 Volunteer measurements

Figure 2.8 shows two B-mode images of the volunteer before and after voiding. The volume of urine in Figure 2.8a was estimated to be 450 ml approximately. After voiding, the bladder has not been fully emptied and some urine has been retained (Figure 2.8b). Normalized frequency spectra from the selected ROIs

from the two measurements are given in Figure 2.8c. The full bladder obviously demonstrates harmonic distortion with a significant level of second harmonic component present in the spectrum. The level of the second harmonic is approximately 30 dB below the fundamental level. The spectrum shows also a third harmonic component that is higher than the second harmonic frequency. The third harmonic frequency component was mainly contained in the transmitted signal, rather than created from nonlinear wave distortion. After voiding, the second harmonic energy has decayed by almost 10 dB due mainly to the absence of liquid paths and the presence of supplementary tissue paths, which causes additional ordinary attenuation; therefore, reducing the effects of harmonic distortion. This very preliminary measurement performed on a volunteer demonstrates the feasibility of the approach based on the difference in harmonic behavior of the US wave, depending on the encountered propagation medium.

2.5 Conclusions

Nonlinear wave distortion and, by that, the generation of harmonic components (second and/or higher harmonics) can be used as an indicator of filling of the bladder to a certain volume extent. The criterion can be such that, if a certain amount of second harmonic (or higher harmonics) is detected in the echo signal from a fixed deep ROI, the device would indicate that the critical volume (or threshold) has been reached. In addition, higher harmonics or superharmonics (Bouakaz et al., 2002) can be used to refine the volume indication. Similar measurements can be carried out at low transmit pressure and be used for calibration purposes. To estimate the volume of urine in the bladder, a look-up table can be created beforehand. The table will contain the correspondence between the harmonic energy and the volume of urine. The table can be used to determine the critical second harmonic threshold also. The study presented in this paper is a preliminary study that demonstrates the feasibility of a new method to measure noninvasively a volume of a cavity; the bladder, in this specific case. Therefore, the technique is currently under further investigation to evaluate its potential and drawbacks compared to existing methods. One of the focuses is to estimate the dependency of the method on different cavity shapes and positions. For this method to perform appropriately, the ultrasonic beam needs to encompass the full bladder volume. Therefore, a new transducer with a wide acoustic beam is required. To circumvent this current limitation in our study, the rotating probe was used in the measurements and the 2-D scans made from different angles simulate, to a certain extent, the wide acoustic beam situation. However, a new transducer design with a wide acoustic field is mandatory if the method is to be evaluated. In conclusion, the principle of this approach will allow the use of a simple single wide beam transducer to

encompass and surround the full bladder volume and to limit aiming problems encountered with other ultrasonic methods.

Acknowledgments

Part of this research was sponsored by Diagnostic Ultrasound Europe BV (DxU) Lage Dijk 14, 3401 RG IJsselstein, The Netherlands.

Chapter 3

Transducer Design and Realization

The most important part of an ultrasound system is, without doubt, the transducer that generates and receives ultrasonic waves. In reception, the transducer converts the "ground truth", i.e. the acoustic waves, to electrical signals that are subsequently processed (in the analogue and digital domain), interpreted and displayed. Any noise or distortion that is added with the conversion from the mechanical to the electrical domain reduces the thruth-to-noise ratio and, with this, the ability to correctly interpret and display the result. The phrase *"Garbage in, garbage out"* is at its place here.

The system used with the pilot study consisted of a conventional ultrasound system, adjusted for experimental purposes, and an experimental fast rotating phased array probe developed for 3D harmonic cardiac imaging. This system is clearly too advanced and costly for the intended application. Also, the system was limited to receiving up to the 2^{nd} harmonic, where the influence of the 3^{rd} and higher harmonics on the volume detection is also of interest. This chapter, therefore, describes the design and implementation of a dedicated measurement system. Because of the extreme requirements on sensitivity, bandwidth and beamforming, the main emphasis lies on the design, modeling and implementation of the special ultrasound transducer.

Initially, a first prototype of a dedicated multilayer transducer was realized. It is composed of a PZT transducer for transmission and a PVDF top-layer for reception. The rationale behind the implementation of a multilayer transducer is to separate the transmission characteristics from the reception properties. In doing so, both properties can be separately optimized for the intended application.

To determine feasibility of the multilayer concept for bladder volume measurements, and to ensure optimal performance, an equivalent mathematical model on the basis of KLM-circuit modeling was generated. The obtained results indicated that a valid model for the multilayer transducer was constructed. The model showed feasibility of the multilayer concept for bladder volume measurements. It also allowed for further optimization with respect to electrical matching and transmit waveform.

To make sure that the multilayer concept was the best choice for the application of bladder volume assessment, it was compared with two other concepts, i.e. a broadband piezo-composite transducer and a multi-element transducer. This comparison included the ability to generate sufficiently high pressures at a fundamental frequency and to receive the generated higher harmonics with sufficient signal-to-noise ratio. The effects of an additional acoustic lens on the beamwidth and generated peak pressures were also considered.

This chapter concludes with the design and realization of a new multilayer transducer that overcomes the problems encountered with the first multilayer prototype.

3.1 Transducer realization

Based on:
 Merks E.J.W., Bouakaz A., Bom N., de Jong N., and van der Steen A.F.W. Design of a multilayer transducer for acoustic bladder volume assessment. *IEEE Transactions on Ultrasonics, Ferroelectrics, and Frequency Control*, 53(10):1730–1738, 2006.

3.1.1 Introduction

In several clinical situations it is important to accurately measure bladder volume. Catheterization remains the "gold standard" for bladder volume assessment, but it is invasive, uncomfortable to the patient, and introduces the risk of infections and traumas (Ord et al., 2003). Acoustic measurement of the bladder volume reduces the need for a urinary catheter (Slappendel and Weber, 1999). As a result, noninvasive acoustic bladder volume measurement methods have gained interest. Previously, a new technique to noninvasively measure the bladder volume on the basis of nonlinear ultrasound wave propagation was described (Bouakaz et al., 2004; McMorrow et al., 2002). It is known that nonlinear effects occur most strongly when ultrasound waves propagate through liquids. In tissue, however, acoustic attenuation influences the nonlinear wave propagation, making the nonlinear effects less dominant. The relationship between nonlinearity and attenuation within a medium is reflected in the so-called "Goldberg number" (Bouakaz et al., 2004). When the number is less than 1, the attenuation dominates the nonlinear effect. For values of the Goldberg number higher than 1, the nonlinear effect dominates the attenuation. The Goldberg number of urine (104) is almost 380 times that of soft tissue (0.27) at an acoustic pressure of 1 MPa and a transmit frequency of 3 MHz. This indicates a much stronger nonlinear behavior for urine than for tissue. Given this feature to differentiate between liquid and tissue, it, therefore, should be possible to find a relationship between the amount of generated harmonics present within echoes received from a region of interest (ROI) behind the posterior bladder wall and the amount of liquid present within the propagation path.

Although a precise relationship between bladder volume and the harmonic levels present within a ROI behind the posterior bladder wall was not obtained, it was shown that bladder volume indeed correlates with the harmonic levels generated at the posterior bladder wall. As other ultrasonic techniques calculate the volume from large amounts of data comprising the bladder geometry (Ganguly and Guiliani; Ganguly et al., 1999), this technique, in combination with a diverging acoustic beam wide enough to encompass the whole bladder, requires in principle only one pulse-echo measurement. Initial

measurements (Bouakaz et al., 2004) were performed with a fast rotating, phased-array transducer capable of three-dimensional (3-D) harmonic imaging (Voormolen et al., 2002). As this transducer was too advanced, and thus too expensive for the application discussed here, the use of a single-element, defocused transducer was suggested. This transducer should be capable of generating pressures sufficiently high to induce nonlinear wave propagation, and it should have sufficient spectral bandwidth and sensitivity to receive at least up to the third harmonic component present within the reflected waves.

With conventional transducer design, a trade-off must be made between bandwidth and sensitivity (Zhang et al., 1997). A single-element, broadband transducer with a -6 dB fractional bandwidth between 110% and 120% is needed for transmission at a fundamental frequency and reception up to the third harmonic frequency with sufficient signal bandwidth. With current transducer design, such bandwidths cannot be obtained (Hossack et al., 2000). Although, PZT ceramics show good efficiency, they thus have insufficient bandwidth for the application described here. However, piezoelectric polymers, like PVDF, show outstanding broadband receiving performances due to their low acoustic impedance, but they have poor transmit characteristics due to the low coupling coefficient and high mechanical and electrical losses (Kino, 1987).

A multilayer transducer was constructed by mounting a PVDF layer on top of an unfocused, single-element PZT transducer. Multilayered transducers exhibit several interesting properties (Zhang et al., 1997; Xu et al., 1988; Smith and Dunhill, 1987; Saitoh et al., 1995; Dion et al., 1997). It is possible to electrically separate the piezoelectric layers for transmission and reception. This leads to a simplification of transmit and receive electronics, particularly with respect to electrical tuning. Individual layer properties such as bandwidth and sensitivity can be optimized. Because PVDF has an acoustic impedance much lower than the acoustic impedance of PZT, the mechanical coupling is minimal, and both layers will work almost independently (Lan). Because of its high efficiency, the PZT transducer will be used as a transmitter, and the PVDF layer will be used as a broadband receiver.

In this first approach, an unfocused (flat) transducer was used to test the multilayer principle for the bladder volume assessment method described. To determine the feasibility of the transducer, several acoustical measurements were performed. These included the measurement of the generated acoustic pressures on the transducer axis, and the pulse-echo response with a flat reflector. The transducer also was tested on bladder phantoms to determine the presence of fluid in the sound beam. To make a general statement about the

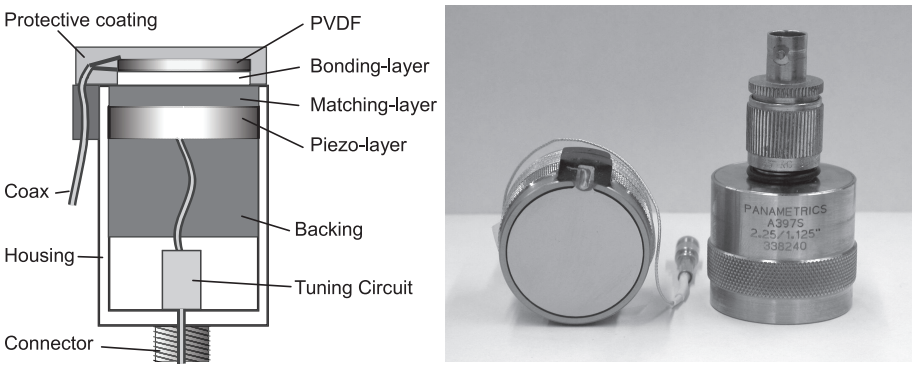

Figure 3.1: The multilayer transducer. Left, Schematic layout. Right, The front view (left) shows the PVDF layer on top of the matching layer of the PZT transducer, as well as the connection between the front electrode and the coaxial cable. An identical PZT transducer without a PVDF layer attached is shown on the right. The piezolayer was connected to the BNC connector at the back of the transducer.

feasibility of the multilayer concept for the bladder volume assessment method, a mathematical model was needed (Lockwood and Foster, 1994). An equivalent mathematical model based on KLM-circuit modeling (Krimholtz et al., 1970) was constructed and validated. The model was used to calculate the transmission and the reception performance of the multilayer transducer.

3.1.2 Materials and methods

Multilayer transducer

A multilayer transducer (Figure 3.1) was constructed using a commercially available, single-element PZT transducer (model A397S, Panametrics-NDT, Waltham, MA) and a PVDF film (Measurement Specialties Inc., Hampton, VA) with a thickness of 52 μm. The PZT transducer has a center frequency of 2.08 MHz and a -6 dB bandwidth of 55%. Both the PZT transducer and the PVDF film have an active diameter of approximately 29 mm.

The PVDF layer was bonded to the matching layer of the PZT transducer using an epoxy. To prevent the electrode from dissolving when the transducer is immersed in water, a protective coating was applied on top of the front-side electrode of the PVDF layer. The electrodes were connected to a thin coaxial cable with a length of 40 cm using a conductive adhesive. The front-side electrode was connected to the common ground of the PZT element for electromagnetic shielding purposes. Except for the common ground, both elements were kept electrically separated.

In this configuration, the PZT transducer will be used for transmission of a narrowband sine wave burst with center frequency of approximately 2 MHz. The PVDF layer will be used for reception of the fundamental frequency up to the third harmonic frequency. The thickness of 52 μm for the PVDF layer was chosen as a compromise between the receive sensitivity, bandwidth, and influence on the transmission characteristics of the PZT transducer. Increasing the PVDF thickness increases the sensitivity, but it lowers the resonance frequency. To obtain a large bandwidth in reception, the PVDF layer should be used away from its resonance frequency. As an unloaded PVDF layer with thickness of 52 μm has a resonance frequency at approximately 21 MHz, which is likely to be lowered due to the mechanical loading of the PZT transducer and the water load, a safe margin with the third harmonic frequency (6 MHz) was obtained. Also, to minimize the influence on the transmission characteristics of the PZT transducer, the PVDF thickness should be kept small. A thickness of 52 μm equals 1/20 of a wavelength at 2 MHz, which can be considered as acoustically invisible to the PZT transducer. Hence, both elements will work almost independently.

Acoustical measurements

To investigate on the capability of the multilayer transducer to generate sufficient acoustic pressures for significant nonlinear wave propagation and the capability of receiving higher harmonics present within the reflected waves, several acoustic measurements were performed. From initial measurements it was found that the PZT transducer exhibited a maximal transmit efficiency at a frequency of 1.9 MHz instead of the given center frequency of 2.08 MHz. Therefore, all acoustic measurements were performed with a Gaussian modulated, 15-cycle sine wave burst with center frequency of 1.9 MHz and -6 dB bandwidth of 15% as transmit waveform. The Gaussian modulation ensures that no higher harmonics were present in the transmitted signal. The waveform was programmed into an arbitrary waveform generator (AWG; model 33220A, Agilent Technologies, Palo Alto, CA). The waveform from the AWG then was amplified with a power amplifier (model A25-25PA, ENI, Rochester, NY). An expander and a passive low-pass filter were used between the power amplifier and the transducer to remove amplifier noise and unwanted frequency components. Data-acquisition was performed with a LeCroy digital oscilloscope (model 9400A, LeCroy Corp., Chestnut Ridge, NY) with sampling frequency of 100 MHz and an 8-bit A-to-D converter. Data were transferred to a computer using a GPIB interface.

1. Axial Pressure Measurements: A calibrated needle hydrophone with an active diameter of 200 μm (Precision Acoustics Ltd., Dorchester, UK) was

used to measure the axial pressures of the PZT transducer in water. The axial pressures generated by the PZT element were measured at drive amplitudes of 60 Vpp and 120 Vpp. The hydrophone was stepped from 2 mm to 180 mm in axial direction away from the transducer surface with step size of 0.5 mm. A total of 30 traces was averaged for each axial position. The recordings then were bandpass filtered to obtain the pressures at the fundamental, second harmonic, and third harmonic frequencies.

2. Pulse-Echo Measurements: Pulse-echo measurements were performed in a water tank with a flat Perspex reflector positioned at 120-mm distance from the transducer surface. The distance was determined to be in the order of the average distance of the posterior bladder wall of patients in the supine position. From these pulse-echo measurements, the receive bandwidth and sensitivity of the PVDF layer were obtained and compared to the pulse-echo response from the PZT transducer. The PVDF responses were measured directly across the 1 MΩ input impedance of the LeCroy oscilloscope. The PZT responses were measured across the BNC-connector of the PZT transducer with a high input impedance probe. The responses were averaged over 30 traces. To observe the change in the level of harmonics, a comparison was made between the responses with a drive amplitude of 60 Vpp and the responses with a drive amplitude of 120 Vpp.

KLM-circuit model

To make a general statement about the usability of the multilayer concept for bladder volume measurements, an equivalent mathematical model on the basis of KLM-circuit modeling was implemented in Matlab (The Mathworks Inc., Natick, MA). The PZT transducer was modeled without PVDF layer attached by means of matching the model with the measured electrical input impedance. The cross correlation between the measured and the simulated pulse-echo responses was used to validate the PZT transducer model. The maximum relative error between the measured and simulated electrical impedance was 9%, which was below the measuring accuracy (12%). The cross correlation between the measured and simulated pulse-echo responses was 0.997. The complete model of the multilayer transducer was obtained by adding the PVDF layer to the model of the PZT transducer. This model then was validated by considering the PVDF layer as a hydrophone on the PZT transducer surface and comparing the measured and simulated PVDF responses of a wave transmitted by the PZT transducer as it propagates from the PZT element through the PVDF layer. To illustrate the close match of the complete equivalent KLM-circuit model, the simulated PVDF response - with water as acoustic load - was compared with the measured response. The broadband transmit pulse (model 33220A, Agilent Technologies) used with this measurement

was first measured across a 50 Ω load using a high-input, impedance probe, then was used as input for the KLM-circuit model. The parameter values used for the complete model are given in Table 3.3 on page 59. The parameters for the electrodes were omitted because of their insignificant influence.

The model also was used to calculate the transmit sensitivity in pascal per volt (Pa/V) of the PZT element and the receive sensitivity in volt per pascal (V/Pa) of the PZT element and the PVDF layer. The PZT and PVDF receive responses - as function of the frequency - were simulated across 50 Ω and 1 MΩ loads, respectively. Simulations were compared with measurements.

In vitro bladder phantom measurements

The multilayer transducer was used in pulse-echo mode on bladder phantoms (Zerdine^{TM}, Computerized Imaging Reference Systems, Inc., Norfolk, VA) to determine whether the transducer is capable of bladder volume assessment. In this setup, the PZT element was used for transmission of the Gaussian modulated waveform previously described with drive level of 120 Vpp. The PVDF layer was used for reception. Before acquisition, the received signals from the PVDF layer were amplified using a Miteq bipolar amplifier (model AU-3A-0110, Miteq, Hauppauge, NY) with a 55 dB gain. B-mode scans were obtained from bladder phantoms with volumes of 133 ml and 500 ml by mechanically moving the transducer in one single plane across the phantom surface with steps of 0.5 mm. At each position 100 radio frequency (RF) traces with a depth of 145 mm were recorded and averaged in the time domain to increase the signal-to-noise ratio (SNR). Only envelope detection was applied for imaging. From each B-mode scan obtained, two ROIs were selected at 120-mm distance from the transducer. The ROIs had a width of 10 mm and a depth of 15 mm. They were selected such that one ROI was preceded with a propagation path through tissue only, and the other has a path through the water-filled cavity. The spectral content within each ROI was calculated as the average of the fast Fourier Transforms (FFTs) of the windowed RF scan lines.

3.1.3 Results

Acoustical measurements

Because the volume measurement technique is based on the generated harmonics due to nonlinear wave propagation, harmonic components in the transmitted signals should be avoided. To determine the spectral contents of the transmitted wave, the PVDF layer was used as a hydrophone to capture the pressure wave that propagated from the PZT element through the PVDF layer. The coaxial cable attached to the PVDF layer was directly connected with the

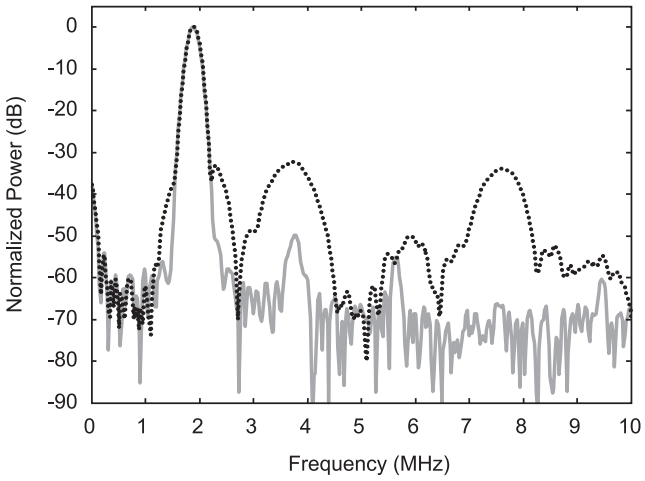

Figure 3.2: Calculated power spectrum of received waveform captured by the PVDF layer as the waveform propagated from the PZT element through the PVDF layer. The dotted line shows the spectrum obtained without filtering. The solid line represents the spectrum when a low-pass filter was applied.

LeCroy oscilloscope with input impedance of 1 MΩ. The power spectrum of the captured waveform is plotted in Figure 3.2. The spectrum (dotted line) clearly shows the presence of higher harmonics, caused by distortions from the power amplifier. To remove these unwanted higher harmonics, a passive ninth order high-power Butterworth low-pass filter with cut-off frequency at 2.5 MHz was used between the power amplifier and the transducer. The spectral results after filtering (solid line) demonstrated the suppression of the transmitted harmonics. The filter was used with all measurements.

From the unfiltered graph it can be seen that the level of the transmitted third harmonic was much lower than for instance the level of the second harmonic. As will be discussed with the model simulations to follow, this was due to the lower transmit efficiency of the PZT element at the third harmonic.

1. Axial Pressure Measurements: The measured peak pressures for three frequency components as a function of axial distance at two different drive amplitudes (i.e., 60 Vpp and 120 Vpp), are shown in Figure 3.3. The axial pressure distributions of the frequency components were normalized to the maximum pressure value of the filtered fundamental component at the particular drive amplitude to demonstrate the difference in harmonic generation. As a result, the distributions of the fundamental frequency components at both drive amplitudes overlap. At the drive amplitude of 120 Vpp, the maximum pressure

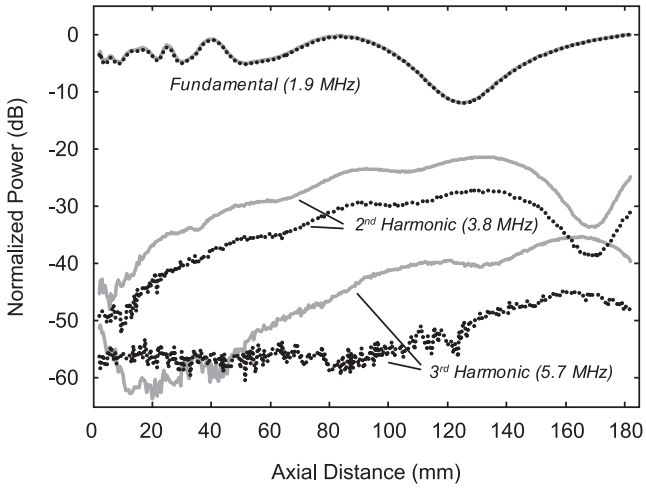

Figure 3.3: Axial pressures measured normalized to the maximum value present within the filtered fundamental component at each drive amplitude. The solid lines represent the spectral components measured at drive amplitude of 120 Vpp. The dotted lines were obtained with drive amplitude of 60 Vpp.

measured in the range of 180 mm from the transducer surface (natural focus at 270 mm) at the fundamental frequency was about 250 kPa at a distance of 82 mm.

The pressures measured close to the transducer surface were 87 kPa and 175 kPa for drive levels of 60 Vpp and 120 Vpp, respectively. This implies linear operation of the transducer. A significant second harmonic component was already visible at the drive amplitude of 60 Vpp. At the drive level of 120 Vpp, both second harmonic and third harmonic components increased significantly. Hence, the transmit efficiency of the multilayer transducer allowed for considerable nonlinear wave propagation in water.

2. Pulse-Echo Measurements: Pulse-echo measurements were performed with the drive amplitudes of 60 Vpp and 120 Vpp using a flat reflector positioned at 120 mm from the transducer surface. To compare the response of the PZT element with the response of the PVDF layer, the backscattered echo was received by both the PZT element and the PVDF layer. Figure 3.4 shows the time waveforms and their normalized power spectra as received by the PVDF layer (black lines) and the PZT element (gray lines). In this case the PZT element was driven with 60 Vpp. Notice the different scaling for the PZT and PVDF time waveforms.

The spectra show that, when normalized to the power level at the funda-

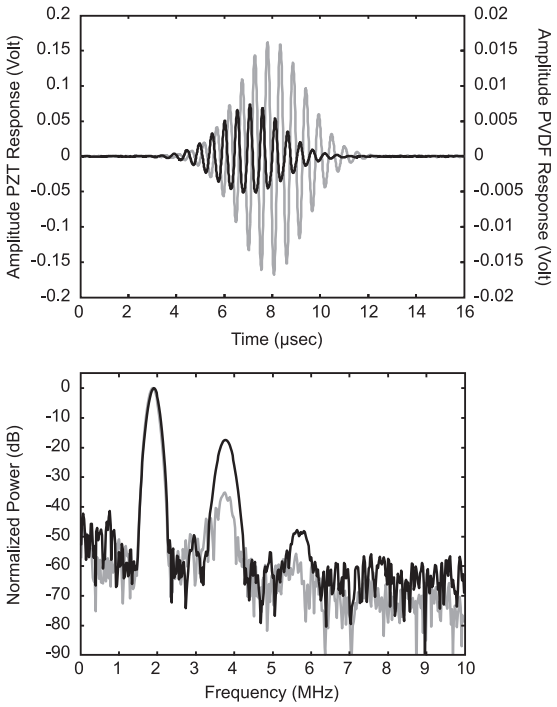

Figure 3.4: Time waveform (top) and normalized power spectra (bottom) of the pulse-echo responses of the PZT element (grey line) and the PVDF layer (black line) using a flat reflector at 120 mm distance from the transducer surface. Transmission with the PZT element was used for transmission of a Gaussian modulated 15-cycle sine wave burst with a center frequency of 1.9 MHz and -6 dB bandwidth of 15% as transmit waveform. The excitation level was 60 Vpp. Notice the different scaling for the PZT and PVDF time waveforms.

mental frequency, the second harmonic level measured with the PVDF layer was only 17 dB below the fundamental level, and the difference between the second harmonic level and the fundamental level measured with the PZT element was 37 dB. The difference between the fundamental level and the level of the third harmonic component measured with the PVDF layer was 48 dB, and this could not be measured with the PZT element. Figure 3.5 shows the pulse-echo responses when the PZT element was driven at 120 Vpp. Clearly, the harmonic levels increased. The response of the PVDF layer even shows the presence of the fourth and fifth harmonics.

With respect to the drive amplitude of 60 Vpp, the differences between the level at the second harmonic and the level at the fundamental frequency decreased with 6 dB with the response of the PVDF layer as well as with the

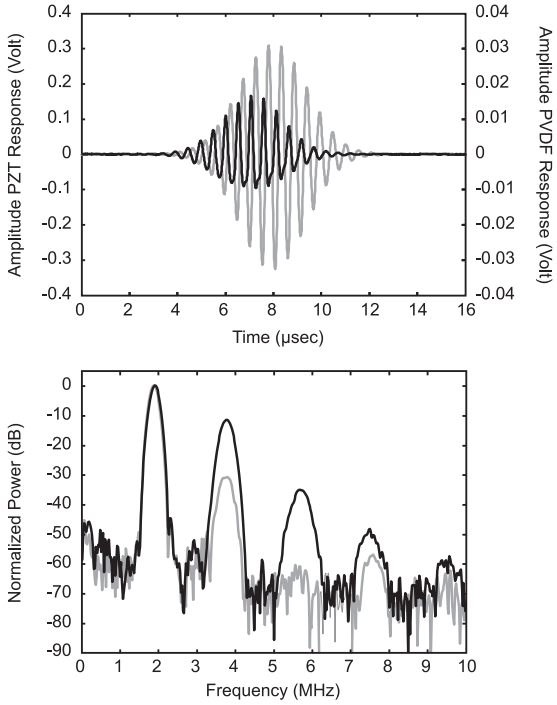

Figure 3.5: Time waveform (top) and normalized power spectra (bottom) of the pulse-echo responses of the PZT element (grey line) and the PVDF layer (black line) using a flat reflector at 120 mm distance from the transducer surface. Transmission was the same as with Figure 3.4, except for an excitation level of 120 Vpp instead of 60 Vpp. Notice the different scaling for the PZT and PVDF time waveforms.

response of the PZT element. The difference at the third harmonic level measured with the PVDF layer decreased with 12 dB, but no change was observed with the response of the PZT element. As expected, it can be concluded that the PVDF layer has a larger receive frequency band compared to the PZT element. From the recorded time waveforms, a time shift of approximately 0.6 μs was noticed between the responses of the PVDF layer and the PZT element. This effect also was observed with model simulations, and it is explained by the PVDF layer being physically closer to the reflector than the PZT element.

KLM-circuit model

The equivalent mathematical model was used to calculate the response of the PVDF layer on a broadband wave transmitted by the PZT-element that propagates from the PZT through the PVDF. Figure 3.6 shows the measured and

Table 3.1: Simulation results on the transmit and the receive sensitivity of the multilayer transducer. Transmission only with the PZT element.

	Transmit		Receive Sensitivity (μV/Pa)		
	Frequency (MHz)	Sensitivity (kPa/V)	Fundam.	2^{nd} Harm.	3^{rd} Harm.
PZT	1.9	2.986	61.6	18.6	2.6
PVDF	1.9	-	2.4	8.6	4.2

simulated time waveforms and corresponding spectra of the PVDF response.

As can be seen, there is a close match between the measurement and the simulation. The spectrum given shows that the PZT-element is able to transmit at the second harmonic (3.8 MHz) with sensitivity of approximately -10 dB below the transmit sensitivity at the fundamental frequency. It also shows a low sensitivity at the third harmonic, which explains for the absence of the third harmonic with the results given in Figure 3.2. This illustrates the importance of filtering the transmit wave from the power amplifier, as previously discussed, and the awareness of the sensitivity of unwanted frequency components during transmission.

The frequency-dependent, transmit sensitivities and the receive sensitivities of the multilayer transducer were simulated. Table 3.1 shows the simulation results. From these results the pulse-echo response could be obtained easily. In transmission as well as in reception, the Gaussian-modulated waveform as previously described - but with the appropriate center frequency - was used.

From the axial pressure measurements, it was found that the pressure at the transducer surface at drive amplitude of 60 Vpp and transmit frequency of 1.9 MHz was measured to be 87 kPa. At a drive amplitude of 120 Vpp, the measured pressure was 175 kPa. From Table 3.1, the calculated acoustic pressures are 90 kPa and 179 kPa at drive amplitudes of 60 Vpp and 120 Vpp, respectively, indicating a close match between measurements and simulations.

The receive sensitivities given in Table 3.1 also explained for the differences between the receive sensitivities of the PZT element and the receive sensitivities of the PVDF layer obtained from the pulse-echo measurements. When the receive sensitivities given in Table 3.1 were normalized to the receive sensitivity at the fundamental frequency, the differences between the PVDF layer and the PZT element were 22.5 dB and 32.4 dB for the second harmonic and third harmonic, respectively. The differences found with the pulse-echo measurements were 22 dB and 35 dB. It must be noted that the relatively low receive sensi-

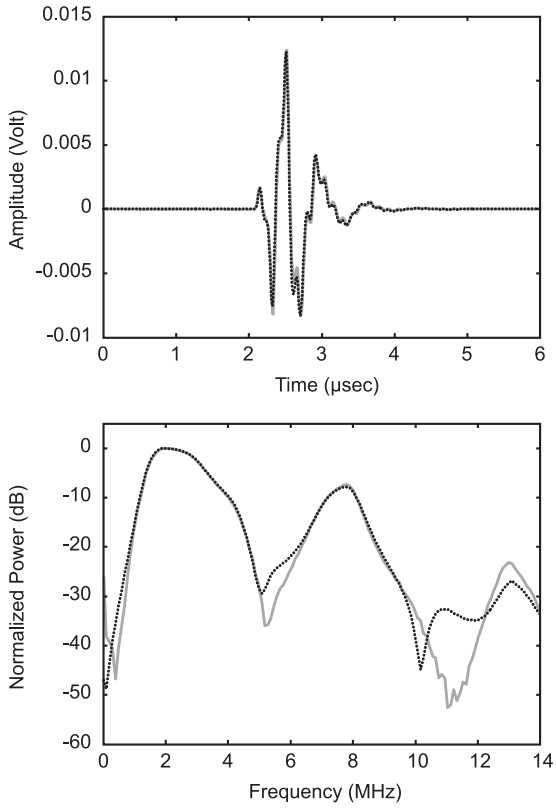

Figure 3.6: Measured (solid lines) and simulated (dashed lines) PVDF responses in water of a wave transmitted by the PZT element as it propagates from the PZT element through the PVDF layer. Top, time waveform. Bottom, spectrum of time waveform.

tivity of the PVDF layer at the fundamental frequency is due to the layered structure of the transducer. This is considered to be advantageous as it reduces the dynamic range needed for the acquisition.

In vitro bladder phantom measurements

B-mode scans were made from bladder phantoms with the Gaussian-modulated transmit waveform previously described and drive amplitude of 120 Vpp. The echoes were received with the PVDF layer. A total of 100 traces with a depth of 145 mm were averaged for each recording to increase the SNR. Figure 3.7 and Figure 3.8 show the B-mode images measured from phantoms containing volumes of 133 ml and 500 ml, respectively. The pulse-echo data shown in

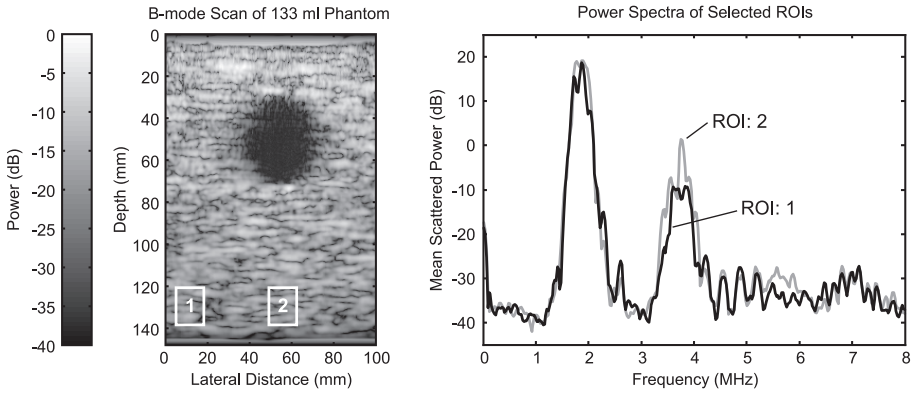

Figure 3.7: B-mode image of unfiltered pulse-echo data (left) and power spectra comparison (right) of selected ROIs measured from a bladder phantom containing a volume of 133 ml.

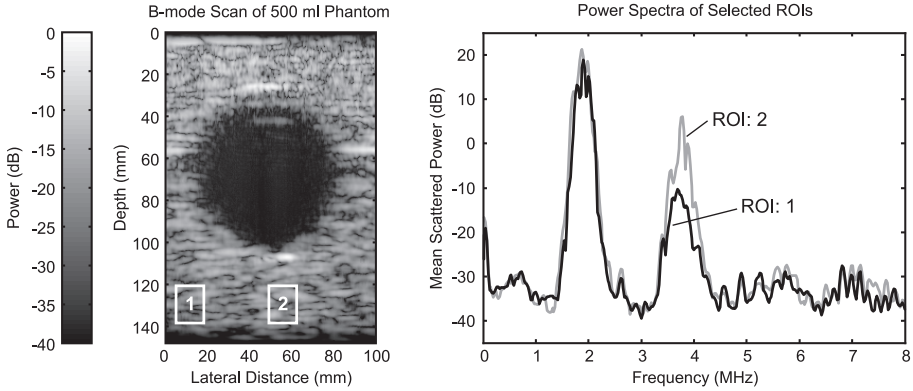

Figure 3.8: B-mode image of unfiltered pulse-echo data (left) and power spectra comparison (right) of selected ROIs measured from a bladder phantom containing a volume of 500 ml.

the B-mode images were unfiltered. Figure 3.7 and Figure 3.8 also show the averaged power spectra of the corresponding ROIs as indicated within the B-mode images. The ROIs were selected at 120-mm distance from the transducer, and had a width of 10 mm and a depth of 15 mm. It is shown that the second harmonic level is higher when a volume is present within the propagation path compared to a path with only tissue. Also, comparing Figure 3.7 and Figure 3.8, it can be concluded that a larger volume corresponds to more generation of second harmonic. Although no third harmonic component was visible, these results demonstrated the principle of measurement as well as the usability of

the multilayer transducer constructed for bladder volume measurements.

3.1.4 Conclusions and discussion

From the acoustical measurements, it can be concluded that the multilayer transducer constructed is capable of transmitting pressures high enough to induce nonlinear wave propagation in water, even though all measurements were performed in the nearfield. In addition, the transducer has sufficient bandwidth and sensitivity in reception. The mathematical model obtained has proven to be a valuable tool in understanding the performance of multilayer transducers. Simulation results closely matched with results from the acoustical measurements. In addition, the model demonstrated the need for a filter at the power amplifier output to remove the unwanted frequency components in the transmitted waves.

B-mode images of bladder phantoms clearly showed an increase of the harmonic levels, especially the second harmonic, in the received echoes from ROIs behind the posterior bladder wall with respect to situations in which only tissue was present within the propagation path. It also showed that a larger volume further increased the level of second harmonic.

The phantom measurements did not show the presence of a third harmonic component. This could be explained by the fact that the induced nonlinear wave propagation was not strong enough to generate a significant third harmonic component. In this case, more acoustic power is required. In addition, the model simulations showed that the PVDF layer has maximal sensitivity at the second harmonic and less sensitivity (-6 dB) at the third harmonic. The lower sensitivity in combination with a limited SNR from the measurement setup could also explain the absence of the third harmonic. The last explanation seems most reasonable, especially with respect to the SNR of the measurement system, when the results of the pulse-echo measurements at drive amplitude of 120 Vpp are considered. Here it was found that the third harmonic level was 35 dB below the fundamental level. However, this was measured in water and with a strong plane reflector. With the phantoms, with randomly distributed reflecting particles and higher frequency dependent attenuation, the third harmonic level will be lower than -35 dB, and possibly even below the maximum obtainable SNR of the measurement setup. Hence, in order to obtain a significant third harmonic level with the multilayer transducer, both the SNR of the measurement setup and the transmitted power need to be increased.

It can be concluded from the phantom measurements that the multilayer transducer constructed allows for determination of the fluid volume in the acoustic beam on the basis of nonlinear wave propagation, which is the concept for noninvasive acoustic bladder volume assessment.

3.2 Transducer modeling

Based on:
 Merks E.J.W., Borsboom J.M.G., Bom N., van der Steen A.F.W., and de Jong N. A KLM-circuit model of a multilayer transducer for bladder volume measurements. *Ultrasonics*, 44 (Suppl. 1):e705–e710, 2006.

3.2.1 Introduction

Initial measurements were performed with a fast rotating phased array transducer capable of 3D harmonic imaging (Voormolen et al., 2002). As this transducer was too advanced for the application, a dedicated multilayer transducer was constructed (Merks et al., 2004). This transducer consists of a PVDF layer mounted on top of an unfocused single element PZT transducer. It was concluded that, when the PZT element is used for transmission and the PVDF layer is used for reception, the transducer is capable of generating pressures sufficiently high to induce nonlinear wave propagation, and has sufficient bandwidth to receive the higher harmonic components present within the reflected waves (Merks et al., 2004). This is in agreement with results from earlier published work (Liu et al., 1999), where it was found that multilayer transducers are useful for applications that require a large bandwidth and good sensitivity at frequencies above 10 MHz. To determine the feasibility of the multilayer concept for the bladder volume measurement technique, which concentrates on frequencies between 1.5 MHz and 8 MHz, to further optimize its design, and to ensure optimal performance, a mathematical model is needed (Lockwood and Foster, 1994). An equivalent KLM-circuit model (Krimholtz et al., 1970) was fitted with data obtained from electrical input impedance measurements and acoustical measurements. The model was also used to observe the effect of mechanical loading of the PVDF layer on the characteristics of the PZT transducer.

3.2.2 Materials and methods

The multilayer transducer constructed (Figure 3.9) consists of a single-element PZT transducer (model A397S, GE Panametrics, USA) and a PVDF film (Measurement Specialties Inc., USA) with a thickness of 52 μm. The PZT transducer has a center frequency of 2.1 MHz and a -6 dB bandwidth of 55%. Both elements have an active diameter of 29 mm.

The PVDF layer was bonded to the matching layer of the PZT transducer using an epoxy. A protective coating was applied to prevent the PVDF-electrode from dissolving when the transducer is immersed in water. The elec-

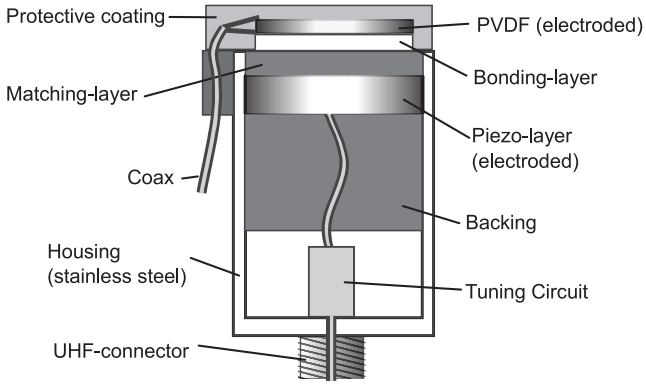

Figure 3.9: Schematic layout of the multilayer transducer. Layer thicknesses are not in scale.

trodes were connected to a thin coaxial cable with length of 40 cm using a conductive adhesive. The front-side electrode was connected to the common ground of the PZT element for EM shielding purposes. Except for the common ground, both elements were kept electrically separated. To make a more general statement about the feasibility of the multilayer concept for the bladder volume assessment method, a mathematical model on the basis of KLM-circuit modeling was implemented in Matlab (The Mathworks Inc., Natick, MA). The model was obtained in two subsequent steps. Firstly, the single element PZT transducer without the PVDF-layer attached was modeled. Secondly, this model was extended with the model of the PVDF-layer. With the use of a graphical user interface (GUI), the model simulations were manually matched with data measured to obtain the initial parameter values to be optimized.

KLM-circuit model of the PZT transducer

Assumptions about the geometry of the PZT transducer were made on the basis of electrical input impedance measurements performed with a vector impedance meter (model 4193A, Hewlett Packard, USA). The electrical impedance was measured with a step size of 50 kHz within the frequency range of 0.4 to 12 MHz. The results shown in Figure 3.10 revealed an electrical tuning circuit consisting of a series and a parallel inductor. The measurements were performed with the transducer held in free air (solid lines) and with the transducer immersed in water (dashed lines). The initially found parameter values were further optimized by matching the electrical impedance calculated with the electrical impedance measured. The Nelder-Mead Simplex method, implemented in Matlab as “fminsearch”, was used to minimize the normalized least-mean-square error (LMSE) with the following cost function:

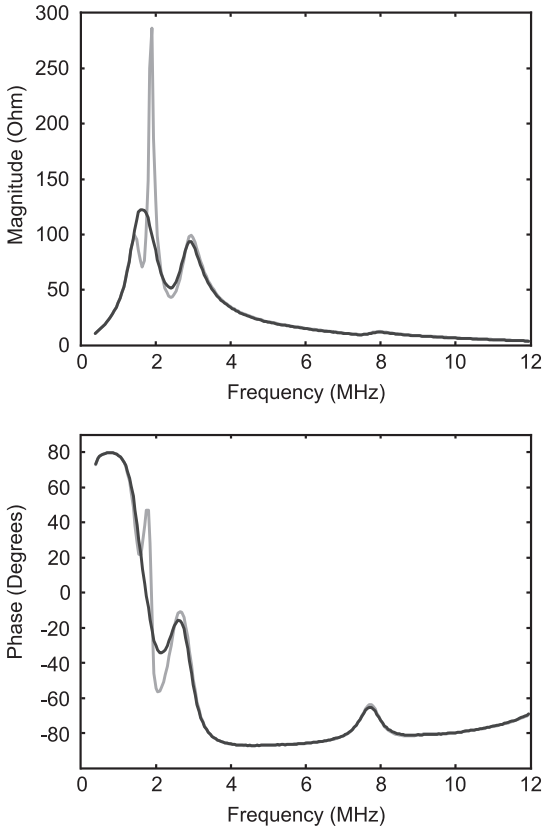

Figure 3.10: Electrical impedance of the PZT transducer measured in free air (gray lines) and in water (black lines). Top: Frequency dependent magnitude. Bottom: Frequency dependent phase.

$$C_{Z\_load} = \frac{1}{N}\sum_{\omega_1}^{\omega_N}\left(\frac{|Z_{elec\_meas}(\omega)| - |Z_{elec\_model}(\omega)|}{|Z_{elec\_meas}(\omega)|}\right)^2\Bigg|_{Z\_load} + \frac{1}{N}\sum_{\omega_1}^{\omega_N}\left(\frac{\theta(Z_{elec\_meas}(\omega)) - \theta(Z_{elec\_model}(\omega))}{\theta(Z_{elec\_meas}(\omega))}\right)^2\Bigg|_{Z\_load} \tag{3.1}$$

$$C_{Total} = C_{Z\_Water} + C_{Z\_Air}$$

where Z_{elec_meas} and Z_{elec_model} are the measured and calculated electrical

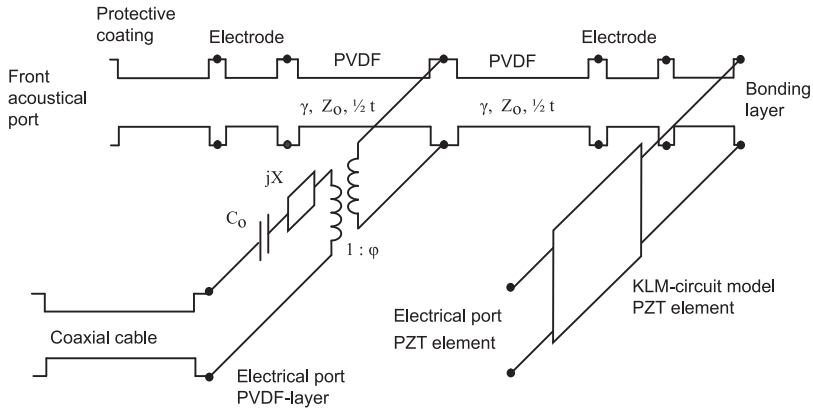

Figure 3.11: The KLM-circuit model used for the multilayer transducer.

impedance, ω the angular frequency (rad/sec) and N is the number of discrete frequencies. This normalized cost function allows for the discrete frequency components to have equal weights and allows for equal optimization of magnitude and phase. The total cost (C_{total}) consists of the sum of costs obtained from observations with water and air as acoustical loads. The cross-correlation between the measured and the simulated pulse-echo responses was used to validate the model. The measurement was performed in water with a flat reflector (Perspex) at 3.5 cm distance. A broadband transmit pulse (Panametrics PR 5052) was used for excitation of the PZT element. It was measured across a 50 Ω load, using a high input impedance probe, such that it could be used as input for the KLM-circuit model.

KLM-circuit model of the multilayer transducer

The complete model of the multilayer transducer was obtained by adding the PVDF-layer, including the bonding-layer, electrodes, coaxial cable and protective coating to the previously found model. Figure 3.12 shows the KLM-circuit model of the multilayer transducer as implemented in Matlab. For simplicity, the PZT element model is represented as a "black box". Because of the high electrical and mechanical losses of PVDF it is difficult to obtain exact parameter values on the basis of electrical impedance matching (Saitoh et al., 1985). However, with the validated PZT model a fully characterized transmitter was obtained. The PVDF-layer was used as a hydrophone being attached to the transducer surface. Its response on a wave transmitted by the PZT element was measured and used to optimize and validate the complete transducer model. Again, the broadband excitation pulse was measured across a 50 Ω load and used as input for the model. The Simplex method was again used to minimize

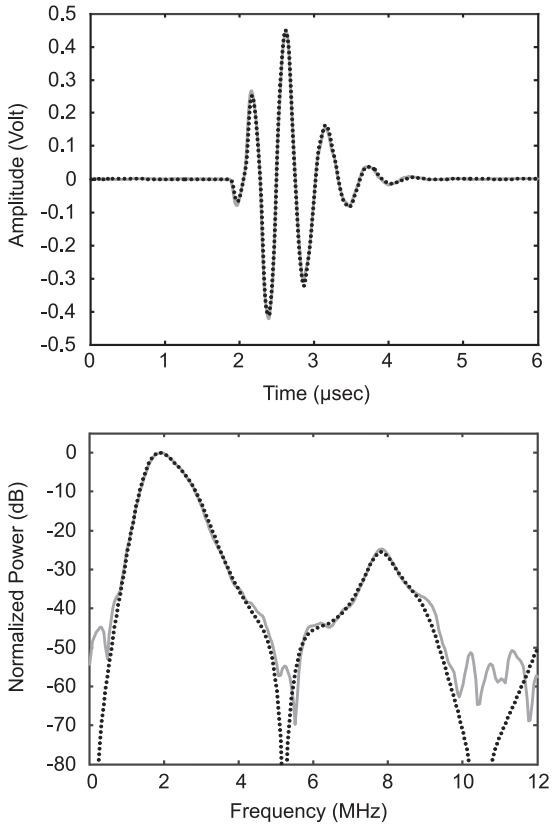

Figure 3.12: The pulse-echo response measured (solid line) and the pulse-echo response calculated (dotted line) of the PZT element in water with a flat reflector at 3.5 cm distance. Top: Time waveforms. Bottom: The corresponding frequency spectra.

the LMSE between the measured and calculated time waveforms. It must be noted that the electrical and the mechanical losses of the PVDF-layer are frequency dependent (Brown and Carlson, 1989). As these losses were difficult to determine correctly, all PVDF parameters were assumed to be frequency independent.

Transducer evaluation

With the model obtained, the transducer behavior and properties were investigated. The effect of mechanical loading of the PVDF-layer on the characteristics of the PZT element was considered. The model was used, with and

Table 3.2: Comparison between the measured and simulated pulse echo responses of the PZT transducer.

	Measurement results	Simulation results
Min. Insertion Loss	16.84 dB	16.73 dB
Frequency at min. Insertion Loss	1.904 MHz	1.904 MHz
Centre frequency	2.075 MHz	2.075 MHz
-6 dB Bandwidth	54.12%	54.12%

without the PVDF-layer, to calculate the transmit sensitivity and the pulse-echo response. Also, the receive sensitivities of both the PZT-element and the PVDF-layer were calculated.

3.2.3 Results

KLM-circuit model for the PZT transducer

From manually matching the simulated electrical impedance to the measured electrical impedance, it was found that PZT-2 best fitted as ceramic material. It was also found that the elements used in the tuning circuit showed some internal resistance. Within the frequency range of interest, the electrode parameters had insignificant influence on the optimization process, and were therefore omitted from the model. Eventually, the model of the PZT transducer contained 17 parameters of which 8 related to the piezoelectric material. Six of these piezoelectric parameters were found from literature (Kino, 1987) and were kept fixed, leaving 11 parameters to be optimized. The electrical impedance matching for the PZT element gave a LMSE of $8.5\text{x}10^{-4}$ (Eq. 3.1). The maximum relative errors found where 9.2% and 3.6% for phase and magnitude respectively. These values are within the accuracy specifications of the HP 4193A (11.8% and 6.3%). Figure 3.13 shows the measured pulse-echo response and the calculated pulse echo response with a flat reflector at 3.5 cm distance. The cross-correlation between both time waveforms is 0.997.

From the comparison between the measured and simulated pulse echo responses (Table 3.2) and from the similarities within Figure 3.12 it can be concluded that the model for the PZT transducer is valid.

KLM-circuit model of the multilayer transducer

The found parameter values for the multilayer transducer after optimization are given in Table 3.3. Figure 3.13 shows the measured and simulated PVDF-responses in air. The cross-correlation between the measured and calculated

Table 3.3: The found parameter values for the KLM-circuit model of the multilayer transducer.
*Values were obtained from Measurement Specialties Inc.
**Values were obtained from Appendix B in (Kino, 1987)

Layer	Material property	Value
Protective coating	Thickness	29.0 μm
	Velocity	2140 m/s
	Density	1075 kg/m^3
	Loss	6.10 dB/(MHz.cm)
PVDF	Diameter	29.2 mm
	Thickness*	52 μm
	Longitudinal velocity*	2210 m/s
	Density*	1780 kg/m^3
	Coupling coeff. (k_t)	0.10
	ϵ_{33}^S *	12
	Mechanical loss	0.17
	Dielectric loss	0.36
Bonding layer	Thickness	18.0 μm
	Velocity	2197 m/s
	Density	1045 kg/m^3
	Loss	5.34 dB/(MHz.cm)
Matching layer	Thickness	0.293 mm
	Velocity	2346 m/s
	Density	1834 kg/m^3
	Loss	6.96 dB/(MHz.cm)
PZT-2	Diameter	27.9 mm
	Thickness	0.844 mm
	Longitudinal velocity**	4410 m/s
	Density**	7600 kg/m^3
	Coupling coeff. (k_t)**	0.51
	ϵ_{33}^S **	260
	Mechanical Q**	680
	Dielectric Q**	200
Backing	Acoustic Impedance	13.9 MRayl
Electrical tuning	Parallel Impedance	1.8+3.6x10^{-6}j$\omega\Omega$
PZT-element	Series Impedance	0.3+3.6x10^{-8}j$\omega\Omega$

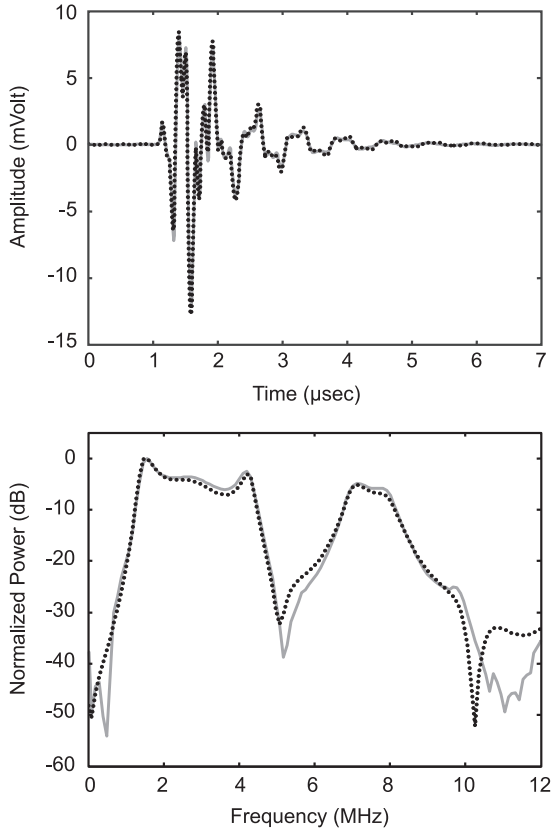

Figure 3.13: The measured (solid lines) and the simulated (dashed lines) PVDF-responses with air as acoustic load. Top: Time waveform. Bottom: The corresponding frequency spectra.

PVDF-responses was 0.988. The results with water as acoustic load were equally satisfying. Hence, the model closely matched with the measurements.

Transducer evaluation

The validated KLM-circuit model allowed for evaluation of the performance of the multilayer transducer constructed. Firstly, the effect of mechanical loading of the additional PVDF layer on the PZT element was observed. Figure 3.14 shows the simulation results of the transmit sensitivity of the PZT element with and without the PVDF layer attached. When no PVDF is attached, the model gave a maximum transmit efficiency of 3.8 kPa/V at a frequency of 1.9 MHz. When the PVDF-layer is present, a maximum transmit efficiency of 3.2

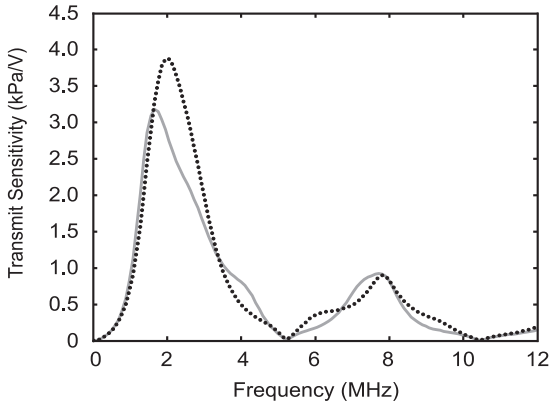

Figure 3.14: Simulated transmit sensitivity (kPa/V) of the PZT-element with (solid line) and without (dotted line) PVDF-layer attached.

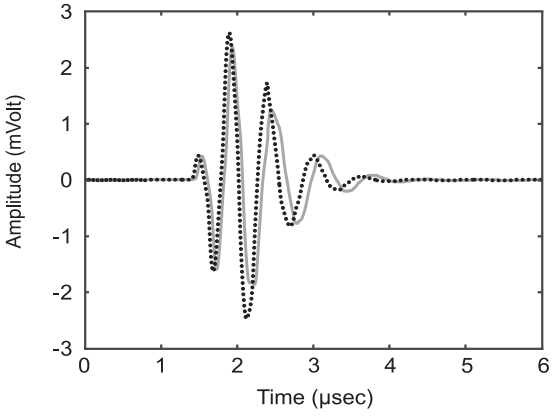

Figure 3.15: Time waveforms of the simulated pulse-echo response of the PZT-element with (solid line) and without (dotted line) PVDF-layer attached.

Table 3.4: Simulation results on the transmit and the receive sensitivity of the multilayer transducer. Transmission only with the PZT element.

	Transmit		Receive Sensitivity (μV/Pa)		
	Frequency (MHz)	Sensitivity (kPa/V)	Fundam.	2^{nd} Harm.	3^{rd} Harm.
PZT	1.7	3.157	65.0	25.4	2.4
	1.9	2.986	61.6	18.6	2.6
PVDF	1.7	-	1.4	7.1	2.9
	1.9	-	2.4	8.6	4.2

kPa/V at a frequency of 1.7 MHz was found. Figure 3.15 shows the effect of mechanical loading on the pulse-echo response of the PZT transducer. The response with PVDF attached shows a small time delay (0.05 μs). Also, the amplitude of the response is less than when no PVDF is present.

Secondly, a comparison was made (Table 3.4) between the transmit frequency used (1.9 MHz) and the calculated optimal transmit frequency previously found (1.7 MHz). Although the highest transmit sensitivity is at 1.7 MHz, 1.9 MHz is preferred because of the higher receive sensitivity.

3.2.4 Discussion and conclusions

A valid model of the multilayer transducer on the basis of KLM-circuit modeling was obtained. The model has proven to be a valuable tool in understanding the performance of the multilayer transducer and observing the effect of mechanical loading of the additional PVDF layer on the PZT element. Optimization using the Simplex method was very sensitive to initial parameter values due to the large amount of parameters used and their interdependency. Further, model accuracy, especially with respect to PVDF, can be improved by incorporating the frequency dependency of the loss factors. With the use of the model, the correct electrical matching circuit and the optimal transmit wave can be calculated. Further, design changes to improve on transducer performance can be easily interpreted.

3.3 Transducer concepts

Based on:
 Merks E.J.W., Lancée C.T., Bom N., van der Steen A.F.W., and de Jong N. Comparison of three different transducer concepts for acoustic bladder volume measurements. *IEEE Ultrasonics Symposium Proceedings*, 4: 2239–2242, 2005.

3.3.1 Introduction

In the previous chapter a new technique to noninvasively measure the bladder volume on the basis of nonlinear ultrasound wave propagation was described (Bouakaz et al., 2004). It uses the medium-specific relationship between the nonlinearity and the attenuation of the acoustic wave propagation, reflected in the so-called "Gol'dberg number" (Bouakaz et al., 2004), to differentiate between urine and tissue. Given a much stronger nonlinear behavior for urine than for tissue, it should be possible to find a relationship between the amount of generated harmonics present within echoes received from a Region of Interest (ROI) behind the posterior bladder wall and the amount of urine present within the propagation path (Figure 3.16). A dedicated transducer is needed to implement this approach. Therefore, the objective of this study is to design an optimal transducer with respect to the transmission and reception sensitivity and beamforming.

Three different transducer concepts were mutually compared using calibrated hydrophone measurements and pulse-echo measurements. As a design criterion, the transmit sensitivity at fundamental frequency should be such that the generated second harmonic peak pressure due to non-linear propagation in

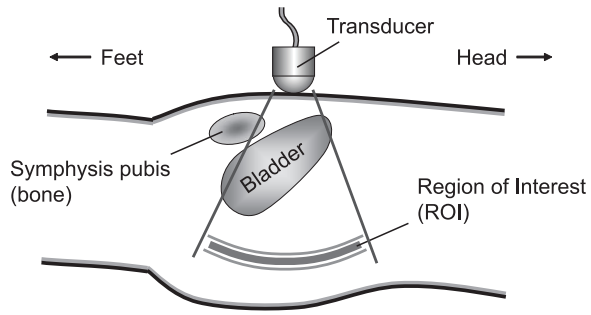

Figure 3.16: Set-up for bladder volume measurements on the basis of nonlinear wave propagation.

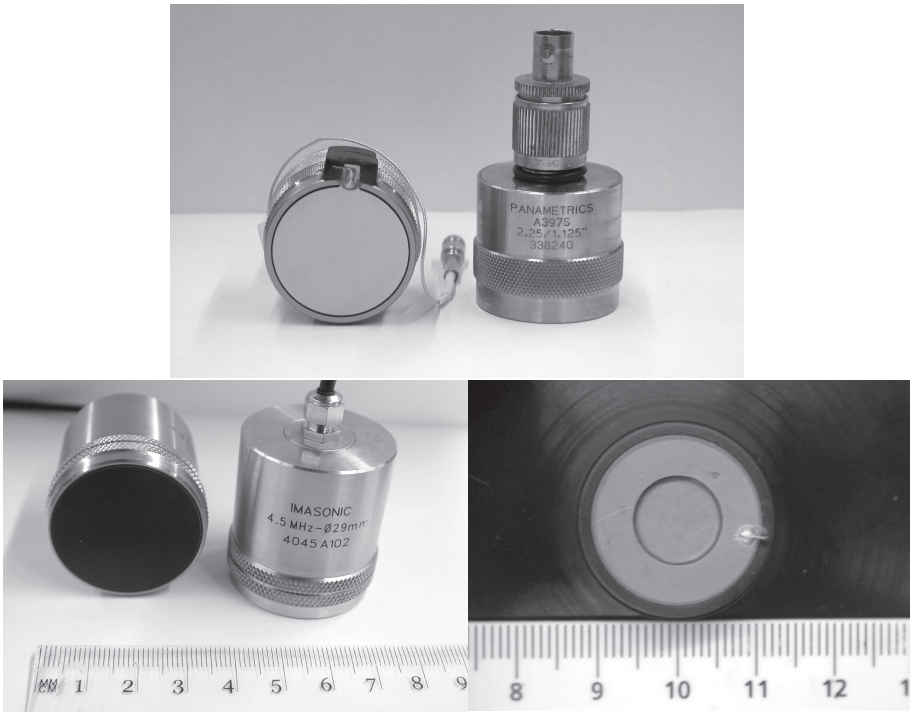

Figure 3.17: The three different transducer concepts. A multilayer transducer (top), a piezo-composite transducer (left) and a multi-element transducer(right).

water is at least 40 kPa at an axial distance of 120 mm. Further, the -6 dB beamwidth at 120 mm should be at least 60 mm to capture a large part of the bladder. With respect to the beamforming, the ultrasound field should be as homogeneous as possible to avoid weighting of the volume due to the field directivity.

3.3.2 Materials and methods

Three different transducer concepts were compared (Figure 3.17):

1. An unfocused multilayer transducer (Merks et al., 2006b) with active diameter of 29 mm, using a single element PZT-transducer (model A397S, GE Panametrics, USA), with 2 MHz center frequency and -6 dB BW of 55%, for transmission, and a 52 μm thick PVDF top-layer (Measurement Specialties Inc., USA) for reception.

2. An unfocused broadband single element 1-3 piezo-composite transducer

(Imasonic, Besançon, France) with active diameter of 29 mm, designed for optimal transmission at 2.25 MHz and reception of the fundamental, second and third harmonics with fractional bandwidths of 10%.

3. An unfocused multi-element transducer consisting of an air-backed PZT ring-element (PXE 5, Morgan Electro Ceramics B.V., the Netherlands) with outer radius of 10 mm and inner radius of 5 mm for transmission at 2.2 MHz, and a broadband unfocused PZT inner-element with active radius of 5 mm for reception (4.5 MHz center frequency, -6 dB BW: 61%).

All three concepts were mutually compared using calibrated hydrophone measurements in water. The measurements were performed, with and without an additional acoustic lens made of Rexolite (Goodfellow Cambridge Ltd., UK) with a radius of curvature (ROC) of 35 mm. This lens is used to obtain a diverging acoustic beam (Figure 3.16). The lens material properties are given in Table 3.5. Pulse-echo measurements on a bladder test phantom were performed, without the acoustic lens attached, to compare the reception sensitivities.

All transducers were excited with a Gaussian modulated 15-cycle sinewave burst with center frequency equal to that of the transducer concept under investigation. To be able to compare the transmit sensitivities, the drive level was set at 200 Vpp. To avoid the presence of harmonic components in the transmitted signal, a passive 9^{th} order Butterworth low-pass filter with cut-off frequency of 2.5 MHz was used between the transducer and the used power amplifier.

Calibrated hydrophone measurements

Calibrated hydrophone measurements were performed in water using a needle hydrophone with active diameter of 200 μm (Precision Acoustics Ltd., UK) to measure the lateral pressure distributions at an axial distance of 120 mm. A total lateral distance of 160 mm was scanned with step size of 2 mm. The hydrophone measurements were performed with and without the additional

Table 3.5: Lens material (Rexolite) properties obtained from literature and measurements. *Obtained from Wang et al. (1999)

	Density (g/cm^3)	Sound speed (m/s)	Acoust.imp. (MRayl)	Transm. coeff.	Acoust.loss (dB/MHz/mm)
Literature*	1.06	2340	2.57	-	0.0367
Measured	1.05	2225	2.33	0.95	0.0370

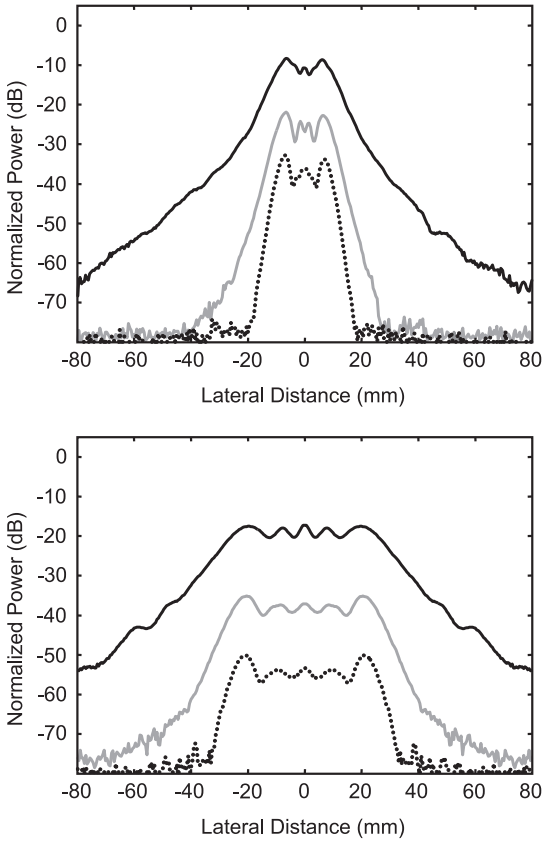

Figure 3.18: Measured lateral pressure distributions, at axial distance of 120 mm, representable for the first two transducer concepts, without (top) and with (bottom) acoustic lens (with ROC of 35 mm) applied. The black lines represent the distributions for the fundamental frequency. The gray and dotted lines represent the distributions for the 2^{nd} and 3^{rd} harmonics, respectively.

acoustic lens to observe the effects on the lateral beamwidth and generated peak pressures. Data-acquisition was performed with a digital oscilloscope (LeCroy model 9400A, LeCroy Corp., USA) with sampling frequency of 100 MHz and an 8-bit A-to-D converter. Data were transferred to a PC using a GPIB interface. A total of 30 RF-traces were averaged for each recording. The recordings were then band-pass filtered at the fundamental, the 2^{nd} harmonic and 3^{rd} harmonic frequencies. The maximum values of these bandpass-filtered signals were plotted to obtain the lateral pressure distributions for each of the frequency components.

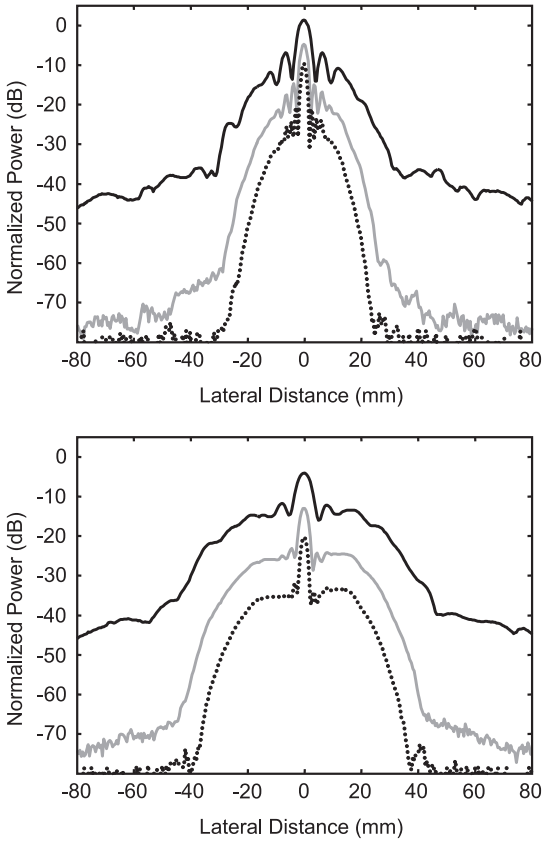

Figure 3.19: Measured lateral pressure distributions, at axial distance of 120 mm, for the multi-element transducer concept, without (top) and with (bottom) acoustic lens (with ROC of 35 mm) applied. The black lines represent the distributions for the fundamental frequency. The gray and dotted lines represent the distributions for the 2^{nd} and 3^{rd} harmonics, respectively.

Pulse-echo measurements on a bladder test phantom

Pulse-echo measurements were performed on a bladder test phantom to compare the receive sensitivities of the three concepts. B-mode images were obtained by mechanically moving the transducers, without the lens, across the phantom with a step size of 2 mm. The same excitation was used as with the hydrophone measurements. Data-acquisition was now performed with a PC oscilloscope (Handyscope 3, Tiepie Engineering, the Netherlands) with sampling frequency of 50 MHz and a 12-bit A-to-D converter. Data were transferred to a PC using a USB 2.0 interface. A total of 100 RF-traces were now averaged for

Table 3.6: Results of the calibrated hydrophone measurements, without acoustic lens applied.

	Fundam. (MPa)	2^{nd} Harm. (kPa)	3^{rd} Harm. (kPa)	-6 dB Beamwidth (mm)
Multilayer	0.39	77	20	26
Composite	0.36	70	20	23
Multi-element	1.14	570	330	5.5

Table 3.7: Results of the calibrated hydrophone measurements, with acoustic lens applied.

	Fundam. (MPa)	2^{nd} Harm. (kPa)	3^{rd} Harm. (kPa)	-6 dB Beamwidth (mm)
Multilayer	0.17	22	4	62
Composite	0.13	16	3	59
Multi-element	0.62	225	95	6.8

each recording, and band-pass filtered at the fundamental, the 2^{nd} harmonic and 3^{rd} harmonic frequencies. The envelopes of these bandpass-filtered signals were then plotted as B-mode images for each frequency component.

3.3.3 Results

Calibrated hydrophone measurements

The results of the hydrophone measurements in water are shown in Figure 3.18 and Figure 3.19. The plots are normalized to a pressure of 1 MPa. As the multilayer and the composite transducers showed similar pressure distributions, only the results of the piezo-composite transducer are shown in Figure 3.18.

A summary on the measured peak pressures and lateral beamwidths is given in Table 3.6 and Table 3.7. The multi-element transducer clearly generates the highest pressures, but has a very narrow -6 dB beamwidth, even with an acoustic lens applied. The design requirement of 60 mm is met when the -20 dB beamwidth is considered. However, the large on-axis sensitivity, which is typical for a concentric ring element, introduces an unwanted weighting of the volume present within the beam. The -6 dB beamwidth increased from 25 mm to 60 mm when the acoustic lens was applied on the first two concepts. The fundamental and second harmonic pressures decreased with 8 dB and 13 dB, respectively, for both transducers. Unlike with the multi-element transducer,

the pressure distributions obtained with these concepts are homogeneous.

Pulse-echo measurements on a bladder test phantom

Figure 3.20 show the B-mode images obtained from the bladder phantom. In this case the acoustic lens was not applied. All concepts allow for 2^{nd} harmonic imaging with sufficient SNR. The multi-element transducer also allows for 3^{rd} harmonic imaging and shows better lateral resolution due to the narrow beamwidth (see Figure 3.19). The images clearly show the presence of harmonics behind the cavity and the absence of harmonics when no cavity is present, illustrating the principle of the new volume measurement technique.

3.3.4 Conclusions and discussion

The results showed that the multi-element concept has the best transmission and reception sensitivity. However, even with an acoustic lens, it has a very narrow -6 dB beamwidth, which is typical for a concentric ring transducer. Although the -20 dB beamwidth is sufficient, an unwanted strong on-axis sensitivity is present. Also, its relatively small active area should be put in perspective with the other concepts. Therefore, the multi-element concept with a concentric ring element is not favorable for bladder volume measurements. The other two concepts do meet the beamwidth requirements. From the B-mode images, the piezo-composite transducer showed to have excellent sensitivity in reception. In transmission however, it is the least sensitive of the three concepts. The multilayer concept performs slightly better in transmission than the piezo-composite transducer, but the PVDF-layer reception sensitivity is relatively low and suffers from electronic noise. The design of the multilayer concept does allow for significant improvements in the transmission and the reception sensitivity, and is therefore preferred for bladder volume measurements above the other two concepts.

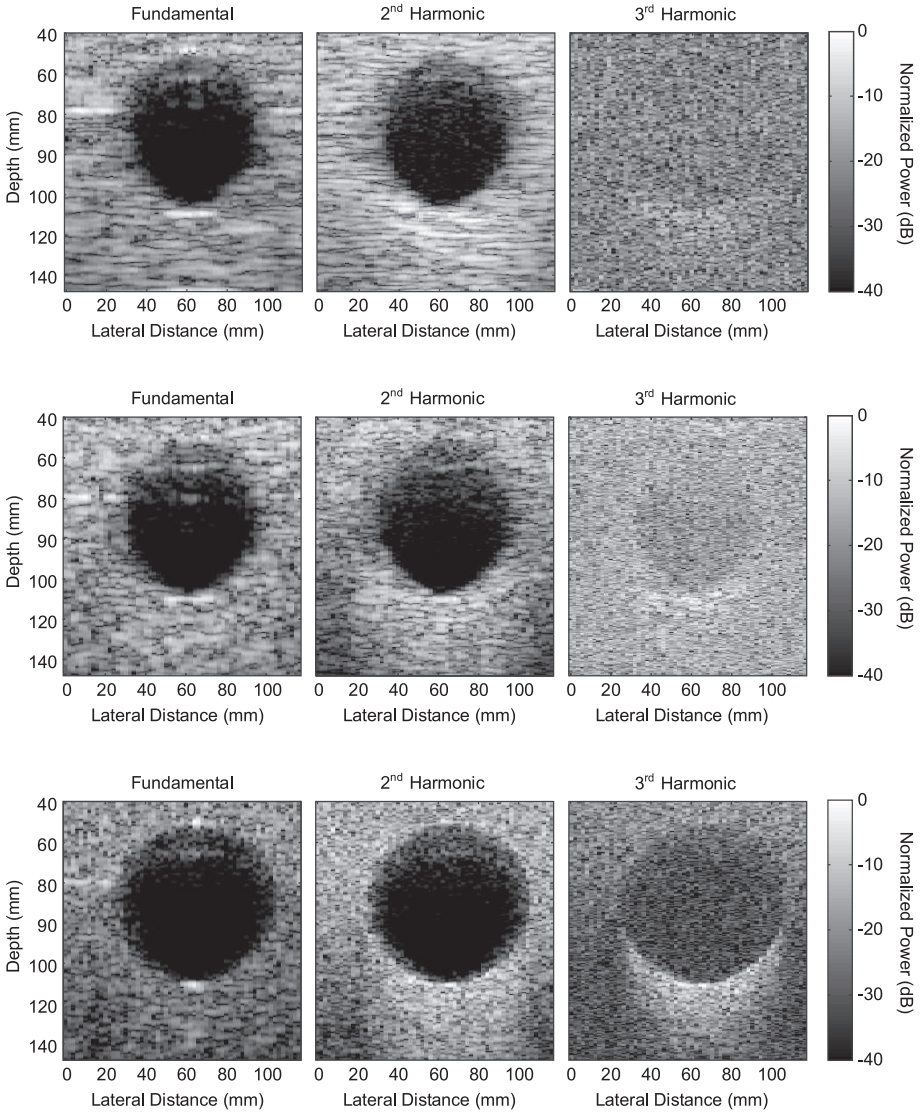

Figure 3.20: B-Mode images obtained from mechanically moving the transducer, without the acoustic lens applied, across a bladder phantom with volume of 500 ml, with step size of 2 mm. The acquired data were filtered to obtain images at the fundamental, 2^{nd} harmonic and 3^{rd} harmonic frequencies. Top: Multilayer; Middle: Piezo-composite; Bottom: Multi-element.

3.4 Inverted multilayer transducer (IMT)

Based on:
 Merks E.J.W., van Neer P., Bom N., van der Steen A.F.W., and de Jong N. Multilayer transducer for acoustic bladder volume assessment on the basis of nonlinear wave propagation. *Ultrasound in Medicine & Biology*, Accepted for publication, 2009.

3.4.1 Introduction and literature

In several clinical situations it is important to accurately measure bladder volume. Catheterization remains the gold standard for bladder volume assessment, but it is invasive, uncomfortable to the patient, and introduces the risk of infections and traumas (Ord et al., 2003). Acoustic measurement of the bladder volume reduces the need for a urinary catheter (Slappendel and Weber, 1999; Hubert et al., 1998). As a result, noninvasive acoustic bladder volume measurement methods have gained interest within the last ten years. Because of the introduction of dedicated devices such as the BladderScan (Verathon Inc., Bothell, WA, USA), acoustic bladder volume measurements have become relatively easy and are valued more and more. These devices are as accurate as urinary catheterization and have proven to be important in clinical practice.

Recently, a new method for acoustic bladder volume assessment on the basis of nonlinear wave propagation has been introduced (Bouakaz et al., 2004; McMorrow et al., 2002). It uses the medium-specific relationship between the nonlinearity and the attenuation of the acoustic wave propagation, reflected in the so-called "Gol'dberg number" (Γ) (Bouakaz et al., 2004), to differentiate between urine and tissue. Given a much stronger nonlinear behavior for urine ($\Gamma = 104$) than for tissue ($\Gamma = 0.27$), the amount of generated harmonics present within echoes received from a Region of Interest (ROI) behind the posterior bladder wall and the amount of urine present within the propagation path are highly correlated. The method uses a single element transducer with a diverging acoustic beam to capture the entire bladder (Figure 3.21). In this way, the bladder volume can be estimated with only one pulse-echo acquisition. This new method is different from the devices currently available because it is instantaneous, and, because of its simplicity and low cost, is especially suitable for miniaturization and thus monitoring purposes and private use.

For this method a dedicated transducer is needed that has sufficient transmit sensitivity at the fundamental frequency ($\sim$2 MHz) to induce significant nonlinear wave propagation, and has sufficient receive sensitivity

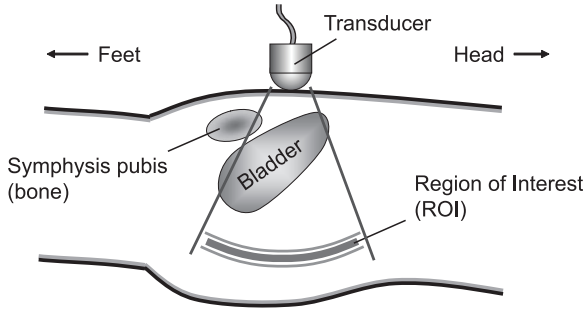

Figure 3.21: Set-up for bladder volume measurements on the basis of nonlinear wave propagation.

and spectral bandwidth to measure up to the 3^{rd} harmonic frequency with sufficient signal bandwidth (1 MHz - 8 MHz). This frequency range was chosen as a trade-off between the volume measurement accuracy and the systems' capability of measuring the acoustic signals with sufficient signal-to-noise ratio (SNR). The 3^{rd} harmonic needs more time to build up to measurable levels and is attenuated more than the 2^{nd} harmonic component. Because the 3^{rd} harmonic is more sensitive to loss, i.e. the amount of tissue in the propagation path, it is also more sensitive to liquid volume variations. The 3^{rd} harmonic is therefore preferred over the 2^{nd} harmonic for volume estimation when the SNR of the pulse-echo data suffices. When the SNR at the 3^{rd} harmonic frequency is too low, the 2^{nd} harmonic is used instead. In practice, this means that larger volumes can be measured more accurately than smaller volumes. The same reasoning can be used for the 4^{th} and higher harmonics, but these higher harmonics are extremely difficult to measure due to the limited SNR. Therefore, the cut-off was set at the 3^{rd} harmonic.

To obtain this dedicated transducer, three different transducer concepts, i.e. a multilayer transducer, a broadband piezo-composite transducer and a multi-element transducer, were compared (Merks et al., 2005). The multilayer transducer concept was previously introduced and its feasibility for bladder volume assessment was proven (Merks et al., 2006a,b). It consisted of a commercially available lead zirconate titanate (PZT) transducer for transmission, including backing and matching layer. A polyvinylidene flouride (PVDF) film was attached on top of the matching layer for broadband reception. The broadband single-element piezo-composite transducer was custom designed for transmission at the fundamental frequency and reception of the fundamental, second and third harmonic frequencies. The multi-element transducer consisted of an air-backed PZT ring-element for transmission and a broadband PZT inner-

element for reception.

It must be noted that the mutual orientation of the transducer and the bladder walls affects the magnitude of the received signals. The signal magnitude is also affected by the different pressure distributions from the different receive frequencies. To reduce these effects a diverging acoustic beam was proposed, which could be created by application of an acoustic lens to the transducer surface.

The multi-element transducer had the highest transmit and receive sensitivity. However, applying an acoustic lens to the multi-element transducer resulted in a large on-axis sensitivity, which is typical for a concentric ring element. This nonuniform acoustic beam would introduce an unwanted weighting of the volume present within the beam. Uniform pressure distributions were obtained with the other two concepts. The multilayer concept and the piezo-composite transducer where therefore preferred (Merks et al., 2005). However, the application of the acoustic lens does not generate a beam wide enough to encompass a full bladder. Hence, in the current setup, the bladder is manually scanned in search of the maximum harmonic-to-fundamental ratio to approximate the true bladder volume.

The multilayer concept had higher transmit sensitivity at the fundamental frequency (1.9 MHz) than the piezo-composite transducer, but the receive sensitivity was relatively low. Additionally, the PVDF film suffered from a high ElectroMagnetic Susceptibility (EMS), i.e. the sensitivity for electromagnetic distortion, which is inherent to the high electrical impedance and broadband characteristics of the PVDF. Hence, to obtain a sufficient SNR, averaging of at least 100 RF traces was required for each measurement. However, in contrast to the piezo-composite transducer, the design of the multilayer concept allowed for significant improvement with respect to sensitivity and noise behavior. Hence, the multilayer concept was preferred for bladder volume measurements above the other two concepts (Merks et al., 2005).

This paper describes the further development of the multilayer transducer concept. To improve on the SNR in reception and to improve on the transmit sensitivity, a new multilayer transducer concept was developed and built. Measurements have been performed to obtain the transmit transfer function, the receive transfer function, the pulse-echo response and the EMS characteristics. The same measurements were performed with a new realization of the old multilayer concept and a broadband piezo-composite transducer for comparison.

3.4.2 Materials and method

An inverted multilayer transducer was built and compared to a previously developed multilayer transducer and a commercially available piezo-composite transducer.

Inverted multilayer transducer concept

The design of the inverted multilayer design is shown in Figure 3.22a. It consisted of a 1 mm thick PZT disc (PXE 5, Morgan Electro Ceramics B.V., the Netherlands) stacked with a 100 μm thick Copolymer film (Precision Acoustics Ltd., Dorchester, UK). Conductive adhesive (Emerson and Cuming, Westerlo, Belgium) was used for bonding the two piezoelectric layers and for ensuring the common ground. The complete stack had a diameter of 20 mm and was mounted in a stainless steel housing. Air-backing was used to achieve the highest transmit sensitivity possible without considering bandwidth requirements. An acoustic matching layer was applied for the acoustic impedance mismatch between the PZT element and water. The PZT element will be used for the transmission of acoustic waves at the fundamental frequency (2.1 MHz) and the copolymer film will be used for the broadband reception of waves at the fundamental up to the 3^{rd} harmonic frequency including sufficient signal bandwidth (1 MHz - 8 MHz). As this geometry resembles an 'inverted' geometry of a previously developed transducer (as will be described next), it will be referred to as the "Inverted Multilayer (IM-)transducer" throughout this paper.

Normal multilayer transducer concept

A second multilayer transducer was built based on a previously developed concept (Merks et al., 2006a,b). It had the same PZT and copolymer layers as the IM-transducer, but it had the copolymer layer mounted on the outside (Figure 3.22b). A protective polyurethane coating was applied to protect the copolymer gold electrode. Again air-backing was used, but no matching layer was applied as the acoustic impedance of the copolymer film was already close to that of water. This transducer will be referred to as the "Normal Multilayer (NM-)transducer."

Piezo-composite transducer

The third transducer used was an unfocused broadband piezo-composite single element transducer (Vermon, Tours, France) with center frequency of 2.4 MHz, -6 dB bandwidth of 85% (as obtained from pulse-echo measurements) and an active diameter of 25 mm.

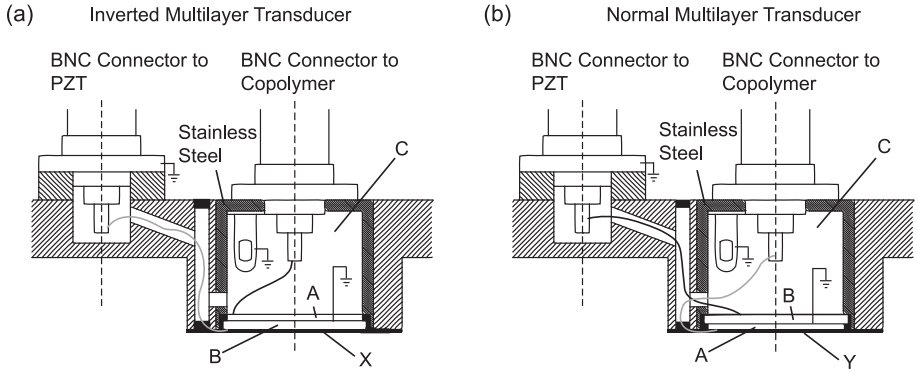

Figure 3.22: Schematics of an inverted multilayer transducer concept (a) and a normal multilayer transducer concept (b). The schematics show the copolymer layer for broadband reception (A), the PZT element for transmission (B), and the air-backing (C). The inverted multilayer transducer has a matching layer (X) and the normal multilayer transducer has a protective coating (Y). Separate BNC connectors are used for both active elements.

Transfer functions

The transmit transfer functions in pascal per volt (Pa/V) and the receive transfer functions in volt per pascal (V/Pa) of the IM-transducer, NM-transducer and the piezo-composite transducer were measured. The transfer functions were calculated by using the methods described in van Neer et al. (2007). For the multilayer transducers, only the transmit transfer functions of the PZT elements were measured. Accordingly, only the receive transfer functions of the copolymer layers were obtained.

The transducer transmit transfer function ($T_{trans}(\omega)$) is defined as (van Neer et al., 2007):

$$T_{trans}(\omega) = \frac{|p_0(\omega)|}{|V_T(\omega)|}, \tag{3.2}$$

where $V_T(\omega)$ is the voltage over the transducer clamps and $p_0(\omega)$ the pressure produced at the transducer surface. To obtain the transmit transfer functions, acoustic measurements with a calibrated hydrophone (Precision Acoustics Ltd., Dorchester, UK, active diameter: 200 μm) were performed. The experimental setup (Figure 3.23a) consisted of a tank filled with saturated water and with the transducer under investigation mounted in the sidewall. The hydrophone was mounted in a holder and controlled by a custom built xyz-system. An

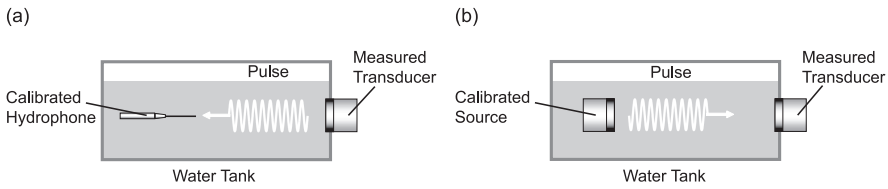

Figure 3.23: Experimental setup used to obtain the transfer functions. A calibrated hydrophone was used to obtain the transmit transfer function (a). A calibrated source was used to obtain the receive transfer function (b).

arbitrary waveform generator (model 33250A, Agilent, Loveland, Colorado, USA) was used to drive the transmitting transducer with 300-cycle sine wave bursts. The waveform generator was controlled by a computer via a general purpose interface bus (GPIB) connection to generate a frequency sweep from 1 MHz till 8 MHz with steps of 50 kHz. The output pressures were kept below 20 kPa at the transducer surface such that nonlinear wave propagation could be neglected. The signals received by the hydrophone were digitized by a digitizer card (DP235, Acqiris, Geneva, Switzerland). In agreement with the method described in van Neer et al. (2007), the hydrophone transfer function was taken into account. The transmitting elements of both multilayer transducers were electronically tuned with a series inductor of 2.7 μH to increase the transmit efficiency. The piezo-composite transducer was electronically tuned by the manufacturer.

The receive transfer function ($T_{rec}(\omega)$) is defined as (van Neer et al., 2007):

$$T_{rec}(\omega) = \frac{|V_{T-open}(\omega)|}{|P_a(\omega)|}, \tag{3.3}$$

with $V_{T-open}(\omega)$ the open circuit voltage produced by the transducer and $P_a(\omega)$ the received pressure averaged across the transducer surface. To obtain the receive transfer functions, direct receive measurements with a calibrated acoustic source were performed. A similar setup as previously described was used where the hydrophone was replaced by a single element transducer (model V310, Panametrics, Waltham, MA, USA) with center frequency of 2.25 MHz and active diameter of 6.35 mm (Figure 3.23b). Again, 300-cycle sine wave bursts were used for transmission and output pressures were kept low. The transducer under investigation was used as a receiver and the received signals were digitized with the digitizer card. Again, the transducers were electronically tuned.

Electromagnetic susceptibility

The electromagnetic susceptibility (EMS) of the IM-transducer, the NM-transducer and the piezo-composite transducer were measured. To mimic *in vivo* measurement conditions with the transducer applied to the abdominal wall, the transducers were placed against the palm of a hand using gel for acoustical and electrical coupling. The transducers were used in reception only. The signals were amplified with a broadband amplifier (model AU-1519-10289, Miteq Inc., Hauppauge, NY, USA) with about 60 dB signal gain and frequency bandwidth of 1 MHz - 300 MHz. Data-acquisition was performed with a PC oscilloscope (Handyscope 3, Tiepie Engineering, the Netherlands) with sampling frequency of 50 MHz and 12-bit resolution. Data were transferred to a PC using a USB 2.0 interface. A low-pass filter with cutoff frequency at 22 MHz together with 20 dB attenuation was used between the amplifier and the oscilloscope to avoid aliasing and clipping. As a reference, the EMS of the complete acquisition system, without a load attached, was also measured.

Additionally, *in vitro* measurements were performed in a controlled setup. The three transducers were immersed in a water tank filled with tap water and were placed within 4 cm from each other. To ensure identical measurement conditions, the transducer responses were measured within 30 seconds. The measurement system was identical to the one used with the *in vivo* EMS measurements, but without 20 dB attenuation.

In vitro pulse-echo measurements

To obtain the responses to a bandwidth limited acoustic wave, two different pulse-echo measurements were performed with all three transducers. Measurements were performed in a water tank with a flat reflector at 2.7 cm distance. Another set of pulse-echo measurements was performed on a 500 ml bladder phantom (Zerdine^{TM}, Computerized Imaging Reference Systems, Inc., Norfolk, VA, USA). The PZT elements of the multilayer transducers and the piezo-composite transducer were excited with a Gaussian modulated 15-cycle sine wave burst with centre frequency of 2.1 MHz and -6 dB bandwidth of 17%. A drive amplitude of 160 Volt peak-to-peak, resulting in peak pressures of approximately 800 kPa at the transducer surface for all three transducers, was used to induce strong nonlinear wave propagation. To prevent the transducers from transmitting harmonic frequency components, a passive 9^{th} order high-power Butterworth low-pass filter with cut-off frequency at 2.5 MHz was used (Merks et al., 2006b) between the power amplifier (model 150A-100B, Amplifier Research, EMV Benelux B.V., the Netherlands) and the transmitting elements. A high-impedance probe (1 MOhm, 1:10) was used to measure the copolymer and the piezo-composite responses. The transmitting elements of both multilayer transducers were electronically tuned with a series

inductor of 2.7 μH to increase the transmit efficiency. The piezo-composite transducer was electronically tuned by the manufacturer.

With the phantom measurements, an 8^{th} order low-pass Bessel filter with cut-off frequency of 12.5 MHz was used before digitalization. A custom built pre-amplifier with high-impedance input (2 kOhm) and 24 dB signal gain was used to measure the copolymer responses. With the piezo-composite transducer, a limiter-configuration, i.e. a series 50 Ohm resistor with a pair of anti-parallel diodes placed parallel to the receive circuitry, was used to protect the receiving pre-amplifier (model AU-1519-10289, Miteq Inc., Hauppauge, NY, USA). Attenuation of 40 dB was used to prevent the amplifier from clipping, leading to a net signal gain of 20 dB for the piezo-composite transducer.

3.4.3 Results

Transfer functions

The transmit transfer functions obtained for the piezo-composite transducer and the PZT elements of the IM-transducer and NM-transducer are shown in Figure 3.24a. The transmit transfer function of the IM-transducer had a centre frequency of 2.1 MHz and -6 dB bandwidth of 73%. The transmit sensitivity at 2.1 MHz was measured to be 9.4 kPa/V. The transmit transfer function of the NM-transducer had a centre frequency of 2.2 MHz, a -6 dB bandwidth of 87% and a transmit sensitivity of 7.3 kPa/V at 2.1 MHz. The piezo-composite had the highest transmit sensitivity of the three transducers at 2.1 MHz (11.4 kPa/V). Its transmit transfer function had a centre frequency of 2.4 MHz and -6 dB bandwidth of 83%, which is in agreement with the specifications given previously. From these results the NM-transducer thus had the largest -6 dB bandwidth. However, from Figure 3.24a, it can be seen that the transmit transfer function of the NM-transducer actually had two high-sensitivity peaks at 1.7 MHz and 2.7 MHz, with -6 dB bandwidths of 24% and 16%, respectively. This indicates that it is not possible to use the full 87% bandwidth in transmission without distorting the transmitted waves.

The measured receive transfer functions of the piezo-composite transducer and the copolymer films of the IM-transducer and NM-transducer are shown in Figure 3.24b. The IM-transducer and the NM-transducer had comparable receive sensitivity at the 2^{nd} harmonic frequency (15.4 μV/Pa), but the IM-transducer had much better sensitivity at the 3^{rd} harmonic frequency (13.2 μV/Pa). The transfer function of the IM-transducer also showed a moderate filtering at the fundamental frequency as the receive sensitivity at 2.1 MHz was measured to be 7.8 μV/Pa. This is advantageous to the dynamic range of the acquisition system, and enables measuring

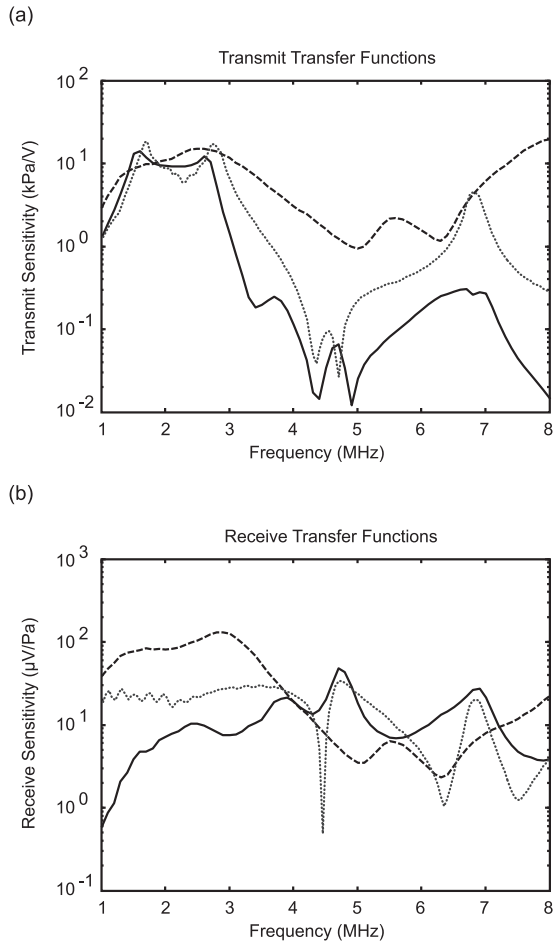

Figure 3.24: Transmit transfer functions (a) and Receive transfer functions (b) obtained for the IM-transducer (solid lines), the NM-transducer (dotted lines) and the piezo-composite transducer (dashed lines).

the fundamental frequency as well as the higher harmonics with sufficient SNR.

The transfer function of the NM-transducer showed sharp low-sensitivity peaks near the 2^{nd} and 3^{rd} harmonic frequencies, which could introduce distortion into the received signals. Since KLM-circuit model simulations also showed these peaks, they are considered specific to the design of the NM-transducer. The KLM-circuit model was adapted from the model used in Merks et al. (2006a). The peaks can be explained by considering the PZT element as a passive layer seen by the copolymer film. Because the media surrounding the

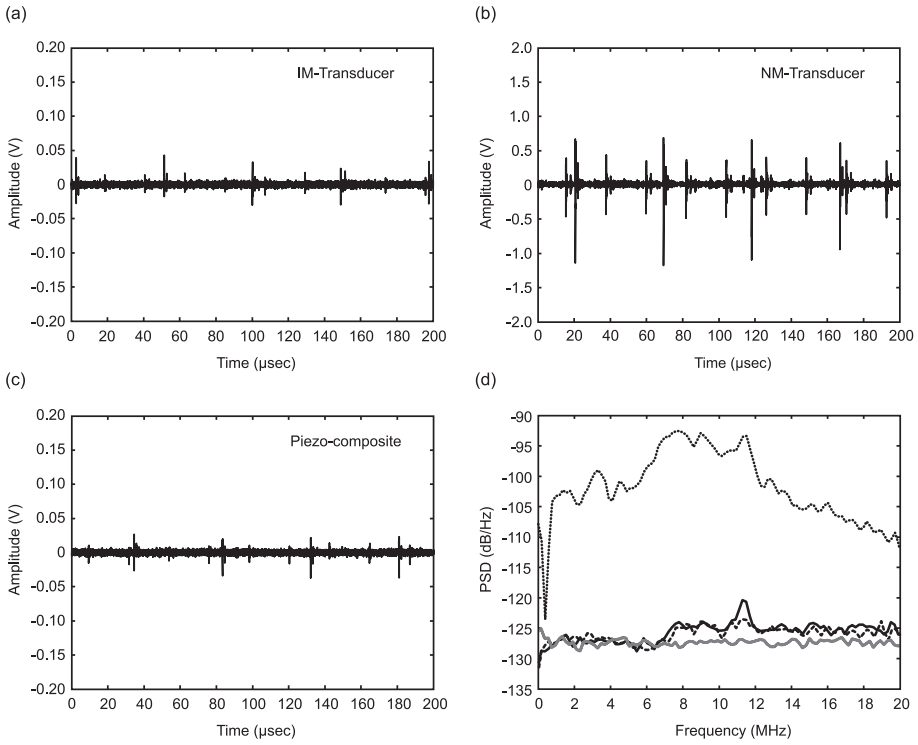

Figure 3.25: RF-recordings from the IM-transducer (a), the NM-transducer (b) and the piezo-composite transducer (c), while the acoustic interfaces were in contact with tissue. Notice the 10 times larger amplitude scaling for the NM-transducer with respect to the other two transducers. The corresponding Power Spectral Density estimates of the IM-transducer (solid black line), the NM-Transducer (dotted line) and the piezo-composite transducer (dashed) are shown at the lower right (d). The solid gray line represents the PSD of the acquisition system without load.

PZT layer have much lower acoustic impedance, standing waves appear within the PZT layer at integer multiples of the fundamental frequency. Because of the specific geometry, the peaks observed within the receive transfer function of the NM-transducer are more pronounced than within the transfer function of the IM-Transducer.

The IM-transducer and the piezo-composite transducer both showed smooth transfer functions near the frequencies of interest. This indicates distortionless transfer of the received signals. The piezo-composite transducer had high receive sensitivity at the fundamental frequency (91.9 μV/Pa), but very low sensitivities at the harmonic frequencies, especially at the 3^{rd} harmonic frequency (6.3 MHz).

Electromagnetic susceptibility

Figure 3.25 shows the recorded RF-data from the IM-transducer, the NM-transducer and the piezo-composite transducer, while the front acoustic interfaces were in contact with tissue. The corresponding Power Spectral Density estimates (PSD) were computed from the RF-data using Welch's method and are shown at the lower right. The solid grey line represents the PSD of the acquisition system without load. Table 3.8 shows the Root-Mean-Square Voltages (V_{RMS}), calculated from the time waveforms, and the measured maximum and minimum values of the received distortion. These values were calculated over a time period of 24 ms to approximate steady state EMS behavior.

The NM-transducer had a very high EMS, which was also the case with the PVDF layer of the previously introduced multilayer transducer. The time waveforms, especially the one from the NM-transducer, showed distortions with a clear repetitive pattern. The largest spikes had a time period of 50 μs and 20 μs, which correspond to switching frequencies of 20 kHz and 50 kHz, respectively. Most likely, this distortion originated from the switching electronic ballasts from fluorescent lamps. In contrast, the EMS of the IM-transducer was very low and could be compared with the EMS from the piezo-composite transducer, which is considered to be optimal. The measured EMS in the frequency range of interest (1 MHz - 8 MHz) was even limited by the system reference.

The setup for the *in vivo* measurements had 40 dB signal gain, whereas for the *in vitro* measurements 60 dB gain was used. The SNR was calculated with 100 Pa acoustic pressure and average receive sensitivity of 10 μV/Pa.

The controlled *in vitro* measurements gave comparable results with respect to the *in vivo* measurements and again showed the high EMS of the NM-transducer relative to the other two transducers (Table 3.8). Also, higher

Table 3.8: Results electromagnetic susceptibility measurements.

	Setup	V_{RMS} *(mV)*	*Max. (mV)*	*Min. (mV)*	*SNR (dB)*
NM-transducer	*in vivo*	50.4	918.9	-1324.3	-22.4
	in vitro	73.0	1093.7	-882.9	-0.8
IM-transducer	*in vivo*	2.6	48.1	-36.8	6.4
	in vitro	2.3	34.0	-34.8	29.2
Piezo-composite	*in vivo*	2.5	32.7	-45.7	6.8
	in vitro	2.4	29.2	-23.6	30.7
System reference	*in vivo*	2.1	10.2	-11.0	19.2
	in vitro	1.7	8.5	-7.9	41.4

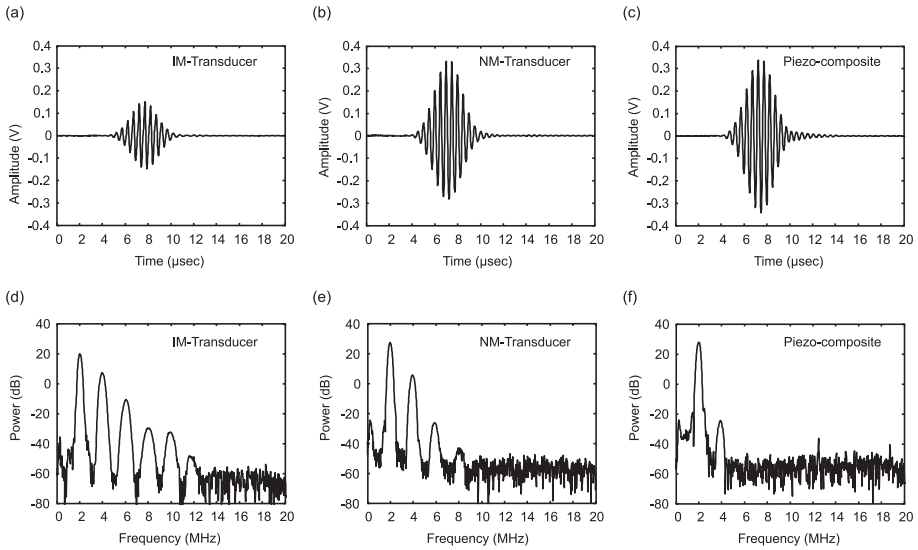

Figure 3.26: Time waveforms and corresponding spectra of the pulse-echo responses of the IM-transducer (a and d), the NM-transducer (b and e) and the piezo-composite transducer (c and f) measured in a water tank with a flat reflector at 2.7 cm distance. With the multilayer transducers, the PZT element was used for transmission and the copolymer layer was used for reception. The time scales represent retarded time.

EMS was apparent *in vivo* than *in vitro*, which explains for the difference in signal attenuation used.

Table 3.8 also shows the estimated SNR when assuming harmonic peak pressures of at least 100 Pa with an average receive sensitivity of 10 μV/Pa. These ratios were calculated by taking the maximum absolute amplitude of the measured distortion, corrected for the applied signal gain. Both the piezo-composite transducer and the IM-Transducer have sufficient SNR ($>$ 6 dB), whereas the NM-transducer has not (-22 dB). Because the part with high EMS, i.e. the piezoelectric film, was shielded by the transducer housing and the electrodes of the PZT element, the large reduction of the EMS, and thus the increase in SNR, of the IM-transducer could be ascribed to the inverted geometry.

In vitro pulse-echo measurements

The measured pulse-echo responses of the IM-transducer, the NM-transducer and the piezo-composite transducer, in a water tank with a flat reflector at 2.7 cm distance, are shown in Figure 3.26. The PZT element was used for transmission and the copolymer layer was used for reception. The piezo-composite

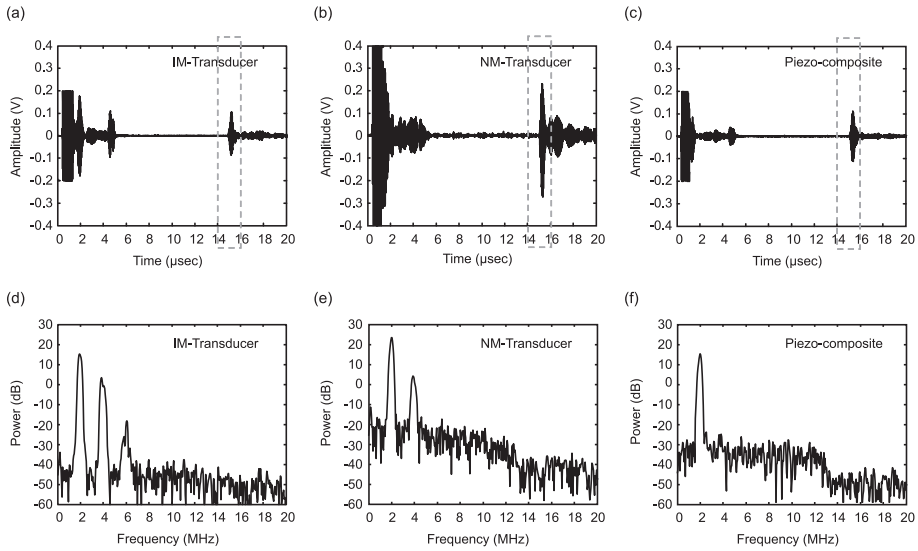

Figure 3.27: Time waveforms and corresponding spectra of the pulse-echo responses of the IM-transducer (a and d), the NM-transducer (b and e) and the piezo-composite transducer (c and f) measured on a 500 ml bladder test phantom. With the multilayer transducers, the PZT element was used for transmission and the copolymer layer was used for reception. The spectra were computed from the RF-signal present within the time segment indicated (dashed box).

transducer was used for transmission as well as reception. In total 100 traces were averaged and a 3^{rd} order Butterworth filter with passband between 200 kHz and 20 MHz was used before the spectra were calculated. The IM-transducer had the best sensitivity at the harmonic frequencies compared to the other two transducers. The spectrum of the IM-transducer also showed the moderate filtering at the fundamental frequency with respect to the higher harmonics. The response of the IM-transducer showed a 3^{rd} harmonic level only 30 dB below the fundamental level. Even at the small reflector distance of 2.7 cm, but with averaging, a significant 6^{th} harmonic was apparent. The NM-transducer also showed a significant 3^{rd} harmonic component, but at 50 dB below the fundamental level. The piezo-composite transducer only showed a small 2^{nd} harmonic component, 50 dB below the fundamental level, and no higher harmonics. Both multilayer transducers are therefore better suited for harmonic pulse-echo applications.

The measured pulse-echo responses of the IM-transducer, the NM-transducer, and the piezo-composite transducer on the CIRS bladder phantom are shown in Figure 3.27. Again, the RF-data were filtered with a 3^{rd} order

Butterworth filter with passband between 200 kHz and 20 MHz before the spectra were calculated. No averaging was done. Also, the measurements were not corrected for the differences in receive circuitry between the copolymer and piezo-composite transducers. The spectra were computed from the filtered RF-signal present within a time segment from 140 tot 160 μs (See Figure 3.27). This segment contained the echoes from the posterior bladder wall. A Hanning window with length equal to the time segment was used to obtain a smooth spectrum with sufficient frequency resolution.

Mainly due to the improved SNR and the moderate filtering at the fundamental frequency, the 3^{rd} harmonic frequency could still be measured with the IM-transducer at 45 dB below the fundamental level. The NM-transducer was capable of measuring only up to the 2^{nd} harmonic frequency with less SNR than the IM-transducer. The spectrum of the piezo-composite showed a very small 2^{nd} harmonic component, which may become apparent when averaging is applied. However, it is shown that the multilayer concepts, and especially the IM-transducer, outperformed the single-element piezo-composite transducer in the current application.

3.4.4 Discussion and summary

An inverted multilayer transducer (IM-transducer) and a normal multilayer transducer (NM-transducer) were developed and built. The IM-transducer was designed to have a high transmit sensitivity as well as broadband receive characteristics. This was achieved by using two separate layers; a PZT element for transmission at the fundamental frequency and a copolymer film for broadband reception. Copolymer was used instead of PVDF because of the higher coupling factor (k_t) and lower dielectric and mechanical losses ($tan\delta_e$ and $tan\delta_m$, respectively) (Lan). The transmit sensitivity was sufficient to cause significant nonlinear wave propagation. The receive sensitivity as well as the receive bandwidth allowed for proper acquisition of the fundamental frequency up to at least the 3^{rd} harmonic frequency component in the reflected signals. The ElectroMagnetic Susceptibility (EMS) was reduced to a level comparable to commercially available PZT and piezo-composite transducers.

The NM-transducer, comparable with the previously introduced multilayer concept (Merks et al., 2006b), had the same PZT and copolymer film as the IM-transducer, but the copolymer layer was mounted on the outside and no matching layer was applied. The NM-transducer showed a very high EMS, which was approximately 20 times the EMS observed with the IM-transducer. The large reduction of the EMS was therefore ascribed to the inverted geometry of the IM-transducer.

Mounting the receiver at the back of the layer stack may raise questions with respect to receive sensitivity. This paper documents that, by comparing the IM-transducer with the NM-transducer, the receive sensitivity was only slightly reduced at the fundamental frequency and not at the higher harmonics. Consequently, it was shown that the IM-transducer concept had better signal-to-noise characteristics than the NM-transducer concept. Improvements with respect to previously published work have thus been the increased sensitivity in transmission and reception, and the significant decrease in EMS.

A broadband high sensitive piezo-composite transducer was also included in this study to show that the IM-Transducer had comparable EMS properties as the piezo-composite, which are considered to be optimal. The IM-Transducer and the piezo-composite had comparable transmit transfer functions (Figure 3.24a), but differed in receive sensitivities. It must be noted that the piezo-composite transducer has a larger active surface (factor 1.56) than both multilayer transducers. This factor has not been corrected for.

From the measured receive transfer functions (Figure 3.24b) it shows that the piezo-composite has the highest receive sensitivity up to 4 MHz, whereas the IM-transducer has a slightly higher sensitivity from 4.5 MHz to 7 MHz. The sensitivity at a transmit frequency between 1.5 MHz and 2.5 MHz for the piezo-composite transducer is an order of magnitude higher than the sensitivities at the higher harmonics, whereas the IM-transducer has receive sensitivities at the same order of magnitude. The IM-transducer is therefore preferable when the dynamic range of the measurement system is limited. When the system dynamic range poses no problem, both the IM-transducer as well as the piezo-composite can be used for bladder volume assessment on the basis of nonlinear wave propagation.

A further advantage of using two separate layers is that the transmit and receive electronics can be optimized separately. This allows for dedicated transmit and receive circuitry, which are more efficient and, additionally, are more simple and less bulky than in the case of a single element broadband transducer. This was also the reason for the lower performance of the piezo-composite transducer in pulse-echo mode, where part of the transmit and receive energy were dissipated in the limiter configuration.

Additionally, it was found that the receive transfer function was affected by electronically optimizing for the transmit layer, i.e. electrically tuning the PZT element. Hence, the transmit transfer functions and receive transfer functions of the IM-transducer, with and without electrically tuning the PZT element with a series inductor (2.7 μH), were obtained (see Figure 3.28).

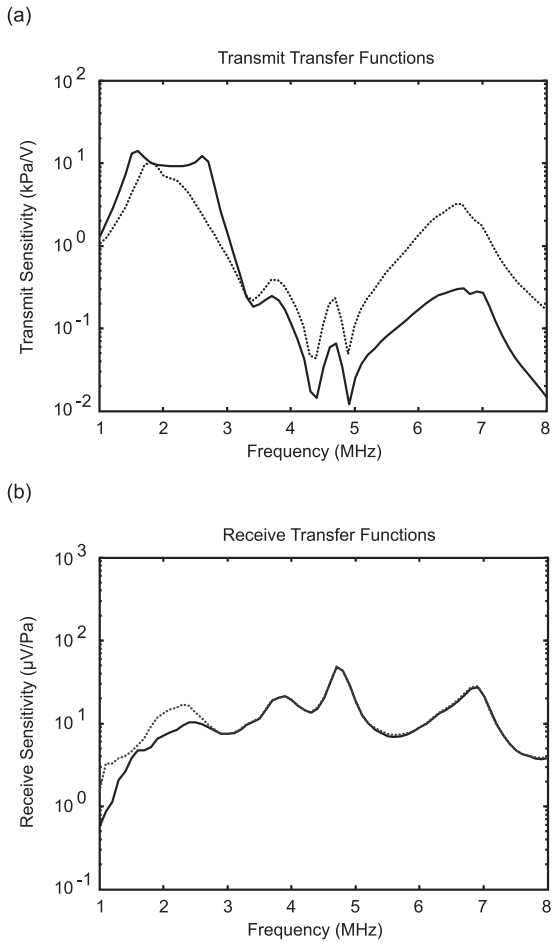

Figure 3.28: Transmit transfer functions (a) and receive transfer functions (b) obtained for the IM-transducer without the PZT element electrically tuned (dotted line) and with the PZT element electrically tuned (solid line) with a series inductor of 2.7 μH.

Figure 3.28a shows a significant increase in transmit sensitivity and bandwidth when the PZT element is electrically tuned. The transmit sensitivity was increased from 7 kPa/V to 9.4 kPa/V. The -6 dB bandwidth increased from 39% to 73%. Figure 3.28b shows that the electrical tuning of the PZT element only affects the receive transfer at the fundamental frequency. The receive sensitivity at the fundamental frequency was reduced with 6 dB. This means that an electronically tuned IM-transducer shows a moderate

filtering at the fundamental frequency with respect to the higher harmonics. This can be explained by the receive transfer function of the PZT, which has a preference for acoustic energy at the fundamental frequency. The PZT thus absorbs large part of the fundamental acoustic energy before the acoustic waves reach the copolymer layer. This is considered beneficial for the dynamic range of the receiving electronics, which has been increased with 6 dB.

Because of these benefits compared to single element implementations and because of the low lateral coupling of copolymer, the new multilayer concept could be beneficial for array transducer applications (Jeong et al., 2007). It is concluded that in order to measure at least up to the third harmonic frequency component with good sensitivity in combination with very high transmit sensitivity at the fundamental frequency, a multilayer structure is optimal. To optimize for the EMS in reception, and hence also the signal-to-noise ratio, an inverted geometry as proposed in this paper has proven to be effective.

Acknowledgments

I would like to thank Wim van Alphen and Geert Springeling (ErasmusMC, Rotterdam, the Netherlands) for building all custom transducers described in this chapter. A job well done! Also, many thanks to Oldelft B.V. (Delft, the Netherlands) for the supply of transducer materials.

Chapter 4

Comparison of Computational Methods: A Simulation Study

E.J.W. Merks and N. de Jong

Acoustic bladder volume measurement is clinically relevant as it reduces the need for a urinary catheter and the likelihood of urinary infection. A method was introduced that acoustically measures the volume on the basis of nonlinear wave propagation. With the original concept a region of interest (ROI) is selected at a fixed location behind the bladder. It was shown that the 2^{nd} Harmonic-to-Fundamental ratio (2HFR) within this ROI correlated well with the urine volume. In this chapter, the performance of the original computational method to quantitatively measure the bladder volume was compared with three alternative algorithms using simulations. Besides giving a good estimation of the urine volume present within the acoustic beam, the algorithm to be used will have to be insensitive to patient variability. The simulations included the modeling of nonlinear wave propagation through layered media using a time-domain implementation of the KZK-equation. The layer media comprised the anterior bladder region, urine region and posterior bladder region. Pulse-echo responses were obtained from a flat reflector situation and scatter phantoms using the spatial impulse responses at the particular scatter position and frequency dependent loss of the backward propagation path. Because of limitations of the simulation model used, only unfocused sound fields were used. Hence, urine path lengths (UPLs) were modeled instead of volumes. From the four proposed algorithms, the original concept gave the best estimation of the urine path lengths present within the unfocused acoustic beam. The 2HFR calculated with this algorithm showed a high sensitivity for the UPLs

and it had lowest sensitivity to the modeled patient variability. This simulation study gave good insight on the observed 2HFR-bladder volume relationship with respect to the effect of patient variability, transducer configuration and, most importantly, the algorithm used.

4.1 Introduction

Acoustic bladder volume measurement is clinically relevant as it reduces the need for a urinary catheter and the likelihood of urinary infection (Slappendel and Weber, 1999). A method was introduced that acoustically measures the bladder volume on the basis of nonlinear wave propagation (Bouakaz et al., 2004; McMorrow et al., 2002). It uses the medium-specific relationship between the nonlinearity and the attenuation of the acoustic wave propagation, reflected in the so-called "Gol'dberg number", to differentiate between urine and tissue. Given a much stronger nonlinear behavior for urine than for tissue, it should be possible to find a relationship between the amount of generated harmonics present within echoes received from a Region of Interest (ROI) behind the posterior bladder wall and the amount of urine present within the propagation path (Figure 4.1). The method proposes to use a single element transducer with a diverging acoustic beam to capture the entire bladder in real time with a minimum number of pulse-echo acquisitions.

With the original concept, as described by Bouakaz et al. (2004), a region of interest (ROI) is selected at a fixed location behind the bladder. As a first approach, it was shown that the 2^{nd} Harmonic-to-fundamental ratio (2HFR) within this fixed ROI correlated well with the urine volume. However, a thorough investigation on the computational method to be used might improve the results on volume estimation.

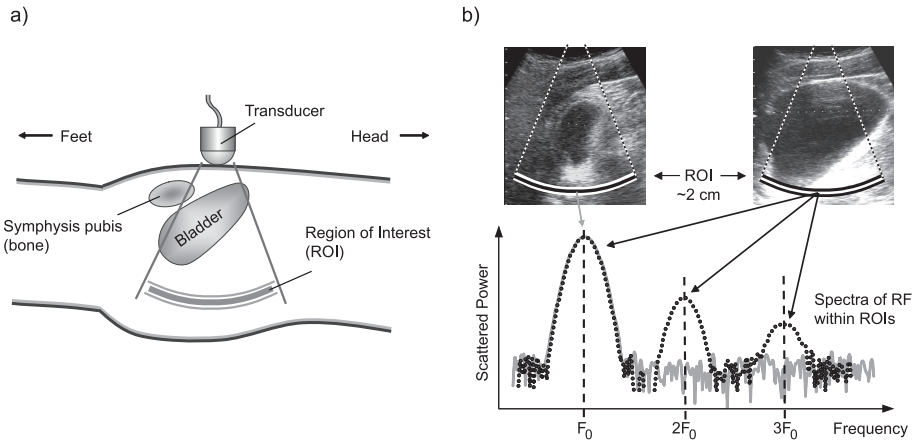

Figure 4.1: Set-up for bladder volume measurements on the basis of nonlinear wave propagation. With the patient in supine position (a) and a single element transducer producing a diverging acoustic beam, the bladder volume is obtained from spectral analysis (b) on a fixed region of interest behind the bladder.

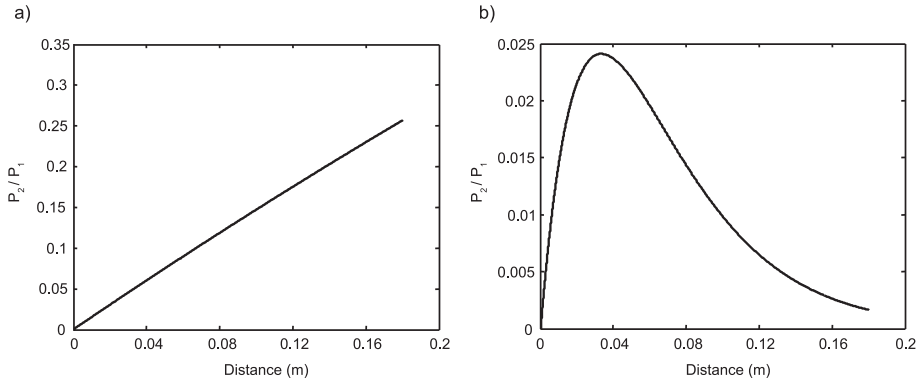

Figure 4.2: 2^{nd} Harmonic - Fundamental pressure amplitudes ratio (2HFR) as function of propagation distance for water (a) and for tissue (b) calculated with equation 1 for plane wave propagation, with $p_0 = 200$ kPa, $f_0 = 2$ MHz, and $\rho_0 = 1\text{kg/dm}^3$. For water: $\beta = 3.5$, $\alpha_1 = 0.13$ Np/m, and $\alpha_2 = 0.51$ Np/m. For tissue: $\beta = 4.5$, $\alpha_1 = 15$ Np/m, and $\alpha_2 = 30$ Np/m.

A good approximation of the 2^{nd} harmonic-to-fundamental pressure amplitude ratio as function of distance including frequency dependent loss was formulated by Thuras et al. (1935) as:

$$\frac{p_2}{p_1} = p_0 \frac{\beta\omega}{2\rho_0 c_0^3} \left[\frac{e^{-(\alpha_2-\alpha_1)z} - e^{-\alpha_1 z}}{2\alpha_1 - \alpha_2} \right], \tag{4.1}$$

where $p_1(z)$ and $p_2(z)$ are the pressure amplitudes of the fundamental and 2^{nd} harmonic frequency at propagation distance z, respectively. p_0 is the source pressure amplitude, β the coefficient of nonlinearity and ω the angular frequency. ρ_0 and c_0 are the density and speed of sound at equilibrium, respectively. The frequency dependent attenuation coefficients are given by α_1 and α_2 (Np/m) for the fundamental and 2^{nd} harmonic. Eq. 4.1 assumes plane wave propagation and z to be much less than the shock formation distance, such that the harmonics higher than the 2^{nd} harmonic can be neglected. Figure 4.2 shows the 2HFR as function of propagation distance for water and for tissue as calculated with Eq. 4.1.

The 2HFR for water only (Figure 4.2a) shows a monotonic relationship with propagation distance. Eventually, the curve will flatten off beyond the shock formation distance due to acoustic saturation. The tissue-only situation (Figure 4.2b) shows an increase of the 2HFR until about 3.5 cm from where the attenuation becomes more significant than the nonlinear propagation and the curve shows an exponential decrease over distance. For humans, in supine

position, the anterior bladder wall lies at an average depth of about 4 cm, which also depends on the bladder filling stage. In most situations, a full bladder will be closer to the abdominal wall than an empty bladder (Figure 4.1b.). The curve from Figure 4.2b thus implies that the anterior bladder region (ABR) affects the 2HFR observed at the posterior bladder wall not only with additional loss of the transmitted wave, but also with the generation of harmonics. With this in mind, the computational method to be used with this method must, besides giving a good estimation of the urine volume present within the acoustic beam, be insensitive to patient variability.

In this chapter, the performance of the original computational method to quantitatively measure the bladder volume was compared with three alternative methods using simulations. As already mentioned, Eq. 4.1 only applies to plane waves. Additionally, it only applies to a single medium and it only describes the amplitudes of the forward propagated waves. Because eventually the algorithms will be used on recorded RF-Data obtained from pulse-echo measurements on the bladder volume *in vivo*, the simulation model must include multiple layered media and scattering. Hence, the approximation given by Eq. 4.1 cannot be used for this purpose. Instead, a time-domain implementation of the Khokhlov-Zabolotskaya-Kuznetsov (KZK) equation (Lee and Hamilton, 1995) was used together with analytically calculated spatial impulse responses of scatter phantoms.

The suggested bladder volume assessment method is based on the use of a widely diverging acoustic beam to capture the complete bladder. The KZK equation becomes less valid for regions close to the source and for angles (20 degrees) far off the axis of the transducer (Averkiou and Hamilton, 1997). Because of these limitations only a non-diverging acoustic beam could be modeled. Hence, in this paper, as a first approach only urine path lengths (UPLs) were modeled instead of volumes.

4.2 Methods

4.2.1 Computer model

A time-domain implementation of the KZK-equation, as described by Lee and Hamilton (1995), was used to simulate the nonlinear acoustic field generated by a unfocused circular transducer in a layered medium. The approach is similar as described in Li et al. (2004); Rielly et al. (2000), where it was validated experimentally that acoustic fields in layered liquid media could be simulated using the KZK-equation by changing the speed of sound, the density, the attenuation and the nonlinearity parameter for each layer.

The layered medium used here contained an ABR, a urine region with a certain urine path length (UPL) and a posterior bladder region (PBR). The

regions were assumed to be isotropic, i.e. homogeneous with constant propagation speed (1480 m/s), density (1 kg/dm^3), nonlinearity and attenuation. The bladder, or tissue, regions were assumed to have a nonlinearity parameter β of 4.5 and frequency dependent loss α_0 of 0.6 dB/MHz/cm. The acoustic properties of the urine region were taken equal to those of water, i.e. $\beta = 3.5$ and $\alpha_0 = 0.002$ dB/MHz^2/cm. A Gaussian modulated sinewave burst with centre frequency (f_0) of 2.1 MHz, a Full-Width-Half-Maximum (FWHM) pulse length of 2.5 μs, and peak amplitude of 300 kPa was used for excitation of an unfocused piston transducer with radius of 1 cm. The simulation sample frequency was chosen at 30 times f_0 (63 MHz).

4.2.2 Pulse-echo scattering

The modeling of the pulse echo scattering was adapted from Frijlink et al. (2006). Scatterers were randomly positioned in the bladder regions to create non-coherent scattering. The complete scatter phantoms ranged from -3 cm to +3 cm in both lateral dimensions and ranged from 0 to 20 cm in the axial dimension. Individual scatter responses were calculated using the spatial impulse response (SIR) $h(r, z, t)$ of an unfocused circular transducer defined as (Stepanishen, 1971):

$$\begin{aligned} h\left(r,z,t\right) &= \frac{c_0}{\pi}\arccos\left(\frac{\left(c_0t\right)^2 - z^2 + r^2 - a^2}{2r\sqrt{\left(c_0t\right)^2 - z^2}}\right), && \text{if } t_1 < t < t_2 \\ &= c_0, && \text{if } r < a \text{ and } t_0 < t < t_1 \\ &= 0, && \text{elsewhere,} \end{aligned}$$

in which

$$\begin{aligned} t_0 &= z/c_0, \\ t_1 &= \frac{\sqrt{z^2 + \left(r-a\right)^2}}{c_0}, \\ t_2 &= \frac{\sqrt{z^2 + \left(r+a\right)^2}}{c_0} \end{aligned} \tag{4.2}$$

where z and r are the axial and the radial coordinates of the scatterer position, respectively, c_0 is the medium specific propagation speed, a is the transducer radius, and t is time. t_1 and t_2 are the shortest and longest distances, respectively, expressed in propagation times from the point scatterer to the transducer edges.

Frequency dependent attenuation of the backward propagation path was also included. As was mentioned in Frijlink et al. (2006), the effective distance of attenuation can be approximated by the shortest distance between the transducer surface and the scatterer position. The effective distance is given by:

$$\begin{aligned} z_{\text{eff}} &= c_0 t_0, \quad \text{if } r < a \\ z_{\text{eff}} &= c_0 t_1, \quad \text{if } r \geq a \end{aligned} \tag{4.3}$$

All scatterers were assumed to have equal scattering strength and frequency dependent backscatter was not taken into account. Weak scattering was assumed such that the backscattered signal propagated linearly and multiple scattering could be neglected.

The backscattered signal for each individual scatterer was obtained by multiplying the calculated SIR, the waveform computed with the KZK-equation at the specific scatterer location and the frequency dependent attenuation factor in the frequency domain, followed by an Inverse Fast Fourier Transformation (IFFT). The complete RF-signal then followed from summing all individual backscattered RF-signals.

To be able to assume first order statistics on the scattering, i.e. such that the RF envelope amplitude showed a Rayleigh probability distribution function, the scatter density needed to be relatively high with respect to the resolution cell of the scanning system used (Thijssen and Oosterveld, 1986). The resolution cell mainly depends on the point spread function and bandwidth (or transmitted pulse length) of the transducer, and is known to vary over depth with a minimum size at the focal distance. From using the method described in Thijssen and Oosterveld (1986), the volume of the resolution cell at focus was calculated at 27 mm^3. ($\text{FWHM}_{\text{axial}} = 1.9$ mm; $\text{FWHM}_{\text{lateral}} = 4.3$ mm). The scatter phantoms were implemented with 750 scatterers/cm^3, which corresponded to at least 20 scatterers per resolution cell. According to Rao et al. (1990) this was sufficient to assume first order statistics on scattering.

4.2.3 Algorithm definition

Four different algorithms to obtain the UPL within the propagation path from pulse-echo data were compared that all use the selection of a ROI with length of 2 cm. Prior to the application of an algorithm, the RF-data was first bandpass

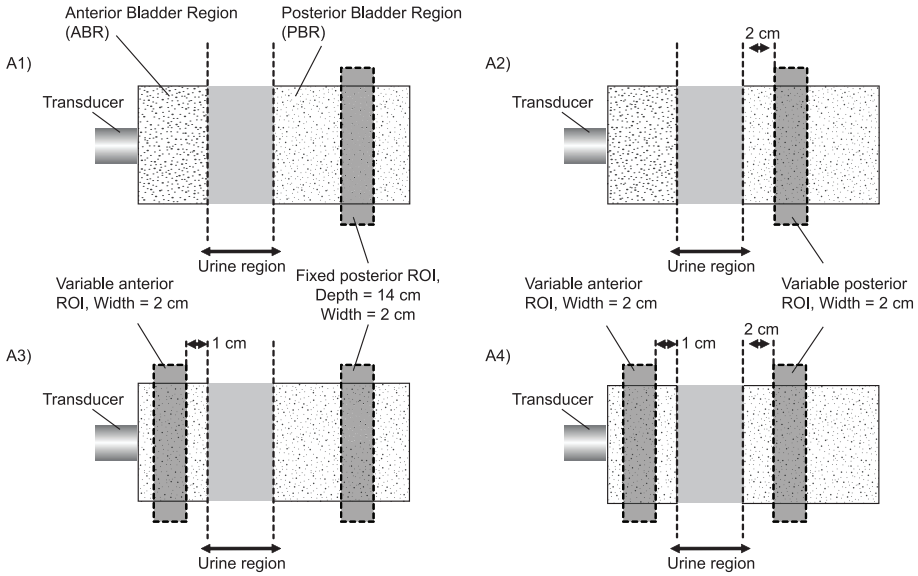

Figure 4.3: Four computational schemes to obtain the urine path length (UPL) present within the propagation path from pulse-echo data.

filtered at the fundamental frequency (2.1 MHz) and the 2^{nd} harmonic (4.2 MHz) using a 3^{rd} order Butterworth filter with transmission bandwidth of 1 MHz. Within the selected ROI, the 2HFR was obtained by dividing the mean envelope value of the 2^{nd} harmonic by the mean envelope value of the fundamental frequency. The algorithms were defined as (See Figure 4.3):

A1) The original concept of selecting a ROI in the PBR at a fixed depth of 14 cm from the transducer surface.

A2) Selecting a ROI in the posterior region 2 cm behind the posterior bladder wall. This implies a variable ROI position and posterior bladder wall detection.

A3) As algorithm 1, but with an additional ROI located 1 cm before the anterior bladder wall. The 2HFR in this ROI is then subtracted from the 2HFR ratio obtained from algorithm 1.

A4) As algorithm 2, but with an additional ROI located 1 cm before the anterior bladder wall. The 2HFR in this ROI is then subtracted from the 2HFR ratio obtained from algorithm 2.

4.2.4 Simulations

Two different simulation situations were investigated and defined as:

A) Increasing UPL with constant ABR. The urine region was increased in length from 0 to 8 cm with steps of 1 cm. The ABR was kept constant at 4 cm.

B) Increasing anterior bladder wall distance with constant UPL. The anterior wall distance was varied from 3 to 8 cm. The UPL was kept constant at 4 cm.

In total 15 individual simulation settings were evaluated, i.e. 9 for situation A and 6 for situation B.

Nonlinear acoustic field simulations

Two-dimensional beam profiles were calculated for the fundamental (2.1 MHz) and second harmonic (4.2 MHz) frequencies through layered media. To observe the effect of the UPL on the harmonic generation, two different phantom configurations were implemented, where the first had a UPL of 3 cm and the second had a UPL of 6 cm depth. Both configurations had an ABR of 4 cm. For comparison, a tissue-only situation was also simulated.

Pulse-echo simulations on a flat reflector

To obtain insight into the 2HFR as function of depth and to avoid the effects scattering and the choice of ROI size, the calculated acoustic field through multiple layers was first used to simulate the pulse-echo response on a flat reflector. Although the reflection coefficient was taken as 1, the reflection from the reflector was assumed to be weak, i.e. the reflected waves propagated linearly, and frequency independent. The response was obtained by first calculating the SIR and frequency dependent loss of the back propagated path, using Eq. 4.2 and Eq. 4.3, at each of the KZK-coordinates corresponding to one plane at a particular axial distance. The pulse response was then obtained by multiplying the SIRs and loss with the corresponding waveforms in the frequency domain, and subsequently applying an IFFT. The pulse responses were then multiplied in the time domain by a weighting factor $w(k)$ defined as:

$$w\left(k\right) = \left(r_{k+1}^2 - r_k^2\right)\pi, \tag{4.4}$$

where r_k is the lateral distance (m) from the transducer axis of the k^{th} lateral simulation step. After applying $w(k)$, the pulse responses were summed to obtain the pulse-echo response on a flat reflector. Situations A and B were both

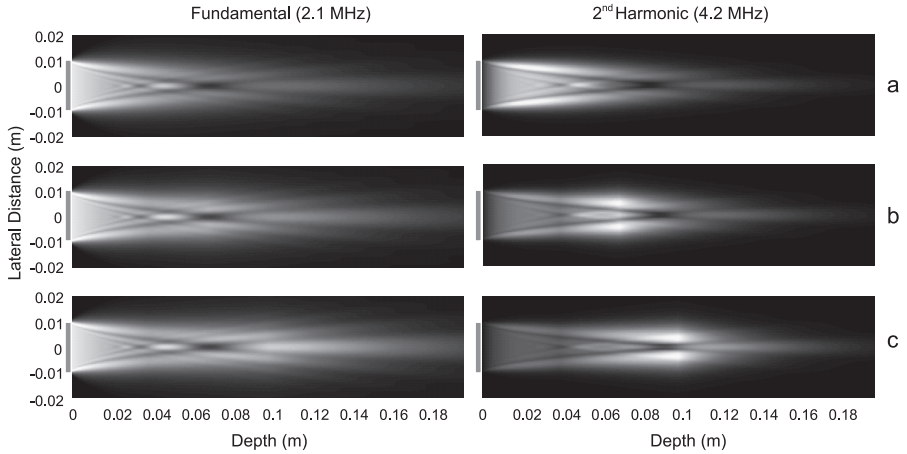

Figure 4.4: Two-dimensional beam profiles plotted at the fundamental frequency (2.1 MHz; left) and at the 2^{nd} harmonic (4.2 MHz; right) for a tissue-only situation (a), for a urine region located between 4 and 7 cm (b) and for a urine region located between 4 and 10 cm (c). All plot were normalized with respect to the maximum values within the individual images. Transducer surfaces are also indicated.

evaluated to observe the effects of changing ABRs and UPLs on the fundamental and generated 2^{nd} harmonic. All four algorithms were used to calculate the 2HFRs at the different simulation settings.

Pulse-echo simulations on scatter phantoms

The pulse-echo evaluation of situations A and B was repeated on scatter phantoms. The RF-signals were obtained as described previously (See section on pulse-echo scattering) and the four proposed algorithms were used to determine the UPL from the 2HFR. To observe the effect of random scattering on the estimated UPL, 6 different scatter phantoms were generated. Hence, the calculation of the RF-data was repeated 6 times.

4.3 Results

Nonlinear acoustic field simulations

The two-dimensional beamprofiles obtained from simulations on nonlinear wave propagation through three different media configurations are shown in Figure 4.4. The fundamental and 2^{nd} harmonic contents were plotted separately to show the effect of the multiple layers. The images have linear scale and were normalized with respect to the maximum values within the individual images.

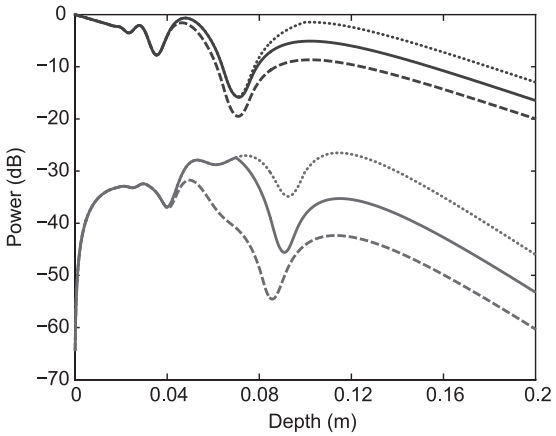

Figure 4.5: Axial beamprofiles of the fundamental frequency (black lines) and 2^{nd} harmonic (gray lines) for the tissue-only situation (dashed), the situation with 3 cm UPL and 4 cm ABR (solid) and the situation with 6 cm UPL and 4 cm ABR (dotted).

Figure 4.4a (top row) represents the tissue-only situation. It is observed that the 2^{nd} harmonic content first increases and then decreases at a faster rate than the fundamental frequency component.

Figure 4.4b and Figure 4.4c represent the situations where the ABR is 4 cm and the UPLs are 3 cm and 6 cm, respectively. Both fundamental plots show higher acoustic energy at larger depths compared to the tissue-only situation. The layered structures are clearly visible in the 2^{nd} harmonic plots. The 2^{nd} harmonic amplitudes clearly show an increase in the urine regions and a decrease in the PBRs.

Figure 4.5 shows the on-axis beamprofiles of the fundamental and 2^{nd} harmonic of the three situations described with Figure 4.4. The 2^{nd} harmonic is more sensitive to the presence of urine and increasing UPL than the fundamental. Because of loss, the natural focus at the fundamental frequency is observed at 10 cm instead of 14 cm for the loss-less case. The shift towards the transducer as function of decreasing UPL is also visible at the local minimum around 9 cm of the 2^{nd} harmonic curves.

Pulse-echo simulations on a flat reflector

The computed nonlinear acoustic fields were used to simulate the pulse-echo response on a flat reflector and to determine the 2HFR as function of distance.

The computed harmonic content and their ratio as function of distance for the situation of an increasing UPL and constant ABR are shown in Figure 4.6a and Figure 4.6b, respectively. The ABR was located from 0 to 4 cm. The UPL

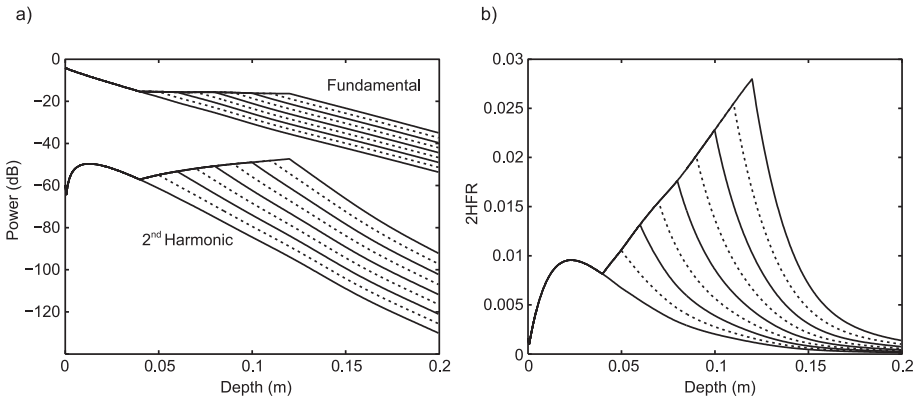

Figure 4.6: The computed harmonic contents (a), normalized to the fundamental frequency component, and the 2HFR (b), obtained in pulse-echo, as function of distance for the situation of an increasing UPL (0 to 8 cm) and constant ABR of 4 cm.

was increased from 0 to 8 cm with steps of 1 cm.

The harmonic content shown in Figure 4.6a was calculated by taking the maximum envelope value of the pulse-echo response at each depth. The 2HFR curve for the tissue-only situation shows an increase up to 2 cm depth, from where the attenuation dominates the nonlinear propagation and the curves show an exponential decay. With a urine region starting at 4 cm, the nonlinearity dominates the loss and the curves show an increase of harmonic contents. After the urine region, loss again dominates the nonlinear wave propagation. As the 2^{nd} harmonic is attenuated more than the fundamental, the 2HFR curves show a strong exponential decay.

The results from the previous section were used to evaluate and compare the 4 different algorithms. The ROIs were selected according to the definition of the algorithms. The differences between the curves obtained with A1 and A2 can be explained by the fact that A1 also includes the frequency dependent acoustic loss of the 2-way propagation path between the ROI and the posterior bladder wall, where A2 only includes the loss in the ABR and nonlinearity in the urine region. Hence, when the UPL increases, A2 only observes an increase in nonlinearity, whereas A1 also observes an additional decrease in loss. This makes A1 much more sensitive to variations in UPL, which is evident in the 2HFR-UPL curves of Figure 4.7b. The curves for algorithms A3 and A4 have identical 2HFR-UPL as those from A1 and A2, respectively, but with a downshift of $9.2\text{x}10^{-3}$.

The computed harmonic content and their ratio as function of distance for the situation of an increasing ABR and constant UPL are shown in Figure 4.8a

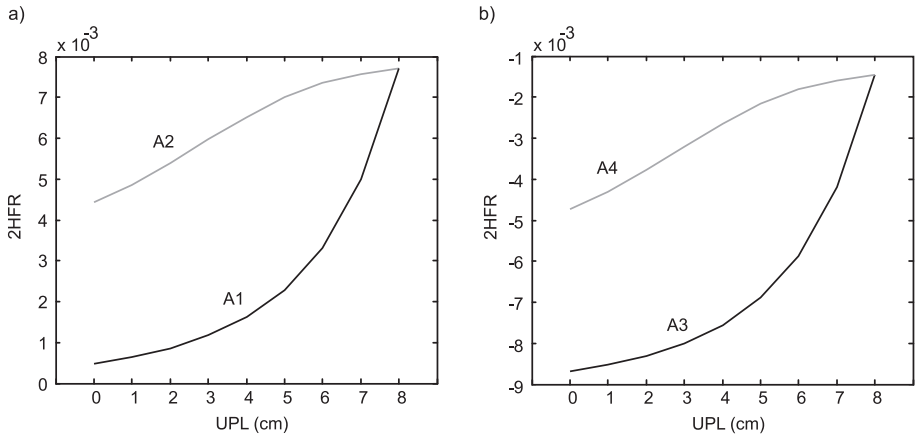

Figure 4.7: Application of the four algorithms on pulse-echo simulations on a flat reflector for the situation of an increasing UPL (0 to 8 cm) and constant ABR of 4 cm. The 2HFR-ABR curves were obtained with A1 and A2 (a) and with A3 and A4 (b). The curves for algorithms A3 and A4 have identical 2HFR-UPL as those from A1 and A2, respectively, but with a downshift of $9.2\text{x}10^{-3}$.

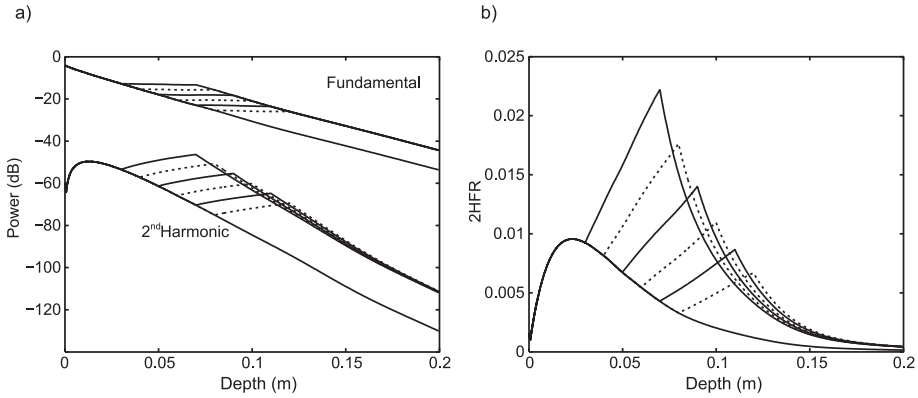

Figure 4.8: The computed harmonic contents (a), normalized to the fundamental frequency component, and the 2HFR (b), obtained in pulse-echo, as function of distance for the situation of an increasing ABR (3 to 8 cm) and constant UPL of 4 cm.

and Figure 4.8b, respectively. In this situation, the UPL was kept constant at 4 cm. The ABR was initially located from 0 to 3 cm and was increased to 8 cm with steps of 1 cm. The tissue-only situation was also added as a reference. It is clear from Figure 4.8a that, at the ABR-urine transition, the 2^{nd} harmonic

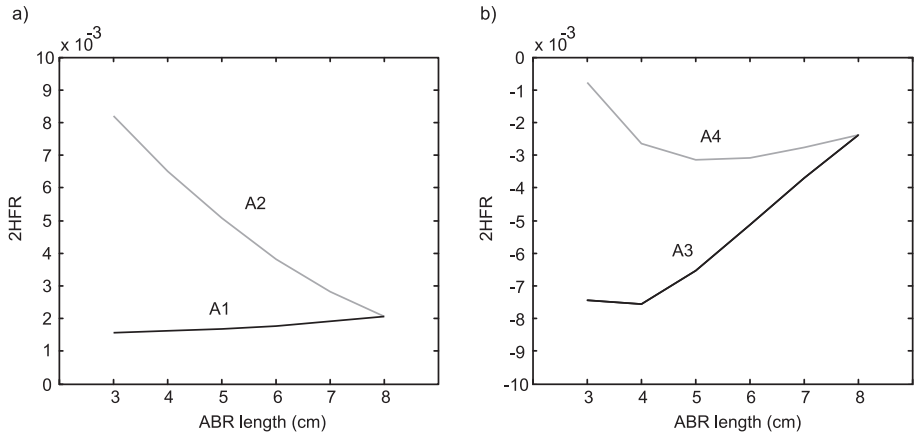

Figure 4.9: Application of the four algorithms on pulse-echo simulations on a flat reflector for the situation of an increasing ABR (3 to 8 cm) and constant UPL of 4 cm. The 2HFR-ABR curves were obtained with A1 and A2 (a) and with A3 and A4 (b).

starts to increase at lower levels with increasing anterior regions, following the tissue-only curve. However, the relative increase of the 2^{nd} harmonic in the urine region remains fairly constant. Because the 2^{nd} harmonic is attenuated more by the ABR than the fundamental frequency, the 2HFR curves of Figure 4.8b show a decreasing slope in the urine regions with increasing ABR. It is interesting to notice that, due to the attenuation in the PBR, the curves of the fundamental frequency and the 2^{nd} harmonic (Figure 4.8a) as well as the 2HFR curves tend to coincide at larger depths. The differences due to the ABR are therefore less visible when observing the harmonic contents at larger depths. As will be shown next, this affects the algorithms' sensitivity to ABR variations.

The results from the previous section were again used to evaluate and compare the 4 different algorithms. Figure 4.9a shows the 2HFR-ABR curves obtained with algorithms A1 and A2. As was already mentioned, algorithm A2 is much more sensitive to variations in the ABR than algorithm A1.

In contrast to the previous section, the harmonic contents of the ROIs selected in the ABR now varied. As a result, the 2HFR curves obtained with A3 and A4 (Figure 4.9b) differed substantially from those obtained with A1 and A2. Algorithm A1 again shows the best result as it is least affected by the changing ABR with a total 2HFR difference of $0.5\text{x}10^{-3}$. When using the additional information of the ABR with algorithm A1, as was defined with algorithm A3, the total 2HFR difference increased to $5.0\text{x}10^{-3}$. Hence, the additional information of the ABR thus increased the sensitivity for ABR vari-

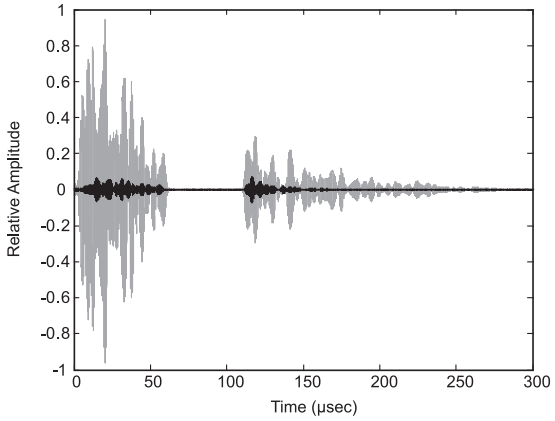

Figure 4.10: Typical RF-responses filtered at the fundamental frequency (2.1 MHz; gray) and the 2^{nd} harmonic (4.2 MHz; black), normalized to the maximum envelope value. The 2^{nd} harmonic was amplified 10 times for illustration purposes.

ations. The 2HFR difference found with algorithm A2 was $6.0\text{x}10^{-3}$. With algorithm A4, using the ABR information, the 2HFR difference decreased to $2.5\text{x}10^{-3}$.

Pulse-echo simulations on scatter phantoms

The four algorithms were applied to the RF data obtained from the simulated nonlinear sound fields and 6 different scatter phantom implementations. From the 6 individual results, the averages and the standard deviations were calculated. A typical RF response obtained from a scatter phantom with urine region between 4 and 8 cm is shown in Figure 4.10. The fundamental and 2^{nd} harmonic components were bandpass filtered with a 3^{rd} order Butterworth filter with transmission bandwidth of 1 MHz.

Figure 4.11 shows the results of the four algorithms on RF data obtained from pulse-echo simulations on scatter phantoms. The UPL was increased from 0 to 8 cm and the ABR was kept constant at 4 cm. The 2HFR-UPL curves are shown in Figure 4.11a and b. The errorbars indicate the standard deviations around the mean from 6 different phantom implementations. Prior to applying the algorithms, the raw RF data were normalized to the mean of the maximum values of all 6 RF lines.

The curves representing the mean values in Figure 4.11 are very similar to the curves from Figure 4.7, except for the 2HFR curve from algorithm A2 and A4. These curves show a clear dip at a UPL of 6 cm (10 cm from the transducer). This might be explained by the local minimum around 9 cm depth

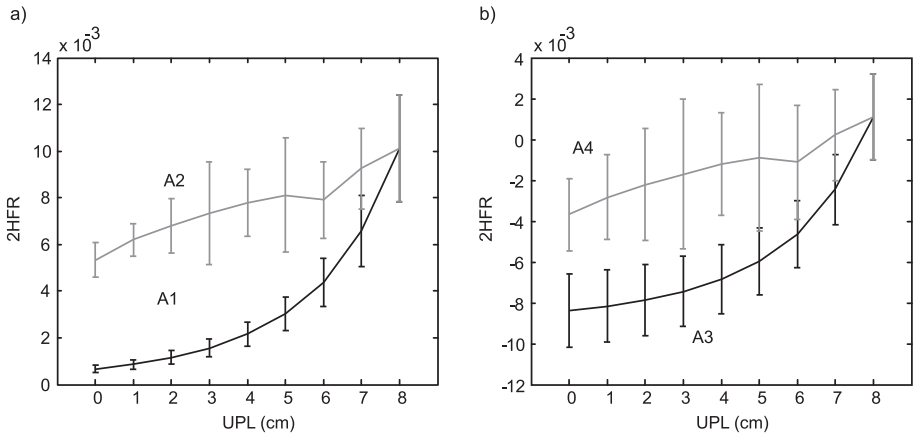

Figure 4.11: Application of the four algorithms on RF data obtained from pulse-echo simulations on scatter phantoms. The UPL was increased from 0 to 8 cm and the ABR was kept constant at 4 cm. The 2HFR-UPL curves were obtained with A1 and A2 (a) and with A3 and A4 (b). Errorbars indicate the standard deviations around the mean from 6 different phantom implementations.

of the 2^{nd} harmonic axial beamprofile observed in Figure 4.4 and Figure 4.5. Although the absolute standard deviations for A1 increase with increasing UPL (Figure 4.11a), the relative standard deviations were constant. This in contrast with the deviations found with algorithm A2, which clearly vary with different UPLs. The relative standard deviations are in the same order of magnitude for both methods, indicating that both methods are equally sensitive to the stochastic scattering of the scatter phantoms. This will be explained in the next section.

As was mentioned in section B2, the 2HFR curves for algorithms A3 and A4, as function of UPL and with constant ABR, are downshifted versions of the curves for algorithms A1 and A2, respectively. The constant found here was $9.0\text{x}10^{-3}$, which is close to the value obtained with the flat reflector simulations. However, the standard deviations did increase substantially for A3 and A4 as the standard deviations for the ABR curves were also included.

Figure 4.12 shows the results of the four algorithms on RF data obtained from pulse-echo simulations on scatter phantoms with various ABR depths. The ABR was increased from 3 to 8 cm and the UPL was kept constant at 4 cm.

The results shown in Figure 4.12a are again comparable with the results from the pulse-echo simulations on a flat reflector. However, the results for algorithms A3 and A4 (Figure 4.12b) differ substantially from those shown in Figure 4.9. The 2HFR calculated from the ABR up to a length of 4 cm is

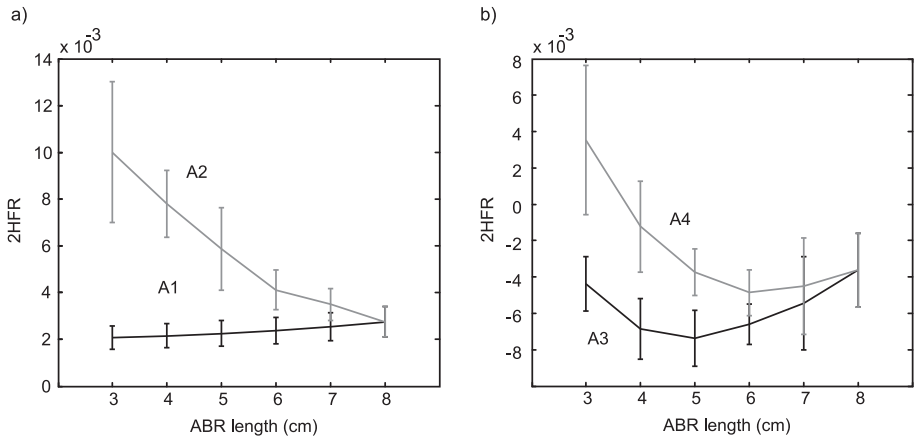

Figure 4.12: Application of the four algorithms on RF data obtained from pulse-echo simulations on scatter phantoms. The ABR was increased from 3 to 8 cm and the UPL was kept constant at 4 cm. The 2HFR curves were obtained with A1 and A2 (a) and with A3 and A4 (b). Errorbars indicate the standard deviations around the mean from 6 different phantom implementations.

higher. The maximum 2HFR differences found over the simulated ABR range are $0.6\text{x}10^{-3}$ for algorithm A1, $7.3\text{x}10^{-3}$ for A2, $3.6\text{x}10^{-3}$ for A3, and $8.4\text{x}10^{-3}$ for A4. Hence, using the ABR, as defined with A3 and A4, does not result in a lower sensitivity to patient variability.

Algorithm comparison

The results from the previous sections were used to compare the four algorithms with respect to the ability to determine the UPL, the sensitivity to patient variability and the sensitivity to stochastic scattering. Figure 4.13 summarizes the results from sections A and B of the scatter phantom simulations for all four algorithms. The UPL and ABR lengths are given as function of the calculated 2HFR.

The ability to determine the UPL and the sensitivity to patient variability should be seen relative to each other over the complete 2HFR range. The 2HFR range that covers the UPL range should be large compared to the 2HFR range related to the ABR lengths. From Figure 4.13 it is clear that Algorithm A1 best fulfills this requirement. The 2HFR is almost insensitive to the ABR, while the UPL shows an exponentially increasing curve. The other algorithms show significant sensitivity to changing ABR. When, for example, the ABR varies between 3 and 5 cm, algorithm A1 still calculates the UPL at approximately 4 cm, whereas algorithm A2 gives and UPL between 0 and 8 cm.

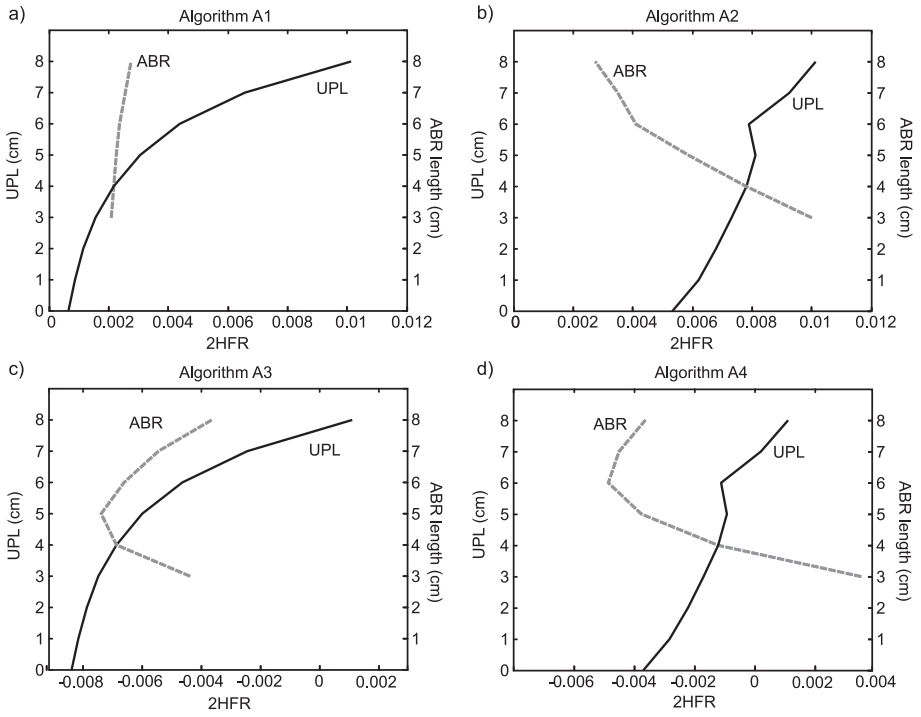

Figure 4.13: Comparison of the four algorithms with respect to the ability to determine the UPL (solid lines) and the sensitivity to patient variability (dashed lines) from simulated RF-data as function of the calculated mean 2HFR. Notice the double y-axis.

4.4 Discussion and conclusions

Four different algorithms to determine the UPL present within the acoustic beam from pulse echo data were compared using simulations. The first algorithm (A1) calculated the 2HFR from a ROI located at a fixed position in the PBR, where the second algorithm (A2) used a ROI with variable locations. To reduce the influence of the possible variations in the ABR, A1 and A2 were extended with selecting a ROI in the anterior region, of which the locations were also chosen to be variable. The 2HFR of this anterior ROI was subtracted from the posterior ROI, resulting in algorithms A3 and A4, respectively.

The simulations included the modeling of nonlinear wave propagation through layered media, comprising the ABR, urine region and PBR, using a time-domain implementation of the KZK-equation. Pulse-echo responses were

obtained from a flat reflector situation and scatter phantoms using the spatial impulse responses at the particular scatter position and frequency dependent loss of the backward propagation path. A non-diverging acoustic beam was used because of the limitations of the KZK implementation. The effect of a diverging acoustic beam on the performance of the computational methods should be studied with an alternative simulation model, which does not use the parabolic approximation (Huijssen et al., 2003), with *in vitro* and *in vivo* measurements.

The simulations showed that the generated harmonics within the anterior bladder wall affect the 2HFR measured in the posterior bladder domain. This influence is emphasized by the additional acoustic loss in this region for the reflected waves. It is likely that the size of the ROI influences the variations observed in the UPL estimates and that a trade-off must be found between sensitivity and variations (Li et al., 1997). A larger ROI averages a larger part of the RF envelope and hence will reduce the temporal variations. However, the sensitivity of the algorithms will be reduced. Reducing the ROI size consequently increases the temporal variations. Also, the chosen location of the ROI affects the estimate.

It is interesting to note that from the results of the scatter phantom simulations it is observed that the methods with variable ROI locations, i.e. algorithms A2 and A4, have 2HFR curves with changing standard deviations over distance. This is explained by the changes in resolution cell sizes over depth, and is closely related to the changing point spread function and loss. It is observed in 2D-echo images as speckle size variations over depth, mainly in the lateral direction (Thijssen and Oosterveld, 1986; Wagner et al., 1983). This also explains the constant relative standard deviations observed with algorithm A1 and A3, where the ROI location was fixed. With respect to the stochastic scattering of the scatter phantoms it can thus be concluded that the variations completely depend on the transducer characteristics and not so much on the algorithm used.

Significant differences were found between the results from pulse-echo simulations on a flat reflector and the scatter phantom results. These differences can be explained by the coherent scattering from a plane parallel to the transducer for flat reflector simulations versus the non-coherent scattering from a ROI, with 10 times the size of a resolution cell, for the scatter phantom simulations. The results from algorithm A1 showed the smallest differences between the two simulation settings. Because the ROI selected by algorithm A1 is situated in the acoustic far field, phase differences from the scattered waves become smaller, approaching the coherent scattering on a flat reflector. This in contrast with the other algorithms, which use (additional) ROIs located in the acoustic near field.

From the four proposed algorithms, A1, i.e. selecting the ROI at a fixed location in the PBR, gave the best estimation of the UPL present within an unfocused acoustic beam. The 2HFR calculated with A1 showed the highest sensitivity for the UPL and it had lowest sensitivity to the variability of the ABR. Consequently, applying a correction for the ABR, i.e. algorithm A3, was not necessary. In contrast with the other 3 algorithms, it does not depend on the performance of a detection method to determine the location of the anterior and posterior ROI. This is considered to be a big advantage.

In conclusion, this simulation study gave good insight on the effect of patient variability, transducer configuration and, most importantly, the algorithm used, on the 2HFR-bladder volume relationship.

Chapter 5

Quantitative Bladder Volume Assessment: First *In Vivo* Results

Based on:
 Merks E.J.W., Bom N., van der Steen A.F.W., and de Jong N. Quantitative Bladder Volume Assessment on the Basis of Nonlinear Wave Propagation. *IEEE Ultrasonics Symposium Proceedings*, pages 1158-1162, 2008.

Abstract-Catheterization remains the gold standard for bladder volume assessment, but it is invasive, uncomfortable to the patient, and introduces the risk of infections and trauma. To reduce the need for a urinary catheter, a new method has recently been introduced that noninvasively and instantaneously measures the bladder volume on the basis of nonlinear wave propagation and using a single diverging acoustic beam. The performance of the original computational method to quantitatively measure volume was compared with an alternative algorithm using simulations on nonlinear wave propagation and *in vivo* measurements. Measurements were performed with an experimental setup including a custom designed multilayer transducer.

5.1 Introduction

Acoustic bladder volume measurement is clinically relevant as it reduces the need for a urinary catheter and the likelihood of urinary infections (Slappendel and Weber, 1999). A new method has recently been introduced that non-invasively and instantaneously measures the bladder volume on the basis of nonlinear wave propagation and using a single diverging acoustic beam (Bouakaz et al., 2004; McMorrow et al., 2002). Given a much stronger nonlinear behavior for urine than for tissue, it should be possible to find a relationship between the 2^{nd} Harmonic-to-Fundamental Ratio (2HFR), present within echoes received from a Region of Interest (ROI) behind the posterior bladder wall, and the amount of urine present within the diverging acoustic beam (Figure 5.1).

Previously obtained results from using a fast-rotating phased array probe proved the feasibility of the new method. A 15 dB increase of the 2^{nd} harmonic frequency was observed *in vitro* on a 500 ml bladder phantom with respect to a tissue-only phantom. Initial *in vivo* measurements on a bladder containing 450 ml urine showed an increase of 10 dB at the 2^{nd} harmonic frequency compared to an empty bladder (Bouakaz et al., 2004).

The objective of this study is to replace the advanced phased array probe and system with a simple transducer that generates a single diverging acoustic beam. This paper will concentrate on the calculation method, or algorithm,

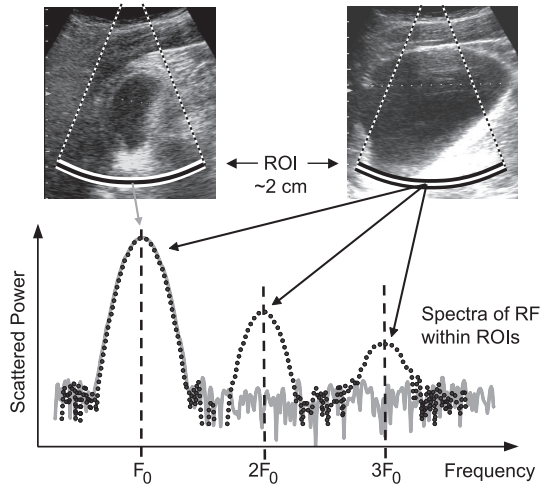

Figure 5.1: Principle of bladder volume measurements on the basis of nonlinear wave propagation. With the patient in supine position and a single element transducer producing a diverging acoustic beam, the bladder volume is obtained from spectral analysis on a fixed region of interest behind the bladder.

that quantitatively relates the spectral contents of the received RF-data to the insonified volume.

As will be shown in this paper, the amount of harmonics present within the received echoes strongly depends on the bladder shape. Especially the size of the anterior bladder region (ABR) has significant effect on the 2^{nd} Harmonic-to-Fundamental Ratio (2HFR) observed in the posterior bladder region (PBR). Hence, besides giving a good estimation of the urine volume present within the acoustic beam, the algorithm to be used must also be insensitive to patient variability and bladder shape.

5.2 Materials and methods

The computational method of the original concept was compared with an alternative algorithm using simulations on nonlinear wave propagation and *in vivo* volunteer measurements.

5.2.1 Nonlinear wave propagation simulations

The simulations included the modeling of nonlinear wave propagation through layered media using a time-domain implementation of the Khokhlov-Zabolotskaya-Kuznetsov (KZK) equation (Lee and Hamilton, 1995). The layered media comprised the anterior bladder region (ABR), a urine region and a posterior bladder region (PBR). Pulse-echo responses were obtained from a flat reflector, while preserving the layered media, and scatter phantoms using the spatial impulse responses at the particular scatter positions and frequency dependent loss of the back propagation path. The method of calculation was adapted from (Frijlink et al., 2006). The KZK equation becomes less valid for regions close to the source and for angles (20 degrees) far off the transducer axis (Averkiou and Hamilton, 1997). Hence, as a first approach, only unfocused sound fields were simulated and urine path lengths (UPLs) were modeled instead of volumes. Two different simulation situations were investigated and defined as:

1. Increasing UPL with constant ABR. The urine region was increased in length from 0 to 8 cm with steps of 1 cm. The ABR was kept constant at 4 cm.
2. Increasing ABR size with constant UPL. The anterior wall distance was varied from 3 to 8 cm. The UPL was kept constant at 4 cm.

5.2.2 *In vivo* volume measurements

Pulse-echo measurements were performed on a healthy volunteer to obtain a specific relationship between the bladder volume and the measured 2HFR. In

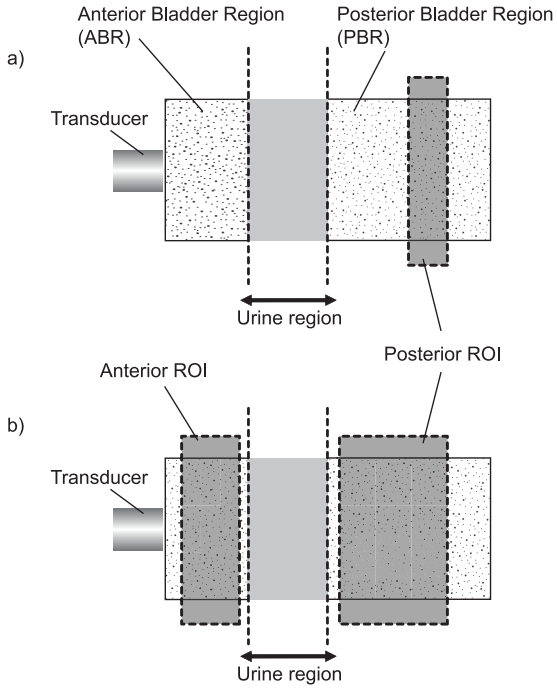

Figure 5.2: The original (a) and alternative (b) computational schemes to obtain the urine path length (UPL) present within the propagation path from pulse-echo data.

total, 3 measurement sets were acquired, with each set containing at least 7 intermediate points. The intermediate measurements included a set of 3 BladderScan® reference measurements (BVI6400, Verathon Inc., Bothell, WA, USA), a set of 10 RF recordings with random probe alignment and the voided volume. The following protocol was used:

- Starting with a full bladder, i.e. a strong urge to void:
  1. Measure the volume with the BladderScan (N=3),
  2. Record RF-signals (N=10),
  3. Void ∼100 ml,
  4. Record real voided volume.
- This cycle was repeated until the bladder was empty.

Algorithm definition

With the algorithm of the original concept (Figure 5.2a), a ROI with length of 2 cm is selected in the PBR at a fixed depth of 14 cm from the transducer surface. Within the selected ROI, the 2HFR was calculated as:

$$2HFR = \frac{1}{N} \sum_{n=n_0}^{N} \frac{H2\,(n)}{F1\,(n)}, \tag{5.1}$$

where F1 and H2 are the envelopes of the RF filtered at the fundamental and 2nd harmonic frequencies, respectively. The alternative algorithm (Figure 5.2b) also uses a ROI in the ABR in addition to the ROI in the PBR. The ROI sizes were variable and the 2HFR was defined as:

$$2HFR_{P-A} = \frac{1}{N_P} \sum_{n=P_0}^{P_T} \frac{H2\,(n)}{F1\,(n)} - \frac{1}{N_A} \sum_{n=A_0}^{A_T} \frac{H2\,(n)}{F1\,(n)}, \tag{5.2}$$

where the first term on the right side is the mean 2HFR of the ROI in the PBR and the second term is related to the mean 2HFR of the ROI selected in the ABR.

Measurement system

The measurement system used with the *in vivo* volume measurements is schematically shown in Figure 5.3. A laptop computer was used to control a PC-based oscilloscope (Handyscope 3 (HS3), Tiepie Engineering, the Netherlands) equipped with an arbitrary waveform generator (AWG) and USB 2.0 interface. The AWG was used to generate a Gaussian modulated 15-cycle sine wave burst with 2.1 MHz center frequency. To remove unwanted frequency components generated by the AWG, this signal was bandpass filtered before amplification by a power amplifier (model 150A-100B, Amplifier Research, EMV Benelux B.V., the Netherlands). A passive 9^{th} order high-power Butterworth low-pass filter with cut-off frequency at 2.5 MHz was used between the amplifier and the transducer to avoid transmitting harmonic frequency components.

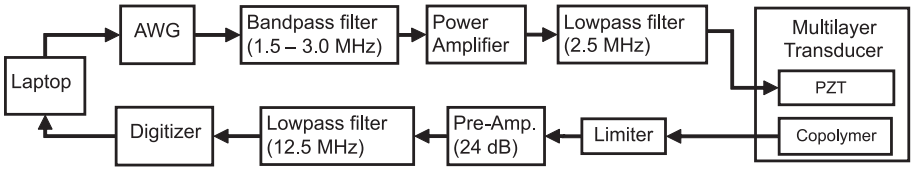

Figure 5.3: Experimental measurement system.

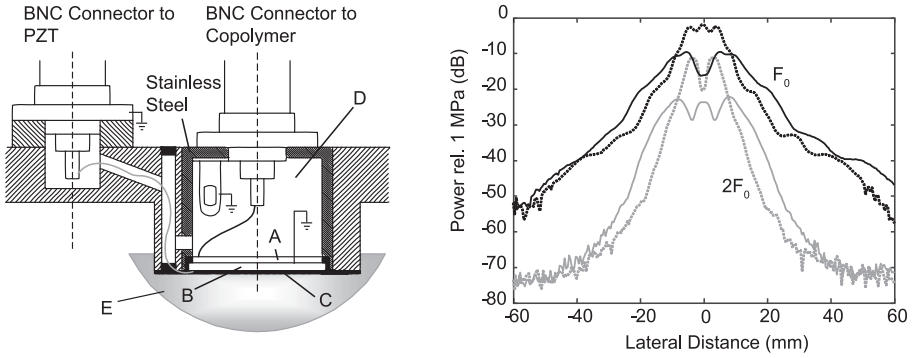

Figure 5.4: Transducer schematics and measured lateral pressure distributions. Left: Schematics of the multilayer transducer, with a copolymer layer for broadband reception (A), a PZT element for transmission (B), a matching layer (C), air-backing (D) and the acoustic lens (E). Separate BNC connectors were used for both active elements. Right: Measured lateral pressure distributions, at axial distance of 90 mm, with (solid) and without (dotted) acoustic lens (with ROC of 35 mm) applied at the fundamental frequency (black) and the 2^{nd} harmonic (gray).

In reception, a limiter was used to prevent a custom built pre-amplifier with 24 dB signal gain from saturation. A lowpass filter with cutoff frequency at 12.5 MHz was used to avoid aliasing. Data-acquisition was performed at a sampling frequency of 50 MHz and 12-bit resolution. Each of the acquisitions contained 100 RF-traces (for averaging) and a single noise-reference measurement.

Custom multilayer transducer

A custom built multilayer transducer (Figure 5.4) was used that has high transmit sensitivity as well as broadband receive characteristics (Merks et al., 2006b, 2009). It consisted of a 1 mm thick PZT disc (PXE 5, Morgan Electro Ceramics B.V., the Netherlands) stacked with a 100 μm thick Copolymer film (Precision Acoustics, UK). The complete stack has a diameter of 20 mm. Air-backing was used to achieve high transmit sensitivity. An acoustic matching layer was applied to match the acoustic impedance of PZT to that of the lens. The PZT element was used for the transmission of acoustic waves at the fundamental frequency (2.1 MHz) and the copolymer film was used for broadband reception (1 MHz - 8 MHz). The transmit sensitivity was sufficient to cause significant nonlinear wave propagation. The receive sensitivity and bandwidth allowed for proper acquisition of the fundamental frequency up to at least the 3^{rd} harmonic frequency component in the reflected signals (Merks et al., 2009).

The defocusing acoustic lens was applied to the transducer surface to create

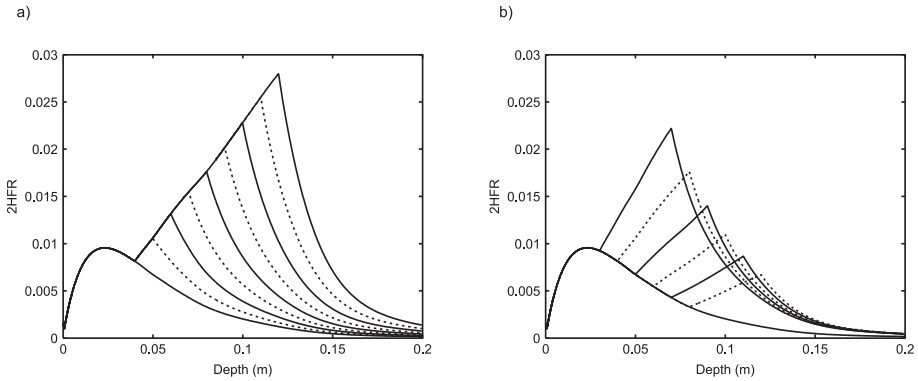

Figure 5.5: Simulated 2HFR obtained in pulse-echo on a flat reflector, as function of distance for (a) situation 1 (Increasing UPL with constant ABR.) and for (b) situation 2 (Constant UPL with increasing ABR.).

the diverging acoustic beam. The right part of Figure 5.4 shows the lateral pressure distributions measured with a calibrated hydrophone at axial distance of 90 mm. Without the lens applied, the -6 dB beamwidth was 16.4 mm at the fundamental frequency. With the lens applied the distribution showed a beamwidth of 31.3 mm. The pressure amplitude dropped with approximately 6 dB and 12 dB for the fundamental frequency and 2^{nd} harmonic, respectively.

5.3 Results

5.3.1 Nonlinear wave propagation simulations

Figure 5.5 shows the results of the pulse-echo simulations on a flat reflector as it was gradually stepped through the layered media. The 2HFR as function of depth for the situation of increasing UPL and constant ABR is shown in Figure 5.5a. The ABR was located from 0 to 4 cm. The UPL was increased from 0 to 8 cm with steps of 1 cm. The harmonic content was calculated by taking the maximum envelope value of the pulse-echo response at each depth. The 2HFR curve for the tissue-only situation shows an increase up to 2 cm, from where the attenuation dominates the nonlinear propagation. With a urine region starting at 4 cm, the nonlinearity dominates the loss and the curves show an increase of harmonic contents. After the urine region, loss again dominates the nonlinear wave propagation. As the 2^{nd} harmonic is attenuated more than the fundamental, the 2HFR curves show a strong exponential decay. The computed 2HFR as function of distance for the situation of an increasing ABR and constant UPL (4 cm) is shown in Figure 5.5b. The ABR was initially

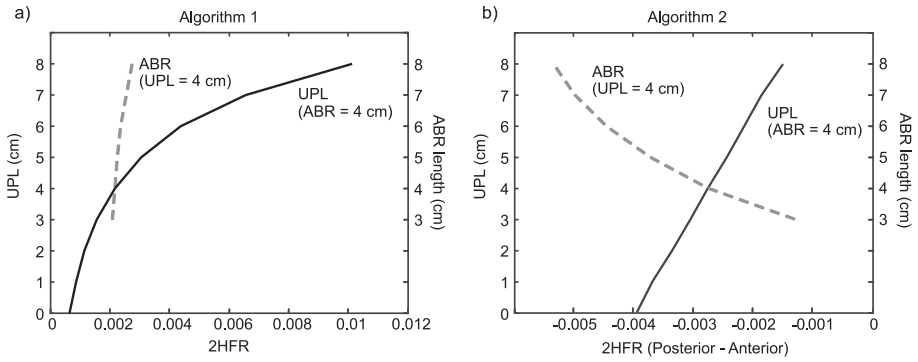

Figure 5.6: Simulation results for Eq. 5.1 (a) and Eq. 5.2 (b). Different UPL (solid lines) and ABR lengths (dashed lines) were simulated.

located between 0 and 3 cm and was increased to 8 cm with steps of 1 cm. Due to the attenuation in the ABR, the different 2HFR curves of Figure 5.5b show a decreasing positive slope in the urine regions with increasing ABR.

Figure 5.6 shows the results of Eq. 5.1 and Eq. 5.2 applied to scatter phantom models. The UPL and ABR lengths are shown as function of the 2HFR. The ability to determine the UPL should be seen relative to the sensitivity to patient variability and bladder shape over the complete 2HFR range. Ideally, the 2HFR range that covers the UPL range should be large compared to the 2HFR range related to the ABR lengths. From Figure 5.6a it is clear that Eq. 5.1 best fulfills this requirement. Here the ABR-curve is almost insensitive to the 2HFR, while the UPL curve increases exponentially with increasing 2HFR. Eq. 5.1 shows a linear relationship between the UPL and 2HFR, but it does show a significant sensitivity to changing ABR. When, for example, the ABR varies between 3 and 5 cm, Eq. 5.1 still calculates the UPL at approximately 4 cm, whereas Eq. 5.2 gives and UPL between 0 and 8 cm.

5.3.2 *In vivo* volume measurements

In total, 3 separate measurement cycles were recorded on the same volunteer. Volumes between 0 and 600 ml with steps of 100 ml were measured. Prior to the application of the algorithms, the RF-data were first bandpass filtered at the fundamental frequency (2.1 MHz) and the 2^{nd} harmonic (4.2 MHz) using a 3^{rd} order Butterworth filter with transmission bandwidth of 1 MHz. Figure 5.7 shows the obtained 2HFR curves for Eq. 5.1 and Eq. 5.2 as function of the recorded BladderScan reference data. The errorbars indicate the standard deviations around the mean of the 10 RF recordings.

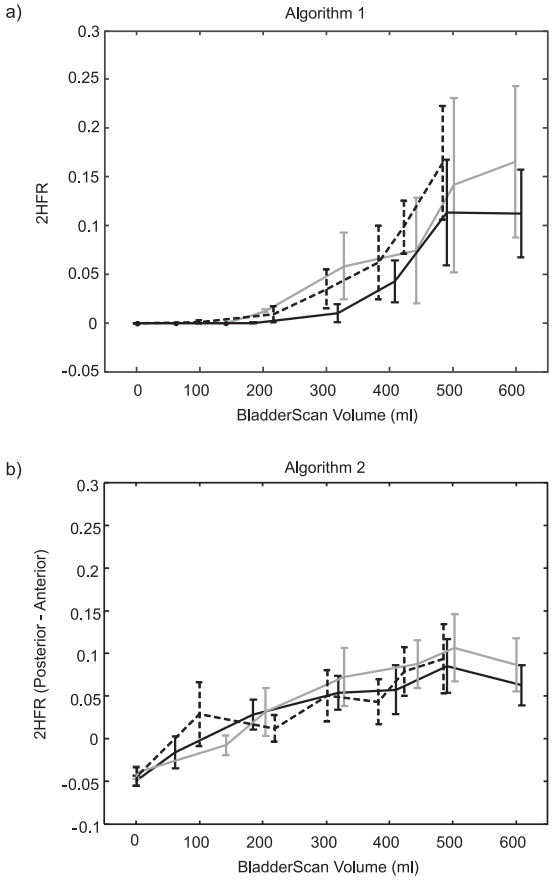

Figure 5.7: Measurement results for Eq. 5.1 (a) and Eq. 5.2 (b) as function of BladderScan reference measurements. The ROIs needed for (2) were manually selected. Only parts of the RF with sufficient signal-to-noise ratio (SNR) were included in the ROI.

It is observed that the curves flatten at volumes above 500 ml. This is explained by the limited width of the acoustic beam with respect to the bladder dimensions. Because of the low SNR at the fixed ROI location with small bladder volumes, the 2HFR curves for Eq. 5.1 show an onset at approximately 150 ml. Also, because Eq. 5.1 generally uses a smaller ROI, the standard deviations observed with Eq. 5.1 are larger than those observed with Eq. 5.2. It can be appreciated that, for both algorithms, the three individual curves are very similar. This indicates the high repeatability of the measurements and methods.

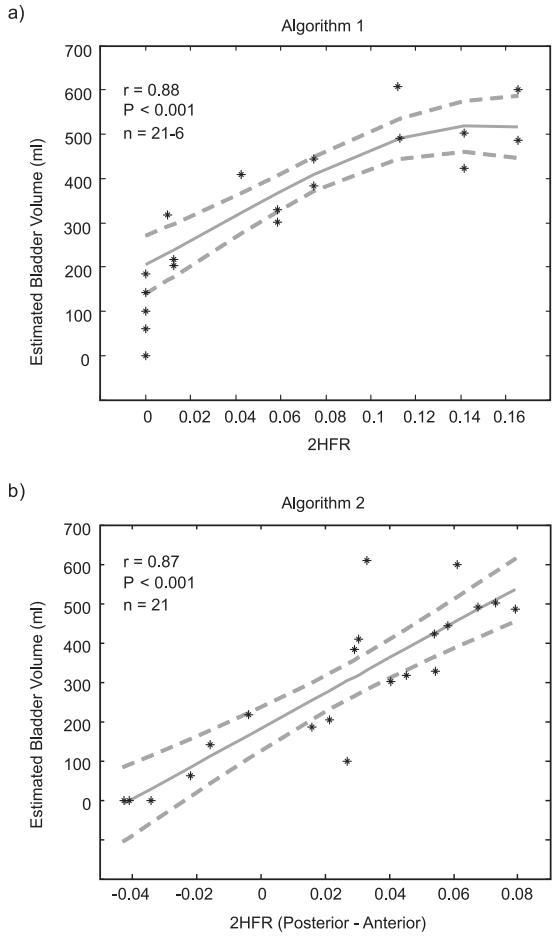

Figure 5.8: Volume estimation using Eq. 5.1 (a) and Eq. 5.2 (b). Polynomial fits (solid lines) and 95% Confidence Intervals (dashed lines) are shown.

Finally, the three separate datasets were used as one larger set. The Pearson's correlation coefficients between the bladder volume and the 2HFR obtained from Eq. 5.1 and Eq. 5.2, were 0.88 and 0.87, respectively, with P-values <0.001. Polynomial fitting was used to deduce the quantitative relationships between the insonified volume and the 2HFR (Figure 5.8). The best fit for the volume estimation function, in liters, as function of 2HFR for Eq. 5.1 was found as:

$$\hat{V} = e^{\left(\alpha \cdot 2HFR^2 + \beta \cdot 2HFR + \gamma\right)},$$
$$\text{with} \tag{5.3}$$
$$\alpha = -40.6,\ \beta = 12.3 \text{ and } \gamma = 5.32.$$

The volume estimation function, in liters, as function of $2HFR_{P-A}$ for Eq. 5.2 was found as:

$$\hat{V} = \alpha \cdot 2HFR_{P-A} + \beta,$$
$$\text{with} \tag{5.4}$$
$$\alpha = 4.42 \text{ and } \beta = 0.18.$$

Figure 5.8 also shows the 95% confidence intervals for the fits. Again, it can be seen that the fits are less accurate at larger volumes. Because of the on-set at low volumes for Eq. 5.1 six datapoints with 2HFR = 0 were not included in the fitting.

5.4 Discussion and conclusion

Both evaluated algorithms allowed for quantitative bladder volume assessment on the basis of nonlinear wave propagation *in vivo*. From simulations, Eq. 5.1 showed to be the least sensitive to patient variability and bladder shape, and does not require additional bladder detection as with Eq. 5.2. However, Eq. 5.2 showed better sensitivity at low volumes with *in vivo* measurements. The measurement results showed a high repeatability for both algorithms, but large volumes could not be measured accurately due to beamwidth limitations.

Acknowledgments

The authors would like to thank Verathon Medical Europe B.V. (IJsselstein, the Netherlands) for their constructive support and for providing the BVI 6400.

Chapter 6

Patient Safety

The previous chapters discussed the development and application of the bladder volume assessment method on the basis of nonlinear ultrasound. A substantial part covered the design of a dedicated transducer. The goal was to obtain a high sensitivity in transmission such that significant nonlinear wave propagation could be induced. Also, a good sensitivity and bandwidth in reception was required to be able to detect the higher harmonic frequency components with sufficient signal-to-noise ratio (SNR). It was shown that a high transmit sensitivity, together with a high drive amplitude, could induce significant nonlinear wave propagation. Additionally, it was suggested that, when the SNR of the received echoes was too low, the drive amplitude should be increased. However, besides the limitations of the driver circuits to increase the drive amplitude, the limitations with respect to patient safety should also be considered. This chapter focuses on patient safety and discusses the new method of bladder volume assessment with respect to the safety regulation limits.

6.1 Introduction

Many studies have addressed the interaction of diagnostic ultrasound with biological tissue. Although there are no confirmed biological effects on patients caused by exposures from present diagnostic ultrasound instruments, the possibility exists that, due to new ultrasound techniques, such biological effects may be identified in the future (Barnett et al., 2000). The method of bladder volume assessment described in this thesis qualifies as such a "new" ultrasound technique, and thus it is essential to determine if this method complies with the given safety regulation limits.

6.1.1 Safety regulation

The U.S. Food and Drug Administration (FDA) initiated the regulation of diagnostic ultrasound in terms of application-specific acoustic intensity limits (Table 6.1). These intensity limits were not based on extensive knowledge of biological effects on patients, but were based on the output capabilities of diagnostic ultrasound systems that were on the market in the late-70s. As, up till then, no biological effects had been observed, the output capabilities of those systems were considered as "safe."

Because of the development of new technology and new image modalities, like Pulsed Doppler, modern ultrasound systems are capable of producing acoustic output levels that exceed the FDA limits as given in Table 6.1. Therefore, the FDA allowed relaxation of these limits provided that the systems are equipped with an output display that can inform the user on the potential of producing biological effects (Barnett et al., 2000).

So far, mechanical and thermal mechanisms have been identified by which ultrasound may induce bioeffects. The American Institute of Ultrasound in Medicine (AIUM) and the National Electrical Manufacturers Association (NEMA) have developed the "Standard for real-time display of thermal and mechanical acoustic output indices on diagnostic ultrasound equipment", also known as the "output display standard" (ODS). This standard provides the means for calculation of acoustic output parameters that are related to the potential of these biological effects. Although the ODS does not specify upper limits to exposure levels, the FDA regulates an upper limit of 720 mW/cm^2 for the derated spatial peak temporal average intensity ($I_{SPTA.3}$) for all applications but the ophthalmic (50 mW/cm^2).

The two biophysical indices given by the ODS are the Mechanical Index (MI) and the Thermal Index (TI). The TI provides information about tissue temperature increase, and the MI provides information about the potential for cavitation. Some international recommendations and guidelines for the safe use of diagnostic ultrasound in medicine with respect to the thermal and mechanical effects are listed in Table 6.2.

Table 6.1: Application-specific acoustic intensity limits given by the FDA. Intensity is derated by 0.3 dB/MHz/cm to compensate for the attenuation by the tissue-path. (O'Brien and Ellis, 1999)

Application	Derated Intensity Values		
	I_{SPTA} (mW/cm^2)	I_{SPPA} (W/cm^2)	I_{m} (W/cm^2)
Cardiac	430	190	310
Peripheral vessel	720	190	310
Ophthalmic	17	28	50
Fetal, abdominal	94	190	310

Table 6.2: A selection of the published recommendations for the safe use of diagnostic ultrasound. (Barnett et al., 2000)

	Thermal effects	Mechanical effects
WFUMB	Temperature rises $\leq$ 1.5°C (38°C) can be used without reservation. Obstetric exposures resulting in a temperature increase of 4°C for 5 min. are potentially hazardous.	When gas (including contrast agents) is present exposure levels and duration should be reduced to the minimum to obtain required information.
AIUM	At the FDA regulatory limit ($\mathrm{I_{SPTA.3}}$ = 720 mW/cm^2) the maximum temperature increase in the conceptus can exceed 2°C.	The threshold value of MI for extravasation of blood cells in mouse lung is approximately 0.3.
ASUM	As per WFUMB + Effects of heating reduced by minimizing duration of exposure. Duplex/Doppler in febrile patients may present additional risk to the fetus or embryo.	Presence of contrast agents should be considered in benefit/risk assessment of ultrasound examinations. Minimize transmit power.
ODS/FDA	FDA does not regulate TI. For general use, TI should be $<$ 6.	For general use, MI should be $<$ 1.9.

6.1.2 Mechanical Index (MI)

Cavitation is the effect of bubble formation caused by the rarefactional phase of the pressure wave. The likelihood of cavitation increases as the peak negative pressure increases, and decreases as the wave frequency increases. Holland and Apfel (1990) described *in vivo* experiments on the behavior of cavitation bubbles and, in particular, the biological effects caused by cavitation. They found that cavitation is in fact a threshold effect. This means that cavitation or any other mechanical effect is not likely to occur unless some output level is exceeded. The mechanical index is expressed as:

$$MI = \frac{p_r}{C_{\mathrm{MI}}\sqrt{f_c}}, \tag{6.1}$$

where p_r is the derated peak negative pressure (in MPa), and f_c the center frequency (in MHz). $\mathrm{C_{MI}}$ is a constant equal to 1 $\mathrm{MPa \cdot MHz}^{-1/2}$ by which the expression of MI remains dimensionless. It must be noted that the given expression does not include the effect of nonlinear wave propagation. It was found that the value of the effective MI, taking in account the nonlinear wave propagation, is much below the value of the MI computed under the assumption of linear wave propagation (Humphrey, 2000). Hence, in order to consider a worst-case configuration, it is reasonable to calculate the MI assuming linear wave propagation.

6.1.3 Thermal Index (TI)

The second biological effect to consider in terms of safety is the heating induced by wave propagation. Wave propagation through tissue is accompanied by absorption and attenuation. The acoustic energy is converted to heat which may lead to a temperature increase of the tissue. A large heat gradient can induce burns, but low rise of temperature can have important consequences as the risk of adverse effects increases with longer exposure times. The Thermal Index has been introduced by the ODS to estimate the harmful effect appearance due to temperature elevation. In general, the TI is defined as:

$$TI = \frac{W_0}{W_{\mathrm{DEG}}}, \tag{6.2}$$

where W_0 is the source power of the ultrasound system (in Watt), and W_{DEG} is the source power necessary to raise the temperature of the targeted tissue with 1°C. Three different Thermal Indices were developed to address three different tissue models and two different scan modes. A comprehensive overview and derivation of these indices can be found in a review by Abbott (1999). The most appropriate TI for the method of bladder volume assessment is the “soft-

tissue thermal index" (TIS), which was derived for the Doppler and B-mode applications and is expressed as (Abbott, 1999):

$$TIS = \frac{W_0 f}{C_{\mathrm{TIS1}}}, \quad \text{when A} \leq 1 \text{ cm}^2 \tag{6.3}$$

$$TIS = \max_{z>1.5D_{eq}} \left[\min \left[\frac{W_{.3} f}{C_{\mathrm{TIS1}}}, \frac{I_{\mathrm{SPTA.3}} f}{C_{\mathrm{TIS2}}} \right] \right], \quad \text{when A} > 1 \text{ cm}^2 \tag{6.4}$$

where $\mathrm{C_{TIS1}} = 210 \text{ mW} \cdot \text{MHz}$ and $\mathrm{C_{TIS2}} = 210 \text{ mW} \cdot \text{MHz} \cdot \text{cm}^{-2}$.

Clearly, a difference is made between apertures with equivalent beam area (A) larger than 1 cm^2 and apertures with A $\leq$ 1 cm^2. In cases when A $\leq$ 1 cm^2 (Eq. 6.3), the temperature increase is controlled by the source power (W_0). In cases when A $>$ 1 cm^2 (Eq. 6.4), the temperature increase is controlled by either the derated output power ($W_{.3}$) or the attenuated spatial-peak temporal average intensity across 1 cm^2 ($\mathrm{I_{SPTA.3}} \cdot 1\text{cm}^2$). To avoid inaccuracies introduced by the intensities measured in the acoustic near field, Eq. 6.4 states that the distance (z) should be larger than 1.5 times the equivalent aperture diameter (D_{eq}).

Acoustic attenuation or loss is known to be frequency dependent, i.e. an increase in frequency causes higher absorption of acoustic energy into the medium. In the case of nonlinear wave propagation, the generated higher harmonics might thus enhance the heat production (Divall and Humphrey, 2000). However, the actual additional effects of the generated higher harmonics on the heat production is unclear. In a recent paper from the World Federation of Ultrasound in Medicine and Biology (Barnett et al., 2000), it was mentioned that the production of higher harmonics due to nonlinear propagation is not properly addressed in calculations of the AIUM/NEMA safety indices. The temperature increment indication provided by the Thermal Index (TI) may significantly underestimate (or overestimate) the actual temperature elevation. Therefore, a conservative approach would be to assume that the temperature increment in tissue is at least as large as the numerical value of the TI and may be higher (Barnett et al., 2000).

With respect to bladder volume assessment on the basis of nonlinear wave propagation, it can thus be stated that, in contrast with the MI, the TI does not represent the worst-case situation. To still be able to determine if the bladder volume assessment method is safe in terms of thermal effects (Table 6.2), temperature simulations and measurements have been performed. These will be described in the following sections.

6.2 Materials and methods

The setup for bladder volume assessment on the basis of nonlinear ultrasound uses a defocused transducer to encompass a large part of the bladder. Hence, the energy dissipation is widely diffused in the media. With this safety study, the worst-case situation is defined, in which both simulations and measurements were done using an unfocused transducer. The deposition of energy thus remains within a much narrower beam, and consequently will induce a higher rise of temperature.

6.2.1 Temperature simulations

To model the temperature elevation induced by ultrasound, the bio-heat transfer equation is used to combine the processes of absorption, medium perfusion and heat conduction via:

$$\frac{dT}{dt} = \kappa \nabla^2 T - \frac{\Delta T}{\tau} + \frac{q_v}{c_v} \tag{6.5}$$

where q_v is the heat source function (the rate of heat production per unit volume), ΔT the temperature rise above the ambient level, κ the thermal diffusivity, τ the time constant for perfusion and c_v is the heat capacity per unit volume of the medium.

The solution to the bio-heat transfer equation, as given by Nyborg (1988), was used to simulate the temperature rise from simulated Root-mean-square (RMS) pressure distributions. The beam profiles were obtained from linear simulations using Field II (Jensen, 1996), and from nonlinear simulations using the time-domain implementation of the KZK-equation (Lee and Hamilton, 1995). The temperature elevation for a point source of heat is given by Nyborg (1988) as:

$$\begin{aligned} \Delta T &= \frac{C}{r}\left(E\left[2 - erfc\left(t^* - R\right)\right] + E^{-1} erfc\left(t^* + R\right)\right) \\ &\text{with} \\ C &= \frac{q_v dv}{8\pi K} = \frac{\alpha I_{TA} dx dy dz}{4\pi K} \\ E &= \exp\left(-r/L\right) \\ L &= \sqrt{\kappa\tau} \\ t^* &= \sqrt{t/\tau} \\ R &= r/\sqrt{4\kappa\tau} = r/2L \end{aligned} \tag{6.6}$$

where r is the distance to the point source, L is the perfusion length and *erfc* the complement of the error function. The thermal conductivity K differs from κ by the factor c_v ($K = c_v \cdot \kappa$).

After a sufficiently long time (t >1000 sec), the *erfc* in Eqn. (6.6) reduces to zero, and the steady state temperature increase for each point source is given as:

$$\begin{aligned} \Delta T &= \frac{2C}{r} \exp\left(-r/L\right) \\ &\text{with} \\ r &= \sqrt{x^2 + z^2} \end{aligned} \tag{6.7}$$

Obviously, the temperature rise in tissue is time dependent. For a short time (< 100 s), the temperature increase is considered as a linear function of time (Nyborg, 1988):

$$\Delta T = 2\alpha I_{SATA}\left(z\right) \cdot t/c_v \tag{6.8}$$

where α is the absorption coefficient, $c_v = 4.184$ J/cm^3°C and $\mathrm{I_{SATA}}(z)$ the spatial average temporal average intensity value at a distance z from the transducer.

As each point source corresponds to a cubic volume containing q_v, the temperature distribution can be defined, using the superposition principle, as the sum of contributions from each point source.

Under the assumption of linear propagation, q_v is defined as $2\alpha \cdot I_{\mathrm{TA}}$, where α is the absorption coefficient (Np/MHz/m). $\mathrm{I_{TA}}$ is the "temporal average intensity", which is the power contained by a small area expressed in Watt. $\mathrm{I_{TA}}$ can be calculated from the pressure distribution as $\mathrm{I_{TA}} = p_{rms}^2/Z$, where Z is the acoustic impedance of the medium.

When nonlinear wave propagation is considered, it is assumed that the temperature calculation can be formulated as a sum of the harmonic contributions $q_v(n) = 2\alpha(n) \cdot I_{TA}(n)$, with n corresponding to the n^{th} harmonic. The total temperature elevation will then be the sum of temperature contributions from every harmonic beam.

6.2.2 Temperature measurements

Temperature elevation as function of time

The temperature simulations were validated by measuring the temperature increase inside a Tissue Mimicking phantom (TMM), while it was insonified by a Panametrics V306 unfocused transducer (Figure 6.1). Sinewave bursts of 20

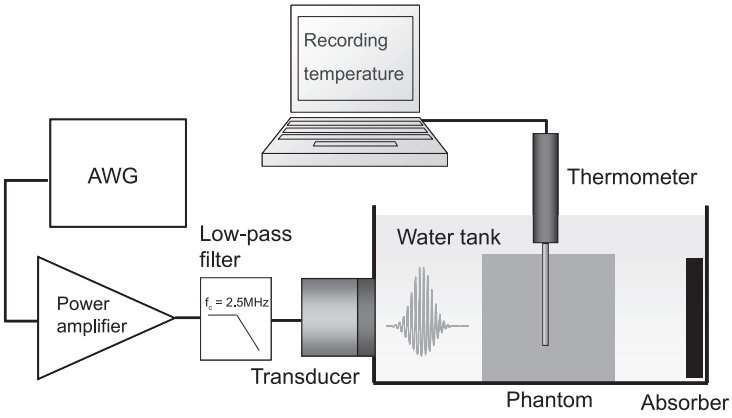

Figure 6.1: Experimental setup for the validation of the model.

cycles with centre frequency of 1.8 MHz and a duty cycle of 20% were used to ensure sufficient energy deposition at the phantom, such that it could be measured by a standard digital thermometer. The accuracy of the digital thermometer (Vernier Software and Technology, Beaverton, OR) was 0.07 K. The setup (Figure 6.1) also shows an additional low-pass high-power Butterworth filter with cut-off frequency at 2.5 MHz. This was used to avoid the transmission of the harmonic components by the transducer (Merks et al., 2006b).

Temperature distribution

A second set of temperature measurements was performed to determine the effect of an acoustic lens on the steady state temperature distribution. Two measurements were performed, each after 45 minutes of insonification, with and without the application of an acoustic lens made of Rexolite (Goodfellow Cambridge Ltd., UK) with a radius of curvature (ROC) of 35 mm. Reference temperature measurements were also taken prior to the 45 minutes. The same system and transmit settings were used as with the temperature elevation measurements. In contrast with the measurements on temperature elevation, where the temperature was measured at only one fixed location, temperatures were now recorded at several grid locations. The distance between gridpoints was defined as 5 mm in the lateral direction and 10 mm in the axial direction of the transducer. To mimic the effect of the abdominal wall on the temperature increase in the posterior bladder region, two phantoms were used. The first phantom had dimensions of approximately 2x10x10 cm and was placed against the transducer surface. The second phantom had dimensions of approximately 17x10x10 cm and was placed at a total distance of 7 cm from the transducer, leaving a waterpath of 5 cm between the two phantoms.

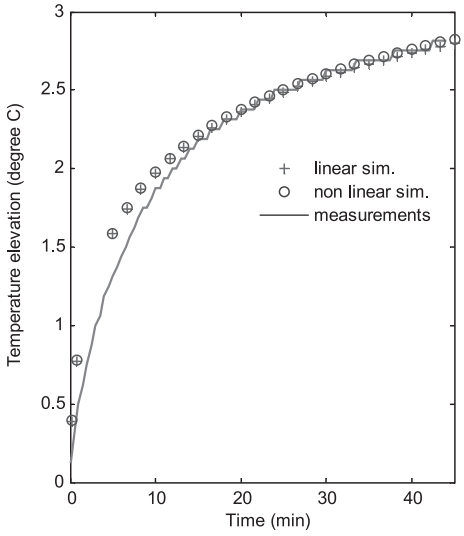

Figure 6.2: Measured and simulated time dependency of the rise of temperature in a tissue mimicking phantom.

6.3 Results

Temperature elevation as function of time

The pressure at the transducer surface was estimated at 200 kPa, the transmit pulse was a 20-cycle sinewave burst with a 20% duty cycle. The measured and simulated time dependency of the rise of temperature is plotted in Figure 6.2. The thermometer was positioned at the location where the simulated maximum rise of temperature was expected. The same power settings were used for the simulation. The thermal diffusivity of the phantom used was measured to be 12 times smaller than the thermal diffusivity of tissue. The acoustical attenuation coefficient of the phantom used with the measurements was measured to be 50 dB/m at 1.8 MHz. Figure 6.2 clearly shows that, with this setup, the harmonic contribution to the temperature increase was not significant.

Temperature distribution

The measured temperature distributions after 45 minutes of insonification, with and without the application of an acoustic lens, are shown in Figure 6.3. The maximum temperature increase in the posterior phantom after 45 minutes was 2.9°C without lens, and was only 1.3°C when the acoustic lens was applied. Both results are below the recommended safety limit of 4°C. With the lens applied, the temperature distribution has approximately twice the width of

the no-lens situation. More importantly, the application of an acoustic lens reduced the temperature increase with about a factor of two. Another effect that can be observed from Figure 6.3 is the rather large temperature increase in the anterior phantom close to the transducer. Without lens, the maximum is found to be 8.4°C. This was not observed with the temperature simulations. Most likely, this temperature increase was due to transducer heating.

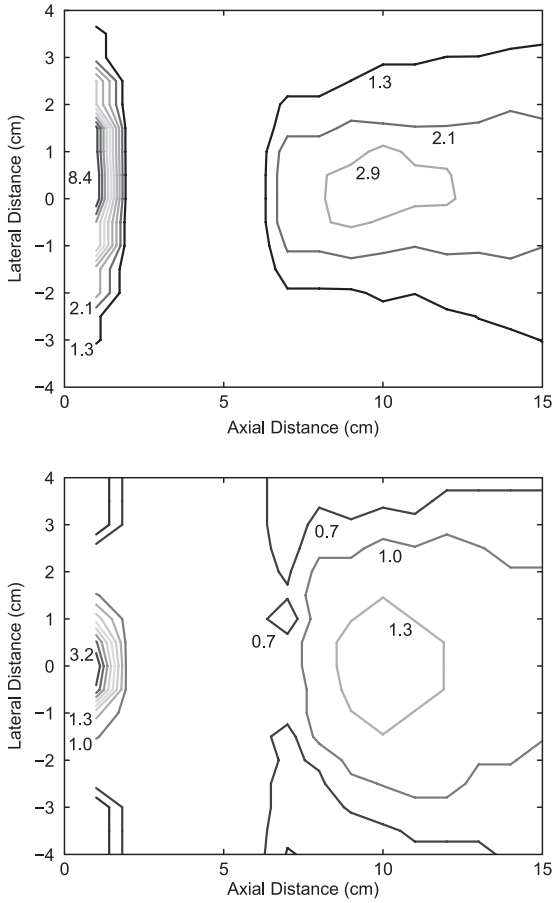

Figure 6.3: Measured temperature distributions after 45 minutes of insonification, without (top) and with (bottom) the application of an acoustic lens (ROC = 35 mm). The numbers next to the contours represent the temperature increase in °C.

6.4 Discussion and conclusions

Additional simulations were done to determine the temperature distribution under a worst case situation. The perfusion time, heat capacity, heat diffusivity, and other properties of tissue were adapted from literature (Duck, 1990). In this worst-case situation, the pressure at the transducer surface was assumed to be 450 kPa. The simulated harmonic beam profiles of this scenario are plotted in the left part of Figure 6.4. The axial beamprofiles of the fundamental, second and third harmonic in a nonabsorbing medium are represented by solid lines. The dashed lines represent simulations on a layered medium. This medium is constituted by an abdominal layer of 2 cm thickness, a water path of 5 cm length, and another layer of tissue to simulate the post bladder domain. It must be noted that the direct heating of the transducer was not included in the simulations. Although it has been neglected here, it might be important to consider this effect, as well as the associated heat conduction, to obtain better temperature estimations. The total temperature elevation is shown in the right part of Figure 6.4. The dashed contours represent the temperature elevation including the harmonic contribution. The harmonic contribution to the total temperature elevation is estimated at 0.21°C.

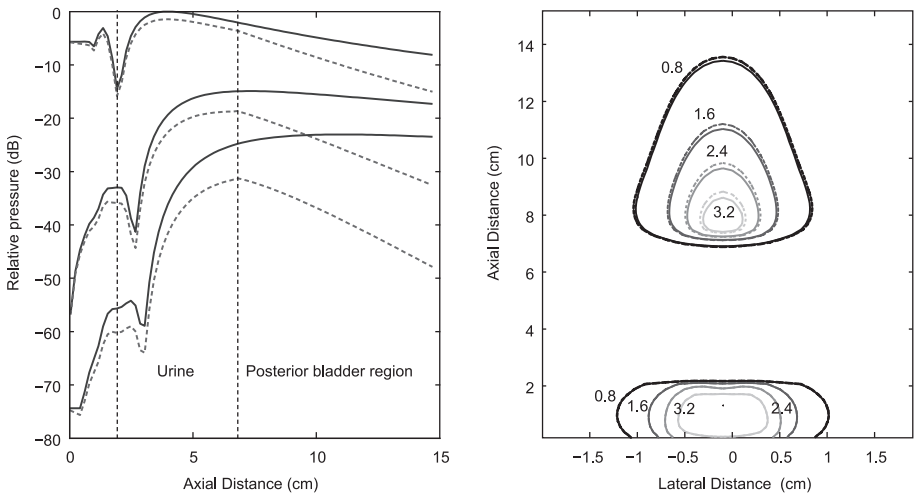

Figure 6.4: Left: Axial nonlinear pressure profiles simulations in water (solid lines) and in a layered medium (dashed lines). Values are normalized to a peak pressure of 800 kPa. Right: Comparison between steady state temperatures calculated from linear propagation (solid lines) and nonlinear propagation (dashed lines).

In conclusion, simulation results and measurement results showed that there were no significant differences in temperature elevation in the case of bladder volume assessment using nonlinear ultrasound. The inclusion of nonlinear wave propagation simulations does not provide a significant increase of temperature compared to linear simulations. Under the experimental conditions required for bladder volume assessment, the TI remains a good indicator of the rise of temperature. In the current stage of the experimental setup, the derated peak pressure reaches 400 kPa at focus (I_m = 10 W/cm^2, I_{SPTA} = 100 mW/cm^2 with 1% duty cycle), which corresponds, in this case, to a TI of 0.9 and a MI of 0.3 (at 1.8 MHz). In case of higher power settings, the contribution of higher harmonics must be taken into account with the temperature calculations.

Chapter 7

Conclusions and Suggestions

7.1 Introduction

In the past 40 years ultrasonography has shown to be very technology dependent. As ultrasound technology became more advanced, the image quality as well as the ability to more accurately perform diagnostic measurements and medical research grew. Quantification of organs with diagnostic ultrasound, especially with 1D and 2D echography, has shown to be less accurate than other diagnostic modalities such as magnetic resonance imaging (MRI) and computed tomography (CT), because of geometric assumptions regarding to organ shape. Additionally, acoustically acquired images are hard to interpret without proper anatomical knowledge and suffer from artifacts related to sound propagation in a inhomogeneous medium. With the introduction of 3D ultrasound, images have become more intuitively interpretable, hence closing the gap with the other modalities. In combination with enhanced detection algorithms, increased computing power and new transducer technology, 3D ultrasound has been proven to be equally accurate as MRI in, for example, cardiac applications (Krenning et al., 2007).

With respect to acoustic bladder volume assessment, the motivation for higher accuracy in volume quantification might not be so obvious. For many years, urinary catheterization has been the golden standard in bladder volume assessment because of its accuracy and its availability, allowing for bedside care. However, it has the serious disadvantage of being invasive and includes the risk of urinary tract infections (UTI) and trauma. Noninvasive acoustic measurement of the bladder volume has been proven to reduce the amount of

unnecessary catheterizations, thus avoiding the risk of infection and trauma. In literature, a clear trend is visible from determining the accuracy of ultrasound for volume assessment towards the clinical benefits versus catheterization. Many publications have stated that, in daily clinical practice, high accuracy is not needed and merely an indication of the bladder filling suffices. For example, measurement of postvoid residual urine volume (PVR), i.e. the amount of urine left after complete voiding, is diagnosed as urine retention when the PVR $\geq$ 300 ml. However, no clear consensus exists on this stated threshold as limit values between 100 ml and 500 ml are reported (Kaplan et al., 2008). The majority of the publications value the benefits of ultrasound, i.e. noninvasive, comfortable to the patient and its availability, over the higher accuracy associated with catheterization. Some papers even reported that equal or better accuracy can be obtained when dedicated ultrasonic bladder volume instruments, like the BladderScan (Verathon Inc., USA), are used. It is therefore reasonable to suggest that the search for higher accuracy in acoustic bladder volume estimation is merely for acceptance within the clinic as an alternative method to catheterization.

7.2 General discussion

In the same line of thought, the method described in this thesis was not developed to improve the accuracy of ultrasonic volume assessment with respect to the currently available devices and methods. Instead, the aim was to design a method that is easy to use, fast and allows for miniaturization. These requirements will make noninvasive bladder volume assessment accessible to a larger public, e.g. nursing homes, general practitioners and personal use. Consequently, it will further reduce the number of unnecessary catheterizations, the associated risks and related the cost of social health care. Most importantly, it will increase the quality of life for those who require bladder volume management.

Currently available handheld devices are capable of accurate volume assessment, but use electronically or mechanically steerable ultrasound beams to detect the bladder walls. The method described in this thesis is based on measuring the presence of harmonics in an echo from a region-of-interest (ROI) at fixed depth beyond the bladder using only one single diverging acoustic beam. The approach takes advantage of the difference in harmonic generation of liquids (urine) and tissues. The transmitted fundamental frequency as well as the generated harmonics are used to define the volume present within the propagation path. The harmonic content in the echo will increase with increase of fluid in the echo path. Feasibility was proven

using in-vitro measurements on bladder phantoms. Also, measurements on a volunteer showed that bladder volume assessment on the basis of nonlinear wave propagation is feasible in-vivo. The results confirmed that the harmonic content of an echo measured at a deep ROI increases for a full bladder and decays strongly after the volunteer has voided. In addition, higher harmonics or superharmonics (Bouakaz et al., 2002) can be used to refine the volume indication.

The system used with this first attempt consisted of a conventional ultrasound system, adjusted for experimental purposes, and an experimental fast rotating phased array probe developed for 3D harmonic cardiac imaging. The transducer and system were clearly too advanced for the application of bladder volume assessment and it would be impossible to integrate its functionality into a low cost handheld device. Also, the system was limited to receiving up to the 2^{nd} harmonic, where, up to that point, the influence of the 3^{rd} and higher harmonics on the volume detection were also of interest. Therefore, it was stressed that a dedicated relatively simple and low cost transducer was needed that is capable of generating a wide acoustic field large enough to capture a (full) bladder. Additionally, the transducer should have high transmit sensitivity to induce significant nonlinear wave propagation, and high sensitivity in reception to measure up to the 3^{rd} harmonic. In the field of transducer design and manufacturing, these requirements are impossible to achieve without making compromises. In general, increasing the bandwidth means sacrificing transmit and receive sensitivity and vice versa. The requirement of the wide acoustic beam additionally requires a high transmit sensitivity as, in the case of a spherical wave, the acoustic pressure decreases proportionally to the inverse of the propagation distance. This clearly puts a limit on the beamwidth that can be achieved.

Three transducer concepts were investigated, i.e. a broadband single element transducer, a multi-element ring transducer and a multilayer transducer. The multilayer transducer was found best due to the combination of high efficiency in transmission and broadband reception and the relatively simple beamforming to create the diverging acoustic beam. However, the first multilayer transducer was very susceptible to electromagnetic distortion (high EMS), resulting in low signal-to-noise ratio (SNR) in the received signals. An equivalent KLM-circuit model of the multilayer transducer was developed. This has proven to be a valuable tool to evaluate and further optimize the multilayer transducer design. Eventually, an "Inverted" multilayer transducer was designed and built. It had very low EMS, high transmit sensitivity and was able to receive up to the 3^{rd} harmonic with good sensitivity. It was concluded that in order to measure at least up to the third harmonic frequency

component with good sensitivity in combination with very high transmit sensitivity at the fundamental frequency, a multilayer structure is optimal. To optimize for the EMS in reception, and hence also the signal-to-noise ratio, an inverted geometry as proposed in this thesis has proven to be effective.

Chapter 4 describes a simulation study that was conducted to define an algorithm that is capable of giving a good estimation of the bladder volume and was not affected by patient variations. Four different algorithms, including the original method of selecting a ROI located at a fixed position behind the bladder, were compared. The simulations included the modeling of nonlinear wave propagation through layered media, comprising the anterior bladder wall, the urine region and the posterior bladder wall, using a time-domain implementation of the KZK-equation. In this case, a non-diverging acoustic beam was used because of the limitations of the KZK implementation. Hence, urine pathlengths (UPL) instead of volumes were modeled. The simulations showed that the generated harmonics within the anterior bladder wall affect the harmonics-to-fundamental ratio measured in the posterior bladder domain. This influence is emphasized by the additional acoustic loss in this region for the reflected waves. It is likely that the size of the ROI influences the variations observed in the UPL estimates and that a trade-off must be found between sensitivity and variations. Also, the chosen location of the ROI affects the estimate. In contrast with the other 3 algorithms, the original method does not depend on the performance of a detection method to determine the location of the anterior and posterior ROI. This is considered to be a big advantage.

Conventional ultrasound scanning can be considered as harmless since no adverse effects have been reported so far. Nonetheless, several guidelines exist that regulate the exposure of ultrasound on humans. The most widely used parameters are the Thermal Index (TI) and the Mechanical Index (MI). With respect to abdominal ultrasound the FDA recommends to stay below a TI of 4.0 and a MI of 1.9. However, these limits were obtained by assuming linear wave theory only, and do not include the effect of the generated harmonic components due to nonlinear wave propagation. It was found that the value of the effective MI, taking in account the nonlinear propagation, is much below the value of the MI computed under the assumption of linear propagation. Additionally, because the generated higher harmonics are absorbed more by tissue, heating of tissues by the absorption of ultrasound might thus be enhanced by nonlinear wave propagation. The TI, calculated from linear theory, might thus underestimate the actual thermal effects of ultrasound exposure.

The study presented in Chapter 6 addressed the safety aspects with respect to the bladder volume assessment using nonlinear ultrasound. Although the method uses a diverging acoustic beam, the study concentrated on an unfocused

(flat) ultrasonic transducer. The results obtained could then be considered as the limiting case, where defocusing of the beam would only decrease the exposure values. Linear and nonlinear wave propagation simulations were used to determine the significance of the additional harmonics on the MI and TI calculations. It readily followed from theoretical analysis that, since the MI is calculated from using the peak rarefactional pressure, which is smaller for the nonlinear case, a worst case situation is found when the MI is calculated under the assumption of linear wave propagation. With respect to the TI, it was found (Chapter 6) that the inclusion of nonlinear simulations for a better estimation of the temperature rise in tissue did not lead to a significant increase of temperature compared to linear simulations. Hence, it was concluded that the TI remains a good indicator for the rise of temperature. Under experimental conditions required for bladder volume assessment, i.e. 400 kPa peak pressure at focus at transmit frequency of 1.8 MHz and with a duty cycle of 1%, the TI was 0.9 and the MI calculated at 0.3. Clearly, these values are on the safe side of the recommended exposure limits, even without the application of a diverging acoustic beam, and indicate that the transmitted power can be further increased to enhance the nonlinear wave propagation. However, it is noted that with higher transmit power, the contribution of the higher harmonics must be taken into account with the temperature calculation.

7.3 Future research suggestions

This thesis showed the first *in vivo* results obtained from a small clinical setting (Chapter 5). Although not mentioned in the previous chapters, numerous other clinical measurements on volunteers were also conducted in the last 4 years. These included using different transducers, lens sizes, system settings and electronics. Although these measurements did not give satisfying results worth publishing, they were extremely useful in identifying practical problems. These problems could not have been detected without actually going to the clinic and do the measurements. Probably the most important conclusion that was obtained from these measurements was that volume estimation is extremely patient dependent.

The measurement setup and results that have led to these important findings are described next:

> Initial clinical measurements of bladder volume assessment were performed in conjunction with ongoing clinical research to noninvasively measure the pressure inside the bladder of male volunteers (de Zeeuw and van Mastrigt, 2007). Each volunteer was subjected to a set of three individual pressure and acoustic measurements. In between

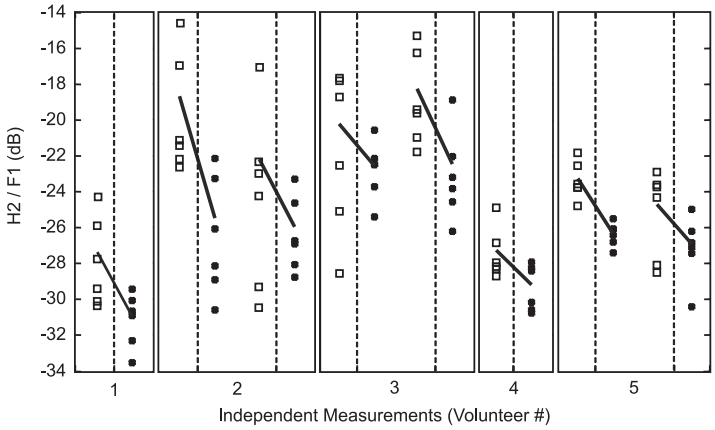

Figure 7.1: Results initial clinical volume measurements for 5 volunteers. Prevoid measurements (squares) and postvoid measurements (dots) are indicated.

these measurements, the volunteer was asked to drink water, and measurements were performed when the volunteer had the sensation of a full bladder. Pre and post void recordings were made.

The results obtained for 5 male volunteers are shown in Figure 7.1. The black solid lines represent the trends between the average harmonic distortion measured before voiding (squares) and the average harmonic distortion measured after voiding (dots). As can be seen from these results, all measurements show a negative trend, which is according to our hypothesis "less volume-less harmonic distortion". The figure has been divided into 5 separate parts corresponding to the measurements of the individual volunteer. Thus, in total 8 measurement sets divided over 5 volunteers are shown.

It can be appreciated from Figure 7.1 that there exists a strong patient dependency. Volunteer 1 and 4 have average ratios below the ratios of volunteers 2, 3 and 5. The large variability of the 6 acquisitions originates from the intended random probe alignment and limited beamwidth.

Clearly, patient dependency plays an important role and should be corrected for to facilitate general application of the volume assessment method. Although, Chapters 4 and 5 already showed that the originally proposed algorithm, i.e. selecting a region of interest at a fixed position behind the bladder, was least sensitive to patient variability, it must be emphasized that

a large clinical study is needed to optimize the algorithm to be used.

Another observation from the clinical measurements as well as from the simulations described in Chapter 4, is the sensitivity to stochastic scattering and spatial averaging. It was concluded that these effects cannot be compensated for by using clever algorithms, but that they completely depend on the transducer properties and the transmitted waves. Further research is therefore necessary to reduce the sensitivity for stochastic scattering. It is suggested that using different pulsing schemes might be beneficial.

It has been noted with the first *in vivo* measurements (Chapter 5) that the used transducer, in combination with the acoustic lens, could not generate a beam wide enough to encompass (full) bladders containing over 500 ml of urine. Although it can be questioned whether the method should be capable of measuring larger volumes, i.e. the current limit already indicates a full bladder, larger beamwidths do avoid aiming problems and hence reduce scanning time. For the same reason, the latest versions of the BladderScan devices (Chapter 1) scan through a 120 degree arc instead of the 97 degree arc used in older versions.

To increase the beamwidth, the radius of curvature (ROC) of the acoustic lens should be decreased, or lens material with higher sound propagation speed should be selected. There are, however, a few problems concerning the use of acoustic lenses. Because of the finite thickness of the lens, reverberations inside the lens are likely to occur. These reverberations cause multiple reflections, which appear as artifacts in the recorded RF-data. The amplitude of these reverberations can be reduced by selecting a lens material that has an acoustic impedance close that of tissue. Matching the impedance to that of tissue, while maintaining a higher sound speed, requires lens material with relatively low density. The material polymethylpentene, better known as TPX (Matsui Plastics, White Plains, NY), has an acoustic impedance close that of tissue and water and is widely used as acoustic window in experimental setups. Because of its low density and high propagation speed it is suitable as lens material. However, it also has a relatively high acoustic loss (6 dB/cm at 2 MHz, (Wang et al., 1999)). Increasing the ROC also implies increasing the propagation path through the lens and thus the total wave attenuation. For this reason Rexolite (Chapter 3), a material with low acoustic loss and impedance comparable to tissue, was previously chosen as lens material instead of TPX.

Instead of using an acoustic lens to create the diverging acoustic beam, a convex transducer aperture might be more effective. This option was not investigated, and hence not covered by this thesis, because priority was set to achieving good transmit and receive sensitivity. The ability of changing

the beamwidth by means of one single element unfocused transducer and different size lenses without having to redesign the transducer, outweighed the lens-associated problems previously discussed. It is because of these problems in combination with the limited beamwidth that the author suggests to determine the feasibility of using convex transducer apertures for bladder volume assessment.

The bladder volume assessment method described in this thesis in combination with other volume measurement techniques, like is being used with the BladderScans (Chapter 1), might increase measurement accuracy. This might become evident with the following example:

> In females, the uterus lies in close vicinity of the bladder. Due to the monthly menstrual cycles, the uterus wall (endometrium) thickens. Since the endometrium is strongly vascular it fills up with blood. At abdominal ultrasound frequencies (2-5 MHz) blood is not visible and the uterus appears as an anechoic region in the image. As a consequence, the uterus might easily be mistaken for the bladder by the automatic border detection algorithm. To overcome this problem, a detection rule might be included that rules out the presence of a second anechoic region to be part of the bladder. However, using the Gol'dberg number, a more robust method might be possible. From Table 1.1 given in Chapter 1 it can be found that urine and blood have about the same nonlinearity parameter, but that the acoustic loss of blood at 1 MHz is 20 times higher than that of urine. The Gol'dberg number for urine is thus approximately 20 times higher, which indicates that blood can be distinguished from urine on the basis of the amount of harmonics present in the echoes originating from the posterior cavity walls.

An advantage of, for example, the BladderScan technology, is that narrow beams are used to detect the borders. With these narrow beams, which are usually also focused, high fundamental pressures can be generated, and the generated harmonics due to nonlinear wave propagation are significantly present. With the previous example in mind, the combination of border detection and medium dependent harmonic generation might then evolve to acoustic spectroscopy of the fluids inside the cavities.

7.4 Conclusions

The work reported in this thesis describes a complete new method to noninvasively and instantaneously measure the volume of liquid filled cavities, in this case the human bladder, using nonlinear ultrasound. Noninvasive acoustic

measurement of the bladder volume has proven to reduce the amount of unnecessary catheterizations, thus avoiding the risk of infection and trauma. Currently available handheld devices are capable of accurate volume assessment, but use electronically or mechanically steerable ultrasound beams to detect the bladder walls. The new method is based on measuring the presence of harmonics in an echo from a region-of-interest (ROI) at fixed depth beyond the bladder using only one single diverging acoustic beam. The transmitted fundamental frequency as well as the generated harmonics are used to define the volume present within the propagation path.

An initial feasibility study showed that bladder volume assessment on the basis of nonlinear wave propagation is feasible. However, it was noted that a dedicated transducer, with an acoustic beam wide enough to encompass a full bladder, is essential.

To obtain the dedicated transducer, three transducer concepts were investigated, i.e. a broadband single element transducer, a multi-element ring transducer and a multilayer transducer. The multilayer transducer was found best due to the combination of high efficiency in transmission and broadband reception and the relatively simple beamforming to create the diverging acoustic beam. It is concluded that in order to measure at least up to the third harmonic frequency component with good sensitivity in combination with very high transmit sensitivity at the fundamental frequency, a multilayer structure is optimal. To optimize for the EMS in reception, and hence also the signal-to-noise ratio, an inverted geometry as proposed in this thesis has proven to be effective.

A simulation study, using the time domain implementation of the KZK-equation, gave good insight on the effect of patient variability, transducer configuration and, most importantly, the algorithm used, on the 2^{nd} Harmonic-to-Fundamental Ratio in relation to the bladder volume. The effect of a diverging acoustic beam on the performance of the computational methods should be studied with an alternative simulation model, which does not use the parabolic approximation, with in-vitro and in-vivo measurements. With respect to the stochastic scattering of the scatter phantoms it is concluded that the variations completely depend on the transducer characteristics and not so much on the algorithm used.

A first *in vivo* evaluation of this method using the new developed transducer, including acoustic lens, and two different computational methods, including the originally proposed algorithm, showed that this method is currently capable of qualitative volume measurement instead of quantitative

measurements. The originally proposed algorithm showed to be the least sensitive to patient variability and bladder shape, and does not require additional bladder detection. However, this method showed a low sensitivity at low volumes with *in vivo* measurements, due to a limited signal-to-noise ratio. The measurement results showed a high repeatability for both algorithms, but large volumes could not be measured accurately due to beamwidth limitations. Clearly, patient dependency plays an important role and should be corrected for to facilitate general application of the volume assessment method. To perform quantitative bladder volume assessment additional research is needed on beamforming and pulsing schemes. Additionally, a large clinical study is needed to optimize the algorithm.

In vitro measurements and simulations showed that the safety limits, the Mechanical Index (MI) and the Thermal Index (TI), were still valid under the assumption of nonlinear wave propagation. It was concluded that the limits were not exceeded and that bladder volume assessment on the basis of nonlinear wave propagation is safe.

From the work presented in this thesis it can be concluded that noninvasive bladder volume measurement using nonlinear ultrasound is feasible. It has the potential of becoming a fast, low cost and easy to use addition to the currently available dedicated portable bladder volume instruments. Although it is not likely that it will rival the obtainable accuracy of current devices, it will make noninvasive bladder volume assessment accessible to a larger public. This was the main goal of this study.

Bibliography

Abbott J.G. Rationale and derivation of mi and ti - a review. *Ultrasound Med Biol*, 25(3):431–441, 1999.

Averkiou M.A. Tissue harmonic imaging. *Proceedings IEEE Ultrasonics Symposium*, 2:1530 – 1541, 2000.

Averkiou M.A. and Hamilton M.F. Nonlinear distortion of short pulses radiated by plane and focused circular pistons. *J Acoust Soc Am*, 102(5):2539–2548, 1997.

Barnett S., ter Haar G., Ziskin M., Rott H.D., Duck F.A., and Maeda K. International recommendations and guidelines for the safe use of diagnostic ultrasound in medicine. *Ultrasound Med Biol*, 26(3):355–366, 2000.

Binard J.E., Perskey L., Lockhart J.L., and Kelly B. Intermittent catheterization the right way! (Volume vs. time-directed). *J Spinal Cord Med*, 19(3): 194–196, 1996.

Bouakaz A. and de Jong N. Native tissue imaging at superharmonic frequencies. *IEEE Trans Ultrason Ferroelectr Freq Control*, 50(5):496–506, 2003b.

Bouakaz A., Lancée C.T., Frinking P., and de Jong N. Simulations and measurements of nonlinear pressure field generated by linear array transducers. *Proceedings IEEE Ultrasonics Symposium*, 2:1511–1514, 1999.

Bouakaz A., Frigstad S., Cate F. Ten, and de Jong N. Super harmonic imaging: A new technique for improved contrast detection. *Ultrasound Med Biol*, 28 (1):59–68, 2002.

Bouakaz A., Lancée C., and de Jong N. Harmonic ultrasonic field of medical phased arrays: Simulations and measurements. *IEEE Trans Ultrason Ferroelectr Freq Control*, 50(6):730–735, 2003a.

Bouakaz A., Merks E., Lancée C.T., and Bom N. Noninvasive bladder volume measurements based on nonlinear wave distortion. *Ultrasound Med Biol*, 30 (4):469–476, 2004.

Brown L.F. and Carlson D.L. Ultrasound transducer models for piezoelectric polymer films. *IEEE Trans Ultrason Ferroelectr Freq Control*, 36(3):313–318, 1989.

Çevik I., Tarcan T., T′urkeri L., Erkurt B., and Akdas A. Comparison of urethral catheterization versus portable ultrasound scanning in the measurement of post-voiding residual urine volume. *Afr J Urol*, 2(1):36–40, 1996.

Coombes G. and Millard R. The accuracy of portable ultrasound scanning in the measurement of residual urine volume. *J Urol*, 152(1):2083–2085, 1994.

de Zeeuw S. and van Mastrigt R. Increased postvoid residual volume after measuring the isovolumetric bladder pressure using the noninvasive condom catheter method. *BJU International*, 100(6):1293–1297, 2007.

Dion J.-L., Cornieles E., Galindo F., and Agbossou K. Exact one-dimensional computation of ultrasonic transducers with several piezoelectric elements and passive layers using the transmission line analogy. *IEEE Trans Ultrason Ferroelectr Freq Control*, 44(5):1120–1131, 1997.

Divall S.A. and Humphrey V.F. Finite difference modeling of the temperature rise in non-linear medical ultrasound fields. *Ultrasonics*, 38(1-8):273–277, 2000.

Djoa K.K., de Jong N., van Egmond F.C., Kasprzak J.D., Vletter W.B., Lancée C.T., van der Steen A.F.W., Bom N., and Roelandt J.R. A fast rotating scanning unit for real-time three-dimensional echo data acquisition. *Ultrasound Med Biol*, 26(5):863–869, 2000.

Duck F. *Physical properties of tissue.* Academic Press Ltd., London, 1990.

Frijlink M.E., Goertz D.E., Bouakaz A., and van der Steen A.F.W. A simulation study on tissue harmonic imaging with a single-element intravascular ultrasound catheter. *J Acoust Soc Am*, 120(3):1723–1731, 2006.

Ganguly D. and Guiliani D. Apparatus and method for non-invasively and automatically measuring the volume of urine in a human bladder.

Ganguly D., Roberts T., and McConaghy R. System for estimating bladder volume. October 1999.

Hakenberg O.W., Ryall R., Langlois S., and Marshall V. The estimation of bladder volume by sonocystography. *J Urol*, 130(2):249–251, 1983.

Hamilton M. and Blackstock D. *Nonlinear acoustics*. Academic Press, San Diego, New York, Boston, London, Sydney, Tokyo, Toronto, 1998.

Haran M. and Cook B. Distortion of finite amplitude ultrasound in lossy media. *J Acoust Soc Am*, 73(3):774–779, 1983.

Harrison N.W., Parks C., and Sherwood T. Ultrasound assessment of residual urine in children. *Br J Urol*, 47(7):805–814, 1976.

Henriksson L. and Maršál K. Bedside ultrasound diagnosis of residual urine volume. *Archives of Gynecology and Obstetrics*, 231(2):129–133, 1982.

Holland C.K. and Apfel R.E. Thresholds for transient cavitation produced by pulsed ultrasound in a controlled nuclei environment. *J Acoust Soc Am*, 88 (5):2059–2069, 1990.

Holmes J.H. Ultrasonic studies of the bladder. *The Journal of Urology*, 97(4): 654–663, 1967.

Hossack J.A., Mauchamp P., and Ratsimandresey L. A high bandwidth transducer optimized for harmonic imaging. *Proceedings IEEE Ultrasonics Symposium*, 2:1021–1024, 2000.

Hubert H.A., Chambers K., Clifton J., and Tasaka J. Clinical utility of a portable ultrasound device in intermittent catheterization. *Archives of Physical Medicine and Rehabilitation*, 79(2):172–175, 1998.

Huijssen J., Bouakaz A., Verweij M.D., and de Jong N. Simulations of the nonlinear acoustic pressure field without using the parabolic approximation. *Proceedings IEEE Ultrasonics Symposium*, 2:1851–1854, 2003.

Humphrey V.F. Nonlinear propagation in ultrasonic fields: measurements, modelling and harmonic imaging. *Ultrasonics*, 38(1-8):267–272, 2000.

Ireton R.C., Krieger J.N., Cardenas D.D., Williams-Burden B., Kelly E., Souci T., and Chapman W.H. Bladder volume determination using a dedicated, portable ultrasound scanner. *J Urol*, 143(5):909–911, 1990.

Jensen J.A. Field: A program for simulating ultrasound systems. *Medical and Biological Engineering and Computing*, 43(1):351–353, 1996.

Jeong J., Seo C., and Yen J.T. Dual-layer transducer array for 3-D imaging. *Proceedings IEEE Ultrasonics Symposium*, pages 2371–2374, 2007.

Kaplan S.A., Wein A.J., Staskin D.R., Roehrborn C.G., and Steers W.D. Urinary retention and post-void residual urine in men: Separating truth from tradition. *The Journal of Urology*, 180(1):47–54, 2008.

Kino G.S. *Acoustic waves: Devices, Imaging and Analog Signal Processing.* Prentice-Hall Inc., Englewood Cliffs, 1987.

Krenning B.J., Voormolen M.M., Geleijnse M.L., van der Steen A.F.W., ten Cate F.J., Ie E.H.Y., and Roelandt J.R.T.C. Three-dimensional echocardiographic analysis of left ventricular function during hemodialysis. *Nephron Clinical Practice*, 107(2):c43–c49, 2007.

Krimholtz R., Leedom D.A., and Mattaei G.L. New equivalent circuit for elementary piezoelectric transducers. *Electronic Letters*, 6(13):389–399, 1970.

Kruczkowski P.J.C., Mylrea K.C., Roemer R.R., and Drach G.M. A non-invasive ultrasound system to determine residual bladder volumes. *Engineering in Medicine and Biology Society, 1988. Proceedings of the Annual International Conference of the IEEE*, 4:1623–1624, 1988.

Kuznetsov V. Equations of nonlinear acoustics. *Sov Phys Acoust*, 16(4):467–470, 1971.

Lee Y.S. and Hamilton M.F. Time-domain modeling of pulsed finite-amplitude sound beams. *J Acoust Soc Am*, 97(2):906–917, 1995.

Lee Y.Y., Tsay W.L., Lou M.F., and Dai Y.T. The effectiveness of implementing a bladder ultrasound programme in neurosurgical units. *Journal of Advanced Nursing*, 57(2):192–200, 2007.

Lewis N. Implementing a bladder ultrasound program. *Rehabil Nurs*, 20(4): 215–217, 1995.

Li W., Lancée C.T., Cespedes E. I., van der Steen A. F. W., and Bom N. Decorrelation of intravascular ultrasound signals: a computer simulation study. *Proceedings IEEE Ultrasonics Symposium*, 2:1165–1168, 1997.

Li Y., Chen Q., and Zagzebski J. Harmonic ultrasound fields through layered liquid media. *IEEE Trans Ultrason Ferroelectr Freq Control*, 51(2):146–152, 2004.

Liu X., Ye S., Gong X., Zhang W., and Lu R. Study of polymer ultrasonic transducer and complex ultrasonic transducer with PZT/PVDF multi-layer structure. *Acustica*, 85:420–426, 1999.

Lockwood G.R. and Foster F.S. Modeling and optimization of high-frequency ultrasound transducers. *IEEE Trans Ultrason Ferroelectr Freq Control*, 41 (2):225–230, 1994.

McMorrow G.J., Baartmans H., Bom N., and Lancée C.T. Instantaneous ultrasonic measurement of bladder volume. *Patent: PCT WO 2004/017834 A1, Diagnostic Ultrasound Europe B.V., Lage Dijk 14, 3401 RG IJsselstein, the Netherlands*, 2002.

Merks E.J.W., Bom N., Bouakaz A., de Jong N., and van der Steen A.F.W. Design of a multi-layer transducer for acoustic bladder volume assessment. *Proceedings IEEE Ultrasonics Symposium*, 1:145–148, 2004.

Merks E.J.W., Lancée C.T., Bom N., van der Steen A.F.W., and de Jong N. Comparison of three different transducer concepts for acoustic bladder volume measurements. *Proceedings IEEE Ultrasonics Symposium*, 4:2239–2242, 2005.

Merks E.J.W., Borsboom J.M.G., Bom N., van der Steen A.F.W., and de Jong N. A KLM-circuit model of a multi-layer transducer for bladder volume measurements. *Ultrasonics*, 44(Suppl. 1):e705–e710, 2006a.

Merks E.J.W., Bouakaz A., Bom N., de Jong N., and van der Steen A.F.W. Design of a multi-layer transducer for acoustic bladder volume assessment. *IEEE Trans Ultrason Ferroelectr Freq Control*, 53(10):1730–1738, 2006b.

Merks E.J.W., van Neer P., Bom N., van der Steen A.F.W., and de Jong N. Multilayer transducer for acoustic bladder volume assessment on the basis of nonlinear wave propagation. *Ultrasound Med Biol*, Accepted for publication, 2009.

Moore D.A. and Edwards K. Using a portable bladder scan to reduce the incidence of nosocomial urinary tract infections. *Medsurg Nursing*, 6(1):39–43, 1997.

Newman D.K. and Palmer M.H. Incontinence and PPS: A new era. *Ostomy / Wound Manage*, 45(12):32–50, 1999.

Nyborg W.L. Solutions of the bio-heat transfer equation. *Phys. Med. Biol.*, 33 (7):785–792, 1988.

O'Brien Jr., W.D. and Ellis D.S. Evaluation of the unscanned soft-tissue thermal index. *IEEE Trans Ultrason Ferroelectr Freq Control*, 46(6):1459–1476, Nov 1999.

Ord J., Lunn D., and Reynard J. Bladder management and risk of badder stone formation in spinal cord injured patients. *Journal of Urology*, 170(5): 1734–1737, 2003.

Palanchon P., van Loon D., Bom N., and Bangma C. Bladder volume measurements with a limited number of fixed ultrasound beams. *Ultrasound Med Biol*, 30(3):289–294, 2004.

Rao N., Mehra S., and Zhu H. Ultrasound speckle statistics variations with imaging systems impulse response. *Proceedings IEEE Ultrasonics Symposium*, 3:803–810, 1990.

Ravichandran G. and Fellows G.J. The accuracy of a hand-held real time ultrasound scanner for estimating bladder volume. *British Journal of Urology*, 55(1):25–27, 1983.

Rielly M., Humphrey V., and Duck F. A theoretical and experimental investigation of nonlinear ultrasound propagation through tissue mimicking fluids. *Proceedings IEEE Ultrasonics Symposium*, 2:1355–1358, 2000.

Saitoh S., Honda H., Kaneko N., Izumi M., and Suzuki S. The method of determining kt and Qm for low Q piezoelectric materials. *Proceedings IEEE Ultrasonics Symposium*, pages 620–623, 1985.

Saitoh S., Izumi M., and Mine Y. A dual frequency ultrasonic probe for medical applications. *IEEE Trans Ultrason Ferroelectr Freq Control*, 42(3):294–300, 1995.

Sedor J. and Mulholland S.G. Hospital-acquired urinary tract infections associated with the indwelling catheter. *Urologic Clinics of North America*, 26 (4):821–828, 1999.

Slappendel R. and Weber E.W. Non-invasive measurement of bladder volume as an indication for bladder catheterization after orthopaedic surgery and its effect on urinary tract infections. *Eur J Anaesthesiol*, 16(8):503–506, 1999.

Smith M.R. and Dunhill A.K. The design and performance of PVDF transducers. *Proceedings IEEE Ultrasonics Symposium*, 1:675–679, 1987.

Stepanishen P.R. Transient radiation from pistons in an infinite planar baffle. *J Acoust Soc Am*, 49(5B):1629–1638, 1971.

Sulzbach-Hoke L. and Schanne L. Using a portable ultrasound bladder scanner in the cardiac care unit. *Crit Care Nurse*, 19(6):289–294, 1999.

Szabo T., Clougherty F., and Grossman C. Effects of nonlinearity on the estimation of in situ values of acoustic output parameters. *J Ultrasound Med*, 18(1):33–41, 1999.

Thijssen J.M. and Oosterveld B.J. Speckle and texture in echography: Artifact or information? *Proceedings IEEE Ultrasonics Symposium*, pages 803–810, 1986.

Thuras A.L., Jenkins R.T., and Neil H.T.O. Extraneous frequencies generated in air carrying intense sound waves. *J Acoust Soc Am*, 6(3):173–180, 1935.

Topper A.K., Holliday P.J., and Fernie G.R. Bladder volume estimation in the elderly using a portable ultrasound-based measurement device. *J Med Eng Technol*, 17(3):99–103, 1993.

van Neer P.L.M.J., Matte G., Sijl J., Borsboom J.M., and de Jong N. Transfer functions of US transducers for harmonic imaging and bubble responses. *Ultrasonics*, 46(4):336–340, 2007.

Verma P.K., Humphrey V.F., and Duck F.A. Broadband measurements of the frequency dependence of attenuation coefficient and velocity in amniotic fluid, urine and human serum albumin solutions. *Ultrasound Med Biol*, 31 (10):1375–1381, 2005.

Voormolen M.M., Bouakaz A., Krenning B.J., Lancée C.T., ten Cate F.J., Roelandt J.R.T.C., van der Steen A.F.W., and de Jong N. A new transducer for 3D harmonic imaging. *Proceedings IEEE Ultrasonics Symposium*, 2:1261–1264, Oct. 2002.

Wagner R.F., Smith S.W., Sandrik J.M., and Lopez H. Statistics of speckle in ultrasound B-scans. *IEEE Transactions on Sonics and Ultrasonics*, 30(3): 156–163, 1983.

Wang H., Ritter T., Cao W., and Shung K.K. Passive materials for high frequency ultrasound transducers. *SPIE Conference Proceedings*, 3664:35–42, 1999.

West K.A. Sonocystography: A method for measuring residual urine. *Scand J Urol Nephrol*, 1(1):68–70, 1967.

Xu Q.C., Madhavan C., Srinivasan T.T., Yoshikawa S., and Newnham R.E. Composite transducer with multiple piezoelectric matching layers. *Proceedings IEEE Ultrasonics Symposium*, 1:507–512, 1988.

Zabolotskaya E. and Khokhlov R. Quasi-plane waves in the nonlinear acoustics of confined beams. *Sov Phys Acoust*, 15(1):35–40, 1969.

Zhang Q., Lewin P.A., and Bloomfield P.E. PVDF transducers - A performance comparison of single-layer and multilayer structures. *IEEE Trans Ultrason Ferroelectr Freq Control*, 44(5):1148–1156, 1997.

Appendix A: Abstract Original Patent Application

(12) INTERNATIONAL APPLICATION PUBLISHED UNDER THE PATENT COOPERATION TREATY (PCT)

(19) World Intellectual Property Organization
International Bureau

(43) International Publication Date
4 March 2004 (04.03.2004)

PCT

(10) International Publication Number
WO 2004/017834 A1

(51) International Patent Classification[7]: A61B 8/08

(21) International Application Number:
PCT/EP2003/007807

(22) International Filing Date: 1 July 2003 (01.07.2003)

(25) Filing Language: English

(26) Publication Language: English

(30) Priority Data:
0218547.8 9 August 2002 (09.08.2002) GB

(71) Applicant *(for all designated States except US)*: **DIAGNOSTIC ULTRASOUND EUROPE B.V.** [NL/NL]; Lage Dijk 14, NL-3401 RG IJsselstein (NL).

(72) Inventors; and
(75) Inventors/Applicants *(for US only)*: **MCMORROW, Gerald, James** [US/US]; 32609 NE 202nd Street, Duvall, WA 98019 (US). **BAARTMANS, Henri** [NL/NL]; Lunenburg 5, NL-3401 HT IJsselstein (NL). **BOM, Nicolaas** [NL/NL]; Kerkweg 85, NL-2825 NA Berkenwoude (NL). **LANCEE, Charles, Theodoor** [NL/NL]; Rijksweg 232, NL-9423 PH Hoogersmilde (NL).

(74) Agent: **CHARIG, Raymond, J.**; Eric Potter Clarkson, Park View House, 58 The Ropewalk, Nottingham NG1 5DD (GB).

(81) Designated States *(national)*: AE, AG, AL, AM, AT, AU, AZ, BA, BB, BG, BR, BY, BZ, CA, CH, CN, CO, CR, CU, CZ, DE, DK, DM, DZ, EC, EE, ES, FI, GB, GD, GE, GH, GM, HR, HU, ID, IL, IN, IS, JP, KE, KG, KP, KR, KZ, LC, LK, LR, LS, LT, LU, LV, MA, MD, MG, MK, MN, MW, MX, MZ, NI, NO, NZ, OM, PG, PH, PL, PT, RO, RU, SC, SD, SE, SG, SK, SL, SY, TJ, TM, TN, TR, TT, TZ, UA, UG, US, UZ, VC, VN, YU, ZA, ZM, ZW.

(84) Designated States *(regional)*: ARIPO patent (GH, GM, KE, LS, MW, MZ, SD, SL, SZ, TZ, UG, ZM, ZW), Eurasian patent (AM, AZ, BY, KG, KZ, MD, RU, TJ, TM), European patent (AT, BE, BG, CH, CY, CZ, DE, DK, EE, ES, FI, FR, GB, GR, HU, IE, IT, LU, MC, NL, PT, RO, SE, SI, SK, TR), OAPI patent (BF, BJ, CF, CG, CI, CM, GA, GN, GQ, GW, ML, MR, NE, SN, TD, TG).

Published:
— *with international search report*

For two-letter codes and other abbreviations, refer to the "Guidance Notes on Codes and Abbreviations" appearing at the beginning of each regular issue of the PCT Gazette.

(54) **Title:** INSTANTANEOUS ULTRASONIC MEASUREMENT OF BLADDER VOLUME

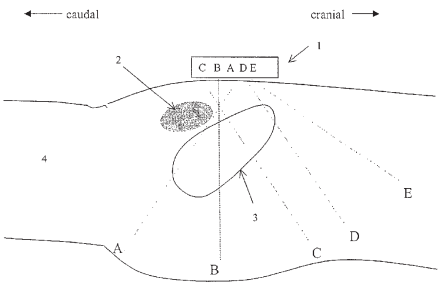

(57) **Abstract:** An apparatus and methods to quantify the volume of urine in a human bladder with a limited number of acoustic beams is disclosed. In a first version the apparatus is composed of a transducers assembly that transmits a plurality of narrow ultrasound beams in different directions towards the bladder and receives the returning ultrasound signals; a receiver detector for processing the returned signals; an analog-to-digital converter; a memory to store the digitized data and a volume display allowing to define the optimal position of the transducer assembly. The apparatus also includes a signal processing software that automatically determines the bladder Depth D and Height H and computes the volume of urine using an empirical formula corrected by specific, empirically measured, filling dependant correction factors. In a second version a single wide angle ultrasound beam transducer transmitting ultrasound signals at fundamental frequency is used to quantify the urine volume. Return signals originating from a depth beyond the usual position of the posterior wall depth of a filled bladder are analyzed for presence of higher harmonic signals which in turn are related to presence or absence of urine. Both methods or a combination thereof can be used as a simple warning device for presence of residual urine after voiding or indicate the presence of a critical bladder urine filling level.

WO 2004/017834 A1

Appendix B: Abstract Continuation In Part (CIP) of the Original Patent Application

(12) INTERNATIONAL APPLICATION PUBLISHED UNDER THE PATENT COOPERATION TREATY (PCT)

(19) World Intellectual Property Organization
International Bureau

(43) International Publication Date
9 March 2006 (09.03.2006)

PCT

(10) International Publication Number
WO 2006/026605 A3

(51) International Patent Classification:
A61B 8/00 (2006.01) *G06K 9/00* (2006.01)

(21) International Application Number:
PCT/US2005/030799

(22) International Filing Date: 29 August 2005 (29.08.2005)

(25) Filing Language: English

(26) Publication Language: English

(30) Priority Data:
60/605,391 27 August 2004 (27.08.2004) US

(71) Applicant *(for all designated States except US)*: **DIAGNOSTIC ULTRASOUND CORPORATION** [US/US]; 21222-30th Drive SE, Suite 120, Bothell, WA 98021 (US).

(72) Inventors; and

(75) Inventors/Applicants *(for US only)*: **MCMORROW, Gerald** [US/US]; 11810 NE 102nd Place, Kirkland, WA 98033 (US). **CHALANA, Vikram** [US/US]; 15302 34th Dr. SE,, Mill Creek, WA 98027 (US). **YUK, Jongtae** [KR/US]; 10106 177th Avenue NE, Redmond, WA 98052 (US). **BAARTMANS, Henri** [NL/NL]; Lunenberg 5, NL-3401 HT IJsselstein (NL). **BOM, Nicolaas** [NL/NL]; Kerkweg 85, NL-2825 NA Berkenwoude (NL). **LANCEE, Charles, Theodoor** [NL/NL]; Rijksweg 232, NL-9423 PH Hoogersmilde, (NL). **MERKS, Egon, J., W.** [NL/NL]; Buitenboogerd 25, NL-2611 WR Delft (NL).

(74) Agent: **BYRNE, Mark, D.**; Black Lowe & Graham Pllc, 701 Fifth Avenue, Suite 4800, Seattle, WA 98104 (US).

(81) Designated States *(unless otherwise indicated, for every kind of national protection available)*: AE, AG, AL, AM, AT, AU, AZ, BA, BB, BG, BR, BW, BY, BZ, CA, CH, CN, CO, CR, CU, CZ, DE, DK, DM, DZ, EC, EE, EG, ES, FI, GB, GD, GE, GH, GM, HR, HU, ID, IL, IN, IS, JP, KE, KG, KM, KP, KR, KZ, LC, LK, LR, LS, LT, LU, LV, MA, MD, MG, MK, MN, MW, MX, MZ, NA, NG, NI, NO, NZ, OM, PG, PH, PL, PT, RO, RU, SC, SD, SE, SG, SK, SL, SM, SY, TJ, TM, TN, TR, TT, TZ, UA, UG, US, UZ, VC, VN, YU, ZA, ZM, ZW.

(84) Designated States *(unless otherwise indicated, for every kind of regional protection available)*: ARIPO (BW, GH,

[Continued on next page]

(54) Title: SYSTEMS AND METHODS FOR QUANTIFICATION AND CLASSIFICATION OF FLUIDS IN HUMAN CAVITIES IN ULTRASOUND IMAGES

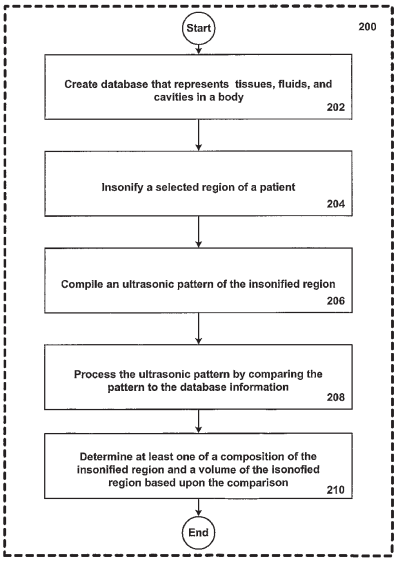

(57) Abstract: Ultrasound imaging systems and methods are disclosed. In one embodiment, an ultrasongraphy method includes creating a database that is representative of a tissue, a fluid, or a cavity of a body, and transmitting ultrasound pulses into a regionof-interest in a patient. Echoes are received from the region of interest, and based upon the received echoes, compiling an ultrasonic pattern of the region-of-interest is compiled. The pattern is processed by comparing the region-of-interest patterns to the pattern information stored in the database. A composition within the region-of-interest of the patient is then determined.

WO 2006/026605 A3

WO 2006/026605 A3

GM, KE, LS, MW, MZ, NA, SD, SL, SZ, TZ, UG, ZM, ZW), Eurasian (AM, AZ, BY, KG, KZ, MD, RU, TJ, TM), European (AT, BE, BG, CH, CY, CZ, DE, DK, EE, ES, FI, FR, GB, GR, HU, IE, IS, IT, LT, LU, LV, MC, NL, PL, PT, RO, SE, SI, SK, TR), OAPI (BF, BJ, CF, CG, CI, CM, GA, GN, GQ, GW, ML, MR, NE, SN, TD, TG).

Published:

— *with international search report*

— *before the expiration of the time limit for amending the claims and to be republished in the event of receipt of amendments*

(88) Date of publication of the international search report:
22 February 2007

For two-letter codes and other abbreviations, refer to the "Guidance Notes on Codes and Abbreviations" appearing at the beginning of each regular issue of the PCT Gazette.

Dankwoord

Dit proefschrift is het resultaat van (al weer) 8 jaar vertoeven op de afdeling *Biomedical Engineering* (voorheen *Experimentele EchoCardiografie*) op de 23^{ste} etage van het ErasmusMC. Het begon allemaal met een afstudeeropdracht, waar ik ruim een jaar gewerkt heb aan het verfijnen van een nieuwe methode om instantaan het volume van de blaas te kunnen meten. Deze methode, welke gebruik maakte van (wel!) vijf ultrageluidstransducenten, werkte uitstekend. Echter, commercieel gezien was vijf toch wel iets te veel, met als gevolg dat het prototype stilletjes in een kast verdween. Door deze opdracht had ik de smaak van het experimentele ultrageluid zeker te pakken en zei daarom volmondig "ja" toen ik door Klaas Bom gevraagd werd voor een ambitieus vervolg. Ik moet toegeven dat mijn beslissing ook bepaald werd door mijn collega's van de afdeling! Zij zorgen dag in dag uit voor een prettige werksfeer en een vruchtbare bodem voor nieuwe ideeën. Dit schrijven heb ik ook aan hen te danken!

Mijn bijzondere dank dus aan alle collega's van de afdeling Biomedical Engineering. Toch wil ik een aantal mensen nog expliciet noemen:

Klaas Bom: Ik ben bevoorrecht om door één der grootsten op het gebied van (medisch) ultrageluid te zijn begeleid. Jouw kennis, inzicht, nuchterheid en gedrevenheid heeft mij door de vele moeilijke momenten tijdens mijn promotie geleid. Mijn stelling 10 heeft zeer zeker betrekking op onze relatie, en ik hoop dat ik in jouw ogen hierin geslaagd ben. Ik moet toegeven dat het mij vaak ook wanhopig heeft gemaakt wanneer er nauwelijks vooruitgang zat in het onderzoek en ik jou als het ware moest teleurstellen. Ik vind het erg jammer dat op de dag van de promotie jij niet mijn promotor kan zijn. Gelukkig zit je wel in de commissie en mag ik twee andere grote heren als mijn promotor noemen. Onze gezamenlijke trips naar Seattle heb ik erg plezierig, gezellig en inspirerend gevonden. Ik hoop dat we nog lang kunnen samenwerken om tot leuke en succesvolle ontwikkelingen te komen. Klaas Bedankt!

Ton van der Steen: Ton, hoewel de fles Rioja Gran Reserva jou (nog) niet

heeft bereikt, wil ik je bij deze ontzettend bedanken dat ik door jouw inspanningen als finalist van de Student Paper Competition naar Beijing ben gegaan. Helaas behoorde ik niet tot de winnaars, maar ik vond het een bijzondere en leerzame ervaring. Bedankt voor je waardevolle opmerkingen en sturing als promotor!

Nico de Jong: Nico, tijd is bij jou een variabel begrip, maar uiteindelijk komt het toch allemaal voor elkaar. Bedankt voor je ondersteuning als promotor, becommentariëren van mijn manuscripten en het pushen als het een keer echt af moest zijn!

Henri Baartmans: Henri jij hebt me laten zien dat het belangrijk is voor wetenschappers om te begrijpen hoe het bedrijfsleven werkt. Beide werelden moeten met elkaar kunnen communiceren en daar heb ik in het verleden zeker aan moeten wennen. Bedankt voor deze ervaring, jouw geduld en het geloof en steun in mij en het project. Tevens bedankt voor de waardering voor mij en Wendy. We hebben genoten van alle uitstapjes. Tevens wil ook alle medewerkers van Verathon Medical Europe bedanken voor hun interesse, vriendelijkheid en behulpzaamheid.

Gerald McMorrow: Thank you Gerald for showing me how a great company should be run. Your vision on how technology can improve Medical Healthcare is inspiring and should be the main drive for other CEOs. Thank you for being a magnificent host during my visits to Bothell. Klaas and I have been treated like kings!

Wouter Serdijn: Wouter bedankt voor je begeleiding als afstudeerdocent en je deelname in de STW gebruikerscommissie. Niet voor niets ben je een volprezen hoogleraar en ik hoop nog vaker samen te kunnen werken. Fijn dat je in mijn commissie zit.

Ron van Mastrigt: Bij de STW gebruikersbijeenkomsten zette jij mij vaak op scherp en ging ik met nieuwe ideeën weer aan het werk. Fijn dat je in mijn commissie zit.

Paul Boontje (STW): Bedankt Paul voor het begeleiden van de STW gebruikersbijeenkomsten en je hulp bij het indienen van financieringsaanvragen.

Charles Lancée: Je hebt geniale mensen en je hebt de overtreffende trap. Jij hoort zeker tot de laatste groep, want veel slimme bedenksels binnen dit project komen van jouw tekentafel. Bedankt voor je innovatieve ideeën en je didactische vaardigheden.

Hans Bosch: Jij bent altijd en overal in geïnteresseerd! Althans, zo kom je bij mij over. Bedankt voor je actieve rol tijdens de STW gebruikersbijeenkomsten en je bijdrage aan het AAA-project.

Marco Voormolen: Ik heb het altijd prettig gevonden om tijdens internationale congressen de kamer met jou te delen. Als het nodig was konden we geconcentreerd de laatste hand leggen aan presentaties of proceedings, maar we hadden ook veel lol. Vooral als ik weer eens in mijn slaap gesproken had:

"Ja, en Marco ook! Hi hi hi!". Ik hoop snel weer eens een biertje met je te drinken.

Ayache Bouakaz: Ayache you kick-started this project and showed the critics that such an ambitious idea should first be explored and its feasibility be checked instead of rejecting it beforehand. All the best to you, Peggy and the kids!

Wim van Alphen: Zonder jouw inzet en kunnen zat ik nu nog aan de tekentafel te speculeren of een 2-laags transducent nu wel zo verstandig was. Alle praktische resultaten heb ik verkregen met jouw speciale en perfect in elkaar gezette brouwsels. Bedankt voor je interesse in mij en het project, en geniet van je vrije tijd!

Leo Bekkering: Samen met Wim heb jij mij geholpen aan allerlei praktische opstellingen. Vooral in mijn afstudeerperiode heb jij veel aan het prototype met de vijf transducenten (later 4) gewerkt. Ook voor het vervaardigen van waterbakken, fantoommallen en transducer behuizingen kon ik bij jou terecht.

Geert Springeling: Een waardevolle opvolger van Wim en Leo. Er zijn al bijzonder mooie en goede dingen uit jouw handen gekomen, en ik hoop natuurlijk op nog veel meer!

Jan Honkoop: "Als iets niet werkt, vraag het dan aan Jan." Vooral in mijn afstudeerperiode heb ik deze uitspraak veelvuldig toegepast. Onder jouw begeleiding heb ik ontzettend veel praktische ervaring opgedaan!

Franc van den Adel en Christian Prins (Oldelft): Bedankt voor jullie adviezen voor alles wat met transducers te maken heeft.

Don Poldermans, Ruud Kuiper, Willem-Jan Flu en J-P van Kuijk: Dank voor jullie inzet en samenwerking in het AAA-project. Als technicus is het zeer leerzaam om zich in de kliniek te begeven, al was het in het begin wel even wennen. Nog wel eens heb ik problemen met het vakjargon. Gelukkig kreeg ik van jullie alle ruimte en begrip om mij ook in de kliniek op mijn gemak te kunnen voelen.

Frits Mastik: Jouw kennis van systemen en software is bewonderenswaardig te noemen. Het is fijn om jou als "backup" te hebben!

Marianne Immerzeel: Bedankt voor al je inspanningen betreft declaraties, borderellen en reserveringen van het filmzaaltje. Je hebt echt tonnen aan werk uit mijn handen genomen, zelfs al durfde ik je het niet te vragen.

Mieke Pruijsten: Jou moet ik vooral bedanken voor je inzet en het feit dat je me achter m'n broek hebt gezeten om alles op tijd in te leveren. Nadat het jou gelukt was om zo snel mogelijk een promotiedatum te bemachtigen, kon ik ook niet anders dan als een bezetene de deadlines halen.

Hans Verdoes: De vraagbaak als het om computer gerelateerde zaken gaat. Bedankt voor je inzet en moeite wanneer een probleempje toch iets groter bleek te zijn.

Sandra de Zeeuw: Bedankt voor je samenwerking in de kliniek. Jij en je

man veel geluk met Milo en met het kleintje op komst.
Cees Pakvis: Er staat nog steeds een project op mij te wachten, waarvan een door jou bedacht inventief hulpmiddel nu nog op mijn bureau staat. Ik ben zeker van plan ermee te gaan werken. Ik hoop je snel met leuke en interessante resultaten te kunnen verassen.
Marcia Emmer: Jouw promotie was als een generale voor de mijne. Bedankt voor je adviezen en hulp met de tekstverwerking.
Jerome Borsboom: Elektrotechnisch ingenieurs hebben een aparte taal en het is prettig als je je daarin kunt uitdrukken. Het denken in systemen is er tijdens de studie aan de TU Delft ingebrand en daardoor zaten wij regelmatig op één lijn.
Martijn Frijlink: Hoewel jij ook elektrotechnisch ingenieur bent liet jij het "in systemen denken" wel eens varen. Dit leverde interessante en leerzame discussies op. Bedankt dat jij je geboortedag met mij wilde delen, ook al was je een jaartje eerder.
Guillaume Matte: Guillaume *"Matte Patat"*, thank you for investigating the patient safety aspects of my project. I know that it was a difficult and rather vague task, but I think you succeeded well. I enjoyed being your supervisor during your graduation project. You were a wonderful colleague and you have proven your scientific and social skills throughout the last few years.
Paul van Neer: Volgens mij ben jij de "waarom?-periode", die we allemaal als kind hebben gehad, nooit ontgroeid. Gelukkig maar, want zo heb ik ook vraagtekens bij menig van mijn bezigheden kunnen zetten. Bedankt voor alle discussies omtrent transducenten en de modellering hiervan. Ik heb prettig met je samengewerkt aan het artikel over de IM-Transducer.
Robert Beurskens: Duits spreken heeft zeker niet mijn voorkeur en bovendien kun jij dat véél beter (Oei!). Bedankt voor al die keren dat ik jouw werkbank heb mogen (mis)gebruiken voor allerlei soldeerfrutsels. Het is goed om over goede tools te kunnen beschikken, en daarvoor kan men zeker bij jou terecht... ook al zijn de handleidingen veelal in de Germaanse taal.
Rik Vos: Nog nooit heb ik iemand zo vaak letterlijk de rug toegekeerd als jou. In tegenstelling tot het spreekwoordelijke is dit bij ons juist een teken van een goede en rustige werkomgeving! Bedankt voor het zijn van een goede vraagbaak en je reflectie betreft complexe problemen. Succes met jouw laatste lootjes!
Sandra Blaak en Margreet Docter: Ik weet dat het nieuwe xyz-systeem bij jullie in goede handen is en dat jullie er al veel tijd in hebben zitten. Ik heb er zelf nog niet mee kunnen werken, maar met jullie hulp gaat het zeker lukken goede resultaten te behalen.

Coot en Peter: Ontzettend bedankt voor jullie hulp in ons huis en de morele steun.

Pa en Ma: Bedankt voor al jullie liefde, zorg, steun en, niet op de laatste plaats, jullie geduld. Ik mag me gelukkig prijzen met jullie als ouders.
Richelle: Je bent en blijft mijn kleine zusje...

Wendy: Wenneke, jij bent mijn steun, mijn maatje. We hebben het de afgelopen tijd erg druk gehad, en ik heb het jou zeker niet gemakkelijk gemaakt. Ik beloof je dat er rustigere tijden komen en dat we van ons huisje, tuin en diertjes kunnen gaan genieten. **Ik hou van je!**

Tot slot ben ik veel dank verschuldigd aan mijn huisdiertjes; de familie konijn (**Charlientje**, **Didi**, **Gizmo** en **Beertje**) en de trotse parkiet **Kwibus**. Bedankt voor jullie liefde en afleiding! **Didi**, ondanks je slechte ruggetje ben je een rolmodel voor enthousiasme. Ik zeg het nogmaals: Velen, inclusief ikzelf, zouden aan jouw doorzettingsvermogen een voorbeeld mogen nemen!

Egon Jacobus Wilhelmus Merks-Swolfs
's-Gravenhage, 28 april 2009

Summary

It is well known that bladder dysfunction is associated with a number of clinical conditions requiring treatment. In many of these cases it is important to accurately determine the volume of the bladder. Under other conditions such as post-operative recovery, where there is temporary loss of bladder sensation and/or loss of the normal voiding mechanism, too much distension of the bladder has to be avoided. Under those conditions voiding by catheter introduction is carried out. Catheterization also remains to be the "golden standard" for bladder volume assessment. However, catheterization has serious disadvantages that range from the uncomfortable situation for the patient to serious possibilities of infection. To be sure that the bladder needs to be emptied, and thus avoiding unnecessary catheterizations, the need for a non-invasive and quick measurement of bladder volume is indicated. The clinical importance is particularly apparent in anesthesiology and urology. Non-invasive procedures for bladder volume estimation are known, but are either unreliable, expensive, or have other significant disadvantages. Recent studies have shown that by the use of portable ultrasound scanners, the number of catheterizations can be reduced significantly, thereby reducing the risks involving this invasive action. However, most ultrasound scanners are very complex and need trained operators. To make noninvasive bladder volume assessment accessible to a larger public, a method is needed that is easy to use, fast, relatively inexpensive and allows for miniaturization.

This thesis describes a completely new instantaneous, non-invasive, and simple bladder volume assessment method with the use of ultrasound. The working principle and a feasibility study is discussed in Chapter 2. While other ultrasound methods require a large amount of ultrasound beams, mechanically or electronically created, to acquire the necessary amount of data of the whole bladder or cross-sections of the bladder, this method only uses a single diverging ultrasound beam. This beam instantly captures the whole bladder, which avoids aiming problems. With the new method a pulsed ultrasonic signal is transmitted at a certain fundamental frequency. The received echoes

that originate from a region of interest (ROI) at a fixed location behind the average position (at approximately 12 cm) of the posterior bladder wall are analyzed for the presence of higher harmonics of the fundamental transmit frequency. The received echoes will contain information about almost the entire bladder as the wide ultrasound beam encompasses the largest part of the bladder. Due to nonlinearity, higher harmonic components will build up during propagation through urine, which can be detected in the returning echo. With empty bladders, the higher harmonics are "absent." Feasibility was proven using *in vitro* measurements on bladder phantoms. Also, measurements on a volunteer showed that bladder volume assessment on the basis of nonlinear wave propagation is feasible *in vivo*.

The system used with this first attempt consisted of a conventional ultrasound system, adjusted for experimental purposes, and an experimental fast rotating phased array probe developed for 3D harmonic cardiac imaging. The transducer and system were clearly too advanced for the application of bladder volume assessment and it would be impossible to integrate its functionality into a low cost handheld device. Therefore, it was stressed that a dedicated relatively simple and low cost transducer was needed that is capable of generating a wide acoustic field large enough to capture a (full) bladder. Additionally, the transducer should have high transmit sensitivity to induce significant nonlinear wave propagation, and high sensitivity in reception to measure up to the 3^{rd} harmonic. Three transducer concepts were investigated, i.e. a broadband single element transducer, a multi-element ring transducer and a multilayer transducer. The multilayer transducer was found best due to the combination of high efficiency in transmission and broadband reception and the relatively simple beamforming to create the diverging acoustic beam.

However, the first multilayer transducer was very susceptible to electromagnetic distortion (high EMS), resulting in low signal-to-noise ratio (SNR) in the received signals. To solve this problem, an equivalent KLM-circuit model of the multilayer transducer was developed. This has proven to be a valuable tool to evaluate and further optimize the multilayer transducer design. Eventually, an "Inverted" multilayer transducer was designed and built. It had very low EMS, high transmit sensitivity and was able to receive up to the 3^{rd} harmonic with good sensitivity. It was concluded that in order to measure at least up to the third harmonic frequency component with good sensitivity in combination with very high transmit sensitivity at the fundamental frequency, a multilayer structure is optimal. To optimize for the EMS in reception, and hence also the signal-to-noise ratio, an inverted geometry as proposed in this thesis has proven to be effective.

In order to define an algorithm that is capable of giving a good estimation of the bladder volume and is not affected by patient variations, a simulation study was conducted. Four different algorithms, including the original method of selecting a ROI located at a fixed position behind the bladder, were compared. The simulations included the modeling of nonlinear wave propagation through layered media, comprising the anterior bladder wall, the urine region and the posterior bladder wall, using a time-domain implementation of the Khokhlov-Zabolotskaya-Kuznetsov (KZK) equation. In this case, a non-diverging acoustic beam was used because of the limitations of the KZK implementation. Hence, urine pathlengths (UPL) instead of volumes were modeled. The simulations showed that the generated harmonics within the anterior bladder wall affect the amount of harmonics measured in the posterior bladder domain. This influence is emphasized by the additional acoustic loss in this region for the reflected waves. The originally proposed algorithm showed to be the least sensitive to patient variability and bladder shape.

A first in-vivo evaluation of this method using the new developed transducer, including acoustic lens, showed that this method is currently capable of qualitative volume measurement instead of quantitative measurements. The measurement results showed a high repeatability for both algorithms, but large volumes could not be measured accurately due to beamwidth limitations. Another observation from the clinical measurements as well as from the simulations described in Chapter 4, is the sensitivity to stochastic scattering of tissue and spatial averaging. It was concluded that these effects cannot be compensated for by using clever algorithms, but that they completely depend on the transducer properties and the transmitted waves. Clearly, patient dependency plays an important role and should be corrected for to facilitate general application of the volume assessment method. To perform quantitative bladder volume assessment additional research is needed on beamforming and pulsing schemes. Additionally, a large clinical study is needed to optimize the algorithm.

The study presented in Chapter 6 addressed the safety aspects with respect to the bladder volume assessment using nonlinear ultrasound. Although the method uses a diverging acoustic beam, the study concentrated on an unfocused (flat) ultrasonic transducer. The results obtained could then be considered as the limiting case, where defocusing of the beam would only decrease the exposure values. *In vitro* measurements and simulations showed that the safety limits, the Mechanical Index (MI) and the Thermal Index (TI), were still valid under the assumption of nonlinear wave propagation. It was concluded that the limits were not exceeded and that bladder volume

assessment on the basis of nonlinear wave propagation is safe.

From the work presented in this thesis it can be concluded that noninvasive bladder volume measurement using nonlinear ultrasound is feasible. It has the potential of becoming a fast, low cost and easy to use addition to the currently available dedicated portable bladder volume instruments. Although it is not likely that it will rival the obtainable accuracy of current devices, it will make noninvasive bladder volume assessment accessible to a larger public, which is the main goal of this study.

Samenvatting

Het is bekend dat het niet goed functioneren van de blaas samen gaat met een aantal behandeling vereisende gezondheidsproblemen. In veel van deze gevallen is het noodzaak het blaas volume nauwkeurig te meten. In andere situaties, zoals na een operatie waarbij tijdelijk het gevoel in de blaas afwezig is en het normale plas mechanisme niet werkt, moet een te grote uitzetting van de blaas vermeden worden. In zulke gevallen wordt de blaas geleegd door middel van het inbrengen van een katheter. Katheterisatie blijft de "Gouden Standaard" voor het meten van het blaas volume, maar heeft als nadeel dat de procedure zeer oncomfortabel is voor de patiënt en dat er een kans op infectie aanwezig is. Om er zeker van te zijn dat de blaas geleegd moet worden, met het doel om onnodige katheterisaties te vermijden, is er een behoefte aan een niet-invasieve instantane meting van het blaas volume. Het klinische belang is vooral duidelijk bij anesthesiologie en urologie. Niet-invasieve methoden voor het bepalen van het blaas volume zijn voorhanden, maar deze zijn onbetrouwbaar, duur, of hebben andere significante nadelen. Recente studies hebben aangetoond dat, door het gebruik van draagbare ultrageluidscanners, het aantal uitgevoerde katheterisaties evenals de samenhangende risico's van invasief handelen drastisch zijn verminderd. Echter, de meeste draagbare ultrageluidscanners zijn complexe apparaten en vergen geoefende gebruikers. Om niet-invasief blaas volume meting toegankelijker te maken voor een groter publiek, is er een eenvoudige, snelle en relatief goedkope methode nodig, welke bovendien klein verpakt kan worden.

In dit proefschrift ligt het accent op een totaal nieuwe, instantane, niet-invasieve en eenvoudige methode om blaas volume te bepalen met behulp van ultrageluid. Het werkingsprincipe en een haalbaarheidsstudie worden besproken in Hoofdstuk 2. Hoewel andere methoden gebaseerd zijn op het mechanisch of elektronisch sturen van veel, nauwe, ultrageluidbundels om voldoende informatie over de hele blaas of doorsneden te verkrijgen, heeft de nieuwe methode slechts één enkele divergente ultrageluidbundel nodig. Met deze bundel wordt in één klap de gehele blaas omvat, waardoor richtproblemen

worden vermeden. Met de nieuwe methode wordt er een gepulseerd ultrageluid signaal verzonden met een bepaalde fundamentele frequentie. Door de wijde ultrageluidbundel bevatten de ontvangen echo's informatie van bijna de gehele blaas. De ontvangen echo's afkomstig van een geselecteerd gebied op een vaste diepte (op ongeveer 12 cm) achter de blaas worden vervolgens geanalyseerd op de aanwezigheid van hogere harmonischen van de fundamentele zendfrequentie. Vanwege niet-lineariteit van de geluidsvoortplanting door de urine ontstaan hogere harmonischen die in het echosignaal kunnen worden gedetecteerd. Bij een lege blaas zijn deze hogere harmonischen "afwezig". De haalbaarheid van deze methode is aangetoond middels fantoom metingen en metingen uitgevoerd op een vrijwilliger.

Het systeem dat gebruikt werd voor de haalbaarheidsstudie bestond uit een conventioneel ultrageluidsysteem, aangepast voor experimentele doeleinden, en een experimentele snel roterende "phased array" probe, welke was ontwikkeld voor 3D harmonische echocardiografie. Het mag duidelijk zijn dat dit systeem te geavanceerd is voor de bedoelde blaas volume meting, en dat het onmogelijk zou zijn deze functionaliteit in een goedkoop en klein apparaat te integreren. Vandaar dat er werd aangegeven dat een speciaal ontwikkelde, simpel en goedkope transducent nodig was. Deze moet bovendien instaat zijn om een brede divergerende bundel te genereren, breed genoeg om een volle blaas te kunnen omvatten. Ook moest de transducer een hoge zendgevoeligheid hebben om voldoende niet-lineaire geluidsvoortplanting te initiëren, en moest de ontvangst gevoeligheid en bandbreedte voldoende zijn om op zijn minst de 3^{de} harmonische te kunnen meten.

Hiertoe werden drie transducent-concepten vergeleken, te weten een breedband enkel-element transducent, een meervoudig ring-element transducent en een meerlaags transducent. De meerlaags transducent werd als beste bevonden vanwege de combinatie van een hoge zendgevoeligheid, een breedbandige ontvangst-gevoeligheid en de mogelijkheid om eenvoudig een brede bundel te creëren.

Het bleek echter dat deze eerste meerlaags-transducent erg gevoelig was voor elektromagnetische storing, waardoor de signaal-ruis-verhouding in de ontvangen signalen erg laag was. Om dit probleem op te lossen werd er een equivalent KLM-circuit model van de meerlaagstransducent ontwikkeld. Dit model is zeer nuttig gebleken als middel om de meerlaags transducent te analyseren en verder te optimaliseren. Uiteindelijk is er een "geïnverteerde" meerlaags transducent ontworpen en gebouwd, welke een zeer lage gevoeligheid had voor elektromagnetische storing. Deze transducent had een hoge zendgevoeligheid en was in staat om tot de 3^{de} harmonische goed

te kunnen ontvangen. Er werd geconcludeerd dat, om op zijn minst de derde harmonische goed te kunnen ontvangen in combinatie met een zeer hoge zendgevoeligheid op de fundamentele frequentie, een meerlaags transducent optimaal is. Om een lage gevoeligheid voor elektromagnetische storing te verkrijgen, en dus de signaal-ruis-verhouding te vergroten, is het gebruik van een geïnverteerde geometrie, zoals voorgesteld is in dit proefschrift, efficiënt bevonden.

Vervolgens is er een simulatie studie uitgevoerd om een algoritme te definiëren welke in staat is een goede schatting te geven van het blaas volume en bovendien niet afhankelijk is van variaties tussen patiënten. Hiervoor werden vier verschillende algoritmen vergeleken, waaronder ook de oorspronkelijke methode waarbij een gebied op een vaste diepte achter de blaas wordt geselecteerd. De simulaties bevatten de modellering van niet-lineair ultrageluid door een gelaagd medium, welke bestond uit een gebeid voor de blaas, een gebied met urine, en een gebied achter de blaas. Er werd gebruik gemaakt de Khokhlov-Zabolotskaya-Kuznetsov (KZK)-vergelijking, welke was geïmplementeerd in het tijdsdomein. Door beperkingen van deze KZK-vergelijking konden alleen niet-divergerende geluidsbundels gesimuleerd worden. Hierdoor konden slechts urinepad lengtes in plaats van volumes gemodelleerd worden. De simulatie resultaten toonden aan dat de harmonischen, welke in het gebied vóór de blaas worden gegenereerd, effect hebben op de hoeveelheid harmonischen gemeten in het gebied achter de blaas. Dit effect wordt nog eens versterkt doordat de gereflecteerde golven extra worden verzwakt. Uit deze simulaties is gebleken dat het oorspronkelijke algoritme het minst gevoelig is voor patiënt variaties en de vorm van de blaas.

Een eerste *in vivo* toepassing van deze methode, inclusief de nieuw ontwikkelde transducent met akoestische lens, toonde aan dat reeds kwalitatieve metingen in plaats van kwantitatieve metingen mogelijk zijn. De metingen vertoonden een hoge mate van herhaalbaarheid. Echter, vanwege de beperkte bundelbreedte konden grote volumes niet nauwkeurig worden gemeten. Een andere waarneming van zowel de klinische metingen als de simulatiestudie (Hoofdstuk 4), is de gevoeligheid voor stochastische reflecties van weefsel en ruimtelijke middeling. Deze effecten bleken geheel afhankelijk te zijn van de eigenschappen van de transducent en van de vorm van de zendpuls. Er kon dus niet voor worden gecompenseerd door de slimme keuze van een algoritme. Het mag duidelijk zijn dat patiënt variaties een grote rol spelen, waarvoor toch echt gecorrigeerd dient te worden om algemene toepasbaarheid mogelijk te maken. Om kwantitatieve blaas volume metingen te kunnen doen is verder onderzoek naar de bundelvorming en de toepassing van verschillende zendpulsen noodzakelijk. Bovendien is een grote klinische studie nodig om het

algoritme te optimaliseren.

Hoofdstuk 6 beschrijft een studie naar het veiligheidsaspect van blaasvolume meting doormiddel van niet-lineair ultrageluid. Hoewel het concept een divergerende bundel gebruikt, concentreerde deze studie zich op een niet-gefocusseerde bundel. Omdat een divergerende bundel een verzwakkend effect heeft ten opzichte van een niet-gefocusseerde bundel, kunnen de resultaten beschouwd worden als een uiterst geval. Uitgevoerde *in vitro* metingen en simulaties toonden aan dat de voorgeschreven veiligheidsmarges, te weten de Mechanische Index (MI) en de Thermische Index (TI), ook geldig zijn in het geval dat sterke niet-lineaire ultrageluids componenten aanwezig zijn. Met betrekking tot de blaasvolume meting werd er geconcludeerd dat de veiligheidsmarges niet werden overschreden, en dat de methode veilig te noemen is.

Uit het werk dat in dit proefschrift is beschreven kan worden geconcludeerd dat niet-invasieve blaasvolume meting door middel van niet-lineair ultrageluid mogelijk is. Deze methode heeft de potentie een snelle, goedkope en makkelijk te gebruiken toevoeging te worden aan de reeds bestaande draagbare blaas volume instrumenten. Hoewel het niet mogelijk wordt geacht dat een gelijke meetnauwkeurigheid als van de huidige apparaten gehaald zou kunnen worden, zal deze nieuwe methode het niet-invasief meten van blaasvolumes beschikbaar maken voor een groter publiek. Dit is het uiteindelijke doel van deze studie.

About the Author

Egon J. W. Merks was born on 20 November 1977 in 's-Hertogenbosch, the Netherlands. He graduated from Delft University of Technology, Delft, the Netherlands, in 2002. He received his MSc. degree in the field of biomedical electrical engineering with a thesis on a novel bladder volume measurement device. From 2002 until the end of January 2005 he was employed by Verathon Medical Europe (formerly Diagnostic Ultrasound, IJsselstein, the Netherlands), but situated at the Erasmus MC, where he worked as a research engineer on a new bladder volume measurement technique on the basis of nonlinear wave propagation. Since February 2005, he continued this research as a PhD-student at the Department Biomedical Engineering of the Thoraxcentre, Erasmus MC, Rotterdam, the Netherlands, under the supervision of Nicolaas Bom, Antonius F.W. van der Steen and Nico de Jong.

Publications and Presentations

Publications

- **E.J.W. Merks**, P. van Neer, N. Bom, A.F.W. van der Steen and N. de Jong, "Multilayer transducer for acoustic bladder volume assessment on the basis of nonlinear wave propagation." Ultrasound Med Biol, Accepted for publication, 2009.

- **E.J.W. Merks**, N. Bom, N. de Jong and A.F.W. van der Steen, "Quantitative Bladder Volume Assessment on the Basis of Nonlinear Wave Propagation, IEEE International Ultrasonics Symposium, November 2008, Beijing, China. [Conference Proceedings]

- Guillaume M. Matte, **Egon J.W. Merks**, Nico de Jong, "Safety aspects of acoustic bladder volume measurements based on the use of higher harmonics, World Conference on Ultrasonics, April 2007, Vienna, Austria. [Conference Proceedings]

- R. Vidakovic, O. Schouten, H.H.H. Feringa, M. Dunkelgrun, S.E. Karagiannis, **E.J.W. Merks**, J. Bosch, N. Bom, A.N. Neskovic, J.J. Bax and D. Poldermans, "Abdominal Aortic Aneurysm Screening Using Non-imaging Hand-held Ultrasound Volume Scanner A Pilot Study, Eur. J. Vasc. Endovasc. Surg., 2006.

- **E.J.W. Merks**, C.T. Lancée, N. Bom, A.F.W. van der Steen and N. de Jong, "Comparison of Three Different Transducer Concepts for Acoustic Bladder Volume Measurements," IEEE International Ultrasonics Symposium, September 2005, Rotterdam, The Netherlands. [Conference Proceedings]

- **E.J.W. Merks**, A. Bouakaz, N. Bom, N. de Jong, A.F.W. van der Steen, "Design of a multi-layer transducer for acoustic bladder volume

assessment, IEEE Trans Ultrason Ferroelectr Freq Control, Vol. 53, No. 10, pp1730-1738, October 2006.

- **E.J.W. Merks**, J.M.G. Borsboom, M.M. Voormolen, N. Bom, A.F.W. van der Steen and N. de Jong, "A KLM-circuit model of a multi-layer transducer for bladder volume measurements, Ultrasonics, Vol. 44, Suppl. 1,pp e705-e710, December 2006. [Refereed Conference Proceedings]

- **E.J.W. Merks**, N. Bom, A. Bouakaz, N. de Jong, A.F.W. van der Steen, "Design of a multi-layer transducer for acoustic bladder volume assessment, IEEE International Ultrasonics Symposium Proceedings, 2004. [Conference Proceedings]

- A. Bouakaz, **E.J.W. Merks**, C.T. Lancée and N. Bom, "Noninvasive Bladder Volume Measurements Based on Nonlinear Wave Distortion," Ultrasound Med Biol., Vol. 30, No. 4, pp. 469-476, April 2004.

Abstracts

- **E.J.W. Merks**, N. Bom, N. de Jong and A.F.W. van der Steen, "Quantitative Bladder Volume Assessment on the Basis of Nonlinear Wave Propagation, IEEE International Ultrasonics Symposium, November 2008, Beijing, China.

- Guillaume M. Matte, **Egon J.W. Merks**, Nico de Jong, "Safety aspects of acoustic bladder volume measurements based on nonlinear wave propagation, Proceedings of the International Congress on Ultrasonics, April 2007, Vienna, Austria.

- **E.J.W. Merks**, J.M.G. Borsboom, M.M. Voormolen, N. Bom, A.F.W. van der Steen and N. de Jong, "A KLM-circuit model of a multi-layer transducer for bladder volume measurements, World Conference on Ultrasonics, September 2005, Beijing, China.

- **E.J.W. Merks**, G. Matte, N. Bom, A.F.W. van der Steen and N. de Jong, "Comparison of Three Different Transducer Concepts for Acoustic Bladder Volume Assessment," IEEE International Ultrasonics Symposium, September 2005, Rotterdam, The Netherlands.

- **E.J.W. Merks**, N. Bom, A. Bouakaz, N. de Jong, A.F.W. van der Steen, "Design of a multi-layer transducer for acoustic bladder volume assessment, IEEE International Ultrasonics Symposium, August 2004, Montreal, Canada.

Presentations

- **E.J.W. Merks**, N. Bom, N. de Jong and A.F.W. van der Steen, "Quantitative Bladder Volume Assessment on the Basis of Nonlinear Wave Propagation, IEEE International Ultrasonics Symposium, November 2008, Beijing, China. [Poster]
- **E.J.W. Merks**, N. Bom, N. de Jong and A.F.W. van der Steen, "Quantitative Bladder Volume Assessment on the Basis of Nonlinear Wave Propagation, IEEE International Ultrasonics Symposium, November 2008, Beijing, China. [Oral]
- **E.J.W. Merks**, "Instantaneous Acoustic Bladder Volume Assessment on the Basis of Nonlinear Wave Propagation, Voorjaarsvergadering SUGB, 24 May 2006, Maastricht. [Oral]
- **E.J.W. Merks**, G. Matte, N. Bom, A.F.W. van der Steen and N. de Jong, "Comparison of Three Different Transducer Concepts for Acoustic Bladder Volume Assessment," IEEE International Ultrasonics Symposium, September 2005, Rotterdam, The Netherlands. [Poster]
- **E.J.W. Merks**, J.M.G. Borsboom, M.M. Voormolen, N. Bom, A.F.W. van der Steen and N. de Jong, "A KLM-circuit model of a multi-layer transducer for bladder volume measurements, World Conference on Ultrasonics, September 2005, Beijing, China. [Poster]
- **E.J.W. Merks**, N. Bom, A. Bouakaz, N. de Jong, A.F.W. van der Steen, "Design of a multi-layer transducer for acoustic bladder volume assessment, IEEE International Ultrasonics Symposium, August 2004, Montreal, Canada. [Oral]

PhD Portfolio Summary

PhD Student:	Egon J.W. Merks
Erasmus MC Department:	Biomedical Engineering, Thoraxcenter
Research School:	COEUR
PhD period:	2004 - 2009
Promotors:	Prof.dr.ir. N. de Jong
	Prof.dr.ir. A.F.W. van der Steen
Supervisor:	Prof.dr.ir. N. Bom

Activity	**Year**	**ECTS**
General academic skills		
Biomedical English Writing and Communication (ErasmusMC)	2004	3.0
Classical Methods for Data Analysis (Nihes, CC02)	2004	6.0
In-depth courses		
Cardiovascular Imaging and Diagnostics (COEUR)	2006	1.5
Good Clinical Practice (Nihes, EWP21)	2007	1.5
International conferences		
IEEE International Ultrasonics Symposium, Beijing, China	2008	0.9
IEEE International Ultrasonics Symposium, New York, USA	2007	0.9
IEEE International Ultrasonics Symposium, Rotterdam, the Netherlands	2005	0.9
IEEE International Ultrasonics Symposium, Montreal, Canada	2004	0.9

Continued on next page

Activity	Year	ECTS
Presentations		
IEEE International Ultrasonics Symposium, Beijing, China (Oral + poster)	2008	1.5
Stichting ultrageluid in de geneeskunde en biologie (SUGB), Maastricht, the Netherlands (Oral)	2006	0.3
IEEE International Ultrasonics Symposium, Rotterdam, the Netherlands (Poster)	2005	0.5
World Conference on Ultrasonics (WCU), Beijing, China (Poster)	2005	0.5
IEEE International Ultrasonics Symposium, Montreal, Canada (Oral)	2004	1.0
Workshops		
Estimation and Imaging of Tissue Motion and Blood Velocity (IEEE short course, Beijing, China)	2008	0.15
Ultrasound Contrast Agents: Theory and Experiment (IEEE short course, New York, USA)	2007	0.15
Nonlinear Acoustics and Harmonic Imaging (IEEE short course, Montreal, Canada)	2004	0.15
Medical Ultrasound Transducers (IEEE short course, Montreal, Canada)	2004	0.15
National Semiconductor - The Power Design Technical Course (Eindhoven, the Netherlands)	2007	0.3
Teaching Activities		
Supervising Master's thesis, Guillaume Matte, ESIL, Marseille, France	2005	4.0
Supervising Master's thesis, Meer Setu, TU-Delft, Delft, the Netherlands	2005-2006	4.0
Other		
Assisting a clinical trial on screening for abdominal aortic aneurysms using a dedicated portable ultrasound system. Location: outpatient clinic of the Department of Vascular Surgery, ErasmusMC, Rotterdam, the Netherlands	2007-2009	4.0
Total		32.3